TECHNICAL UNIVERSITY OF LIBEREC
FACULTY OF EDUCATION

Department of Physics

Study program: secondary school

Specialization: mathematics and physics

Dielectric Studies of Ferroelectric Phase Transitions in $Sn_2P_2(Se_xS_{1-x})_6$ Crystals

Dielektrické Studium Ferroelektrických Fázových Přechodů v Krystalech $Sn_2P_2(Se_xS_{1-x})_6$

Dielektrische Untersuchungen des Ferroelektrischen Phasenüberganges in Einkristallinem $Sn_2P_2(Se_xS_{1-x})_6$

Diploma Thesis: *07*–FP–KFY-062

Author: Iryna TYAGUR

Signature: .....

Address:
Bestuzheva 4/69, 88 009 Uzhgorod
Ukraine

Supervisor: **RNDr. Petr Hána, CSc.**

Consultant: **Dr. Rüdiger, Andreas**

pages	words	figures	tables	bibliography
91	17947	40	13	20

In Liberec: 07-05-2007

Prohlášení

Byla jsem seznámena s tím, že na mou diplomovou práci se plně vztahuje zákon č. 121/2000 Sb. o právu autorském, zejména § 60 – školní dílo.

Beru na vědomí, že Technická univerzita v Liberci (TUL) nezasahuje do mých autorských práv užitím mé diplomové práce pro vnitřní potřebu TUL.

Užiji-li diplomovou práci nebo poskytnu-li licenci k jejímu využití, jsem si vědoma povinnosti informovat o této skutečnosti TUL; v tomto případě má TUL právo ode mne požadovat úhradu nákladů, které vynaložila na vytvoření díla, až do jejich skutečné výše.

Diplomovou práci jsem vypracovala samostatně s použitím uvedené literatury a na základě konzultací s vedoucím diplomové práce a konzultantem.

Datum

Podpis

ACKNOWLEDGEMENTS

My profound thanks to the *Department of Physics* for given opportunity to work in the piezoelectric laboratory, for freedom in choosing the field of research and for support making the facilities available for the investigations.

I am thankful to the *Institute of Physics and Chemistry* of Uzhgorod National University for obtained samples for my research work.

I thank all the staff of the *Physical Department of Technical University* of Liberec for their timely help. A special gratitude to *Mgr.Panoš Stanislav, Ph.D.* for help with programming of software for measurements.

I would like to thank to *Dr. Andreas Rudiger*, Institute of Solid State Research, Juelich, for the scientific discussion and useful suggestions during the period of my research work.

I am very indebted to my *parents* and *friends* for moral support. I thank each and every one of my family members for their support and constant encouragement.

My profound gratitude is to my *father* for fruitful discussion and useful suggestions in various stages of my work.

Finally, I thank to my supervisor *RNDr. Petr Hána, CSc*. for guiding me constantly, for help during the measurements, making the facilities available for the investigations and for useful suggestions and scientific discussion during the period of my research work.

Summary

Since 1880, when Jacques and Pierre Curie discovered an unusual characteristic of certain crystalline minerals, which is now called piezoelectricity; piezoelectric materials have been adapted to an impressive range of applications, where the interconversion of mechanical and electrical energy is required. The effect is of the order of nanometers, but nevertheless finds useful applications such as production and detection of a sound, generation of high voltages, electronic frequency generation, and ultra fine focusing of optical assemblies. The most common piezoelectric materials technically used are the single crystal materials and piezoelectric ceramics.

This work is devoted to study of ferroelectric semiconductor crystals of $Sn_2P_2(Se_xS_{1-x})_6$ crystal family due to their good physical properties and strong piezoelectric effect. Since the interest of $Sn_2P_2(Se_xS_{1-x})_6$ crystals is rare, a special study is devoted to the frequency investigations and temperature measurements of the dielectric properties and their behavior in the vicinity of the phase transition temperature. For further investigations crystals with concentration of selenium x = 5%, x = 10% and x = 15% were used to study dielectric properties and to improve their importance as crystals with strong piezoelectric effect with possible useful applications.

Anotace

Už od roku 1880, kdy Jacques a Pierre Curie objevili neobyčejnou vlastnost určitých krystalických látek, kterou nyní známe pod názvem piezoelektricita, jsou piezoelektrika využívána v mnoha aplikacích, kde je požadována vzájemná přeměna mechanické energie v elektrickou. Tento mikroskopických efekt, nachází uplatnění ve velkém množství užitečných aplikací, jako jsou: detekce a reprodukce zvuku, generování vysokých napětí… Nejpoužívanějšími piezoelektrickými materiály jsou monokrystaly a piezoelektrická keramika.

Tato práce je věnována studiu ferroelektrických polovodičových krystalů $Sn_2P_2(Se_xS_{1-x})_6$ z důvodu jejich dobrých fyzikálních vlastností a výraznému piezoelektrickému jevu. Zvláštní pozornost je věnována frekvenčním a teplotním měřením dielektrických vlastností krystalů $Sn_2P_2(Se_xS_{1-x})_6$ a jejich chování v okolí teploty fázového přechodu. Pro studium byly zvoleny krystaly o koncentraci selenu x = 5%, x = 10% a x = 15% pro ověření výrazného piezoelektrického jevu a jeho možného využití v užitečných aplikacích.

Zusammenfassung

Seit 1880, als Jacques und Pierre Curie eine ungewöhnliche Eigenschaft bestimmter Mineralien entdeckten, die seither als Piezoelektrizität bekannt ist, sind Piezoelektrika in einer beeindruckenden Vielzahl von Anwendungen anzutreffen, vor allem dort, wo die Umwandlung elektrischer in mechanischer Energie erforderlich ist. Auch wenn der Effekt lediglich auf einer Längenskala weniger Nanometer stattfindet, so findet er doch Einzug in die Erzeugung und Detektion von Schall, von Hochspannung, als Frequenzgenerator und der ultragenauen Fokussierung von optischen Bauelementen. Am häufigsten finden piezoelektrische Materialien Einsatz als Einkristalle oder als Keramik.

Diese Arbeit widmet sich dem Studium des ferroelektrischen Halbleitermisch-kristallsystems $Sn_2P_2(Se_xS_{1-x})_6$ aufgrund seines sehr hohen piezoelektrischen Effektes in Verbindung mit anderen vorteilhaften physikalischen Eigenschaften. Da dieses System bislang wenig Aufmerksamkeit auf sich gezogen hat, ist ein besonderer Teil dieser Arbeit frequenz- und temperaturabhängigen Messungen der dielektrischen Eigenschaften in der Nähe des Phasenüberganges gewidmet. Für weitere Untersuchungen sind Kristalle mit einem Selengehalt von x = 5%, x = 10% and x = 15% verwendet worden. Die Ergebnisse belegen einen hohen piezoelektrischen Effekt und ein hohes Anwendungspotential.

CONTENT

List of Figures

List of Tables

Chapter 1

1. INTRODUCTION

This chapter consists of four paragraphs. History and fundamentals of piezoelectricity are presented in the first and the second paragraph. In the third paragraph a mathematical descriptions of the piezoelectric effect, the mechanism of the direct and converse piezoelectric effects are described. The fourth paragraph dealt with the characterization of the main piezoelectric coefficients.

1.1. A Brief History of Piezoelectricity

People always were interested in the study of different unknown materials and their new properties. Hundreds of years ago, natives from Ceylan and India already noticed an interesting property of tourmaline crystals. Tourmaline crystals when warmed become positively charged at one end and negatively charged at the other. All tourmaline hemimorphic crystals are piezoelectric and as well often pyroelectric. Tourmaline's unusual electrical properties made it famous in the early 18th century. Those days, tourmalines were brought to Europe in large quantities by the Dutch East India Company as oddities and gems. The tourmaline was called *Ceylon magnet.*

Then, in 1756, the german physicist Aepinus presented the electrical origin of such behavior of some materials. That behavior was named pyroelectricity by the scottish physicist D. Brewster in 1824. French mineralogist René Just Hauy firstly observed the presence of electric charges on the surface of the stressed tourmaline crystals in 1817. And later, it was firstly demonstrated and discovered by brothers Jacques and Pierre Curie in 1880. Their experiment consisted of a conclusive measurement of surface charges appearing on specially prepared crystals (tourmaline, quartz, topaz, cane sugar and Rochelle salt among them) which were subjected to mechanical stress. These experiments led them to elaborate the early theory of piezoelectricity. This theory was completed by works of G. Lippman, who presented mathematical deduction of the inverse piezoelectric effect, confirmed experimentally by brothers Curie in 1881. And the further works of W.G.Hankel, who introduced term of piezoelectricity and works of Lord Kelvin and W. Voigt (the beginning of the XX^{th} century). Published Voigt's "Lehrbuch der Kristallphysik" became the standard reference work embodying the understanding

which had been reached.

Piezoelectric crystals were first used in 1917 by P. Langevin and his french co-workers in connection with their research efforts in underwater acoustics using ultrasonic transducers. In 1919, using Rochelle salt, Alexander Nicolson first demonstrated a variety of piezoelectric devices, including loudspeakers, phonograph pickups, and microphones. The first serious applications appeared in the period of First World War with the *sonar.* In sonar piezoelectric quartz are used to produce ultrasonic waves (P. Langevin). In the twenties, the use of quartz to control the resonance frequency of oscillators was proposed by an american physicist W.G. Cady.

Problems of manufacturing crystals with uniformity and the necessary shapes prevented the commercial production of any of these devices. Almost 10 years later, C.B. Sawyer and C.H. Tower developed processes to manufacturer uniform complex-shaped piezo-crystals. This paved the way for many piezoelectric or crystal transducers, as they were first called.

In just over 100 years, piezoelectricity moved from being a laboratory curiosity to a big business. Since the period of the First World War most of the piezoelectric applications which are familiar for us now were invented (transducers, sensors, lighters, microphones …).

During the Second World War in the U.S., Japan and the Soviet Union isolated research groups working on improved capacitor materials discovered that certain ceramic materials exhibited dielectric constants up to 100 times higher than common cut crystals. The discovery of easily manufactured piezoelectric ceramics with astonishing performance characteristics launched a revival of intense research and development into piezoelectric devices.

In contrast to the "secrecy policy" practiced among U.S. piezoceramic manufacturers at the outset of the industry, several Japanese companies and universities formed a "competitively cooperative" association, established as the Barium Titanate Application Research Committee, in 1951. Persistent efforts in materials research had created new piezoceramic families which were competitive with Vernitron's PZT, but free of patent restrictions. With these materials available, Japanese manufacturers quickly developed several types of piezoceramic signal filters, which addressed requirements arising in television, radio, and communications equipment markets; and piezoceramic igniters for natural gas/butane appliances.

The commercial success of the Japanese efforts attracted the attention of industry in many other nations and spurred a new effort to develop successful piezoceramic products. The development of electronics and the discovery of ferroelectric ceramics increased the practical use of piezoelectric materials. Especially, use of piezoelectric materials as actuators and sensors for noise and vibrations control has been demonstrated extensively over the last years of the end of XX^{th} century (Forward, 1981; Crawley and de Luis, 1987). During this period, several

technologies were developed to use the piezoelectric effect. In turn, each of these technologies has become an essential component of many types of electronic products.

The search for perfect piezo product opportunities is now in progress. Judging from the increase in worldwide activity, and from the successes encountered in the last quarter of the XX^{th} century, important economic and technical developments seem certain.

1.2. Fundamentals of Piezoelectricity

Since 1880, when Jacques and Pierre Curie discovered an unusual characteristic of some crystalline materials, the piezoelectric effect is often used in daily life, for example in lighters or loudspeakers... In a gas lighter, pressure on a piezoceramic generates an electric potential high enough to create a spark.

So, piezoelectric materials are used to convert electrical energy into mechanical energy and vice-versa. This behavior of certain materials was named the direct piezoelectric effect and the converse piezoelectric effect.

The piezoelectric effect appears only in crystals that lack inversion symmetry. Among the thirty-two crystal classes, twenty-one are non-centrosymmetric, and of these, twenty exhibit direct piezoelectricity (the 21st is the cubic class 432). Ten of these are polar (i.e. spontaneously polarized), having a dipole in their unit cell and exhibit pyroelectricity. If this dipole can be reversed by the application of an electric field, the material is said to be ferroelectric.

- *Piezoelectric Crystal Classes*: 1, 2, m, 222, mm2, 4, -4, 422, 4mm, -42m, 3, 32, 3m, 6, -6, 622, 6mm, -62m, 23, -43m
- *Pyroelectric*: 1, 2, m, mm2, 4, 4mm, 3, 3m, 6, 6mm, 3mm

1.3. Mathematical Description of Piezoelectricity

Let us consider our crystal as a thermodynamic system: its equilibrium state can be defined by the values of a number of variables. The internal energy of such a system can be expressed as a function of the mechanical stress and the electrical stress, or the mechanical and the electrical strains, in addition to temperature and entropy. Of these four variables we can chose two of them as independent, the other two as dependent. Generally, it is easier to vary the external stress and the applied electric fields, so it is logical to assume the strains and

polarization as dependent variables.

Thus, piezoelectricity is described mathematically by a constitutive equation which defines dependence among the piezoelectric material's stress (**T**), strain (**S**), charge density displacement (**D**) and electric field (**E**). This is described by two coupled equations in *Strain-Charge form*:

$$\mathbf{D} = \mathbf{d} \cdot \mathbf{T} + \varepsilon_{\mathbf{T}} \cdot \mathbf{E} \quad (1)$$

$$\mathbf{S} = \mathbf{s}_{\mathbf{E}} \cdot \mathbf{T} + \mathbf{d}^{\mathbf{t}} \cdot \mathbf{E} \quad (2)$$

where **(D)** is the dielectric displacement, **(T)** is the stress, **(ε)** is the dielectric permittivity, **(S)** is the strain, **(E)** is the applied electric field, **(s)** is the compliance and **(d)** is the piezoelectric coefficient. The superscript (t) stands for matrix-transpose; and the superscript (E) indicates a zero, or constant electric field; the superscript (T) indicates a zero, or constant stress field.

We must realize, that **(D)** and **(E)** are vectors (three components), that is a Cartesian tensor of 1-rank, the permittivity **(ε)** is Cartesian tensor of 2-rank. Strain and stress are tensors of 4-rank, but because they are symmetric tensors they appear to have the "vector form" of 6 components. Consequently, **(S)** appears to be a 6 by 6 matrix instead of 4-rank tensor.

Equation (1) describes the *direct* piezoelectric effect; equation (2) describes the *converse* piezoelectric effect.

The four state variables (**S**, **T**, **D**, and **E**) can be rearranged to give additional 3 forms for a piezoelectric constitutive equation. Instead of coupling matrix (**d**) they contain the coupling matrices **e**, **g**, or **q**. It is possible to transform the piezo constitutive data from one form into another. These transformations are important because vendors typically publish material data for **d** and **g**, whereas certain finite elements codes require piezo data entered as **e**. The four possible forms for piezoelectric constitutive equations are shown below. The names for each of the forms were taken from the two dependent variables on the left side of each equation. Note, that the voltage and electric field variables are related via gradient.

Table I. Four possible forms of piezoelectric constitutive equations

Strain – Charge Form:	*Stress – Charge Form:*
$\mathbf{S} = \mathbf{s}_E \cdot \mathbf{T} + \mathbf{d}^t \cdot \mathbf{E}$ $\mathbf{D} = \mathbf{d} \cdot \mathbf{T} + \varepsilon_T \cdot \mathbf{E}$	$\mathbf{T} = \mathbf{c}_E \cdot \mathbf{S} - \mathbf{e}^t \cdot \mathbf{E}$ $\mathbf{D} = \mathbf{e} \cdot \mathbf{S} + \varepsilon_s \cdot \mathbf{E}$
Strain – Voltage Form:	*Stress – Voltage Form:*
$\mathbf{S} = \mathbf{s}_D \cdot \mathbf{T} + \mathbf{g}^t \cdot \mathbf{D}$ $\mathbf{E} = -\mathbf{g} \cdot \mathbf{T} + \varepsilon_T^{-1} \cdot \mathbf{D}$	$\mathbf{T} = \mathbf{c}_D \cdot \mathbf{S} - \mathbf{q}^t \cdot \mathbf{D}$ $\mathbf{E} = -\mathbf{q} \cdot \mathbf{S} + \varepsilon_s^{-1} \cdot \mathbf{D}$

Matrix transformations for converting of piezoelectric constitutive data from one form into another are shown below. Only 4 out of the 6 possible combinations are shown.

Table II. Matrix transformations for converting of piezoelectric constitutive data from one form into another

Strain – Charge to Stress – Charge:	*Strain – Charge to Strain – Voltage:*
$\mathbf{c}_E = \mathbf{s}_E^{-1}$ $\mathbf{e} = \mathbf{d} \cdot \mathbf{s}_E^{-1}$ $\varepsilon_S = \varepsilon_T - \mathbf{d} \cdot \mathbf{s}_E^{-1} \cdot \mathbf{d}^t$	$\mathbf{s}_D = \mathbf{s}_E - \mathbf{d}^t \cdot \varepsilon_T^{-1} \cdot \mathbf{d}$ $\mathbf{g} = \varepsilon_T^{-1} \cdot \mathbf{d}$
Stress – Charge to Stress – Voltage:	*Strain – Voltage to Stress – Voltage:*
$\mathbf{c}_D = \mathbf{c}_E + \mathbf{e}^t \cdot \varepsilon_S^{-1} \cdot \mathbf{e}$ $\mathbf{q} = \varepsilon_S^{-1} \cdot \mathbf{e}$	$\mathbf{c}_D = \mathbf{s}_D^{-1}$ $\mathbf{q} = \mathbf{g} \cdot \mathbf{s}_D^{-1}$ $\varepsilon_S^{-1} = \varepsilon_T^{-1} + \mathbf{g} \cdot \mathbf{s}_D^{-1} \cdot \mathbf{g}^t$

1.3.1. Mechanism of the Direct Piezoelectric Effect

Certain materials exhibit the following phenomenon: when the material is mechanically strained, or when the material is deformed by the application of an external stress, electric charges appear on certain material surfaces; and when the direction of the strain reverses, the polarity of the electric charge is reversed. This is called the *direct piezoelectric effect*, and

materials that exhibit this phenomenon are called as *piezoelectric materials*.

A direct piezoelectric effect piezoelectric material generates an electrical charge during mechanical distortion. So, applied mechanical stress T_{jk} on the piezoelectric element induces an electrical polarization P_i. In this case, mechanical and electrical values are in linear dependence. The direct piezoelectric effect is described by the following four equations:

$$P_i = d_{ijk} T_{jk} \tag{3}$$

$$P_i = e_{ijk} S_{jk} \tag{4}$$

$$E_i = -g_{ijk} T_{jk} \tag{5}$$

$$E_i = -h_{ijk} S_{jk} \tag{6}$$

where P_i and E_i are electrical polarization and electric field correspondingly, T_{jk} is a tensor of mechanical stress and S_{jk} is a tensor of strain, coefficients d_{ijk}, $e_{ijk,}$ $g_{ijk,}$ h_{ijk} are tensors called piezoelectric coefficients.

Direct piezoelectric effect: convert mechanical energy into electrical (Pierre Curie in 1880)

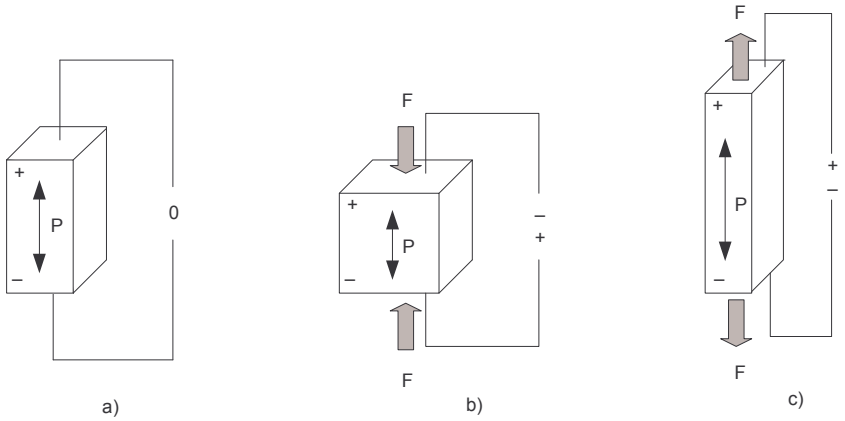

Figure 1. Piezoelectric effect under the influence of the external forces F
a) No forces applied **b) Compression** **c) Tension**

Depending on the force's direction electrical charges with corresponding polarity are generated.

1.3.2. Mechanism of the Converse Piezoelectric Effect

The opposite effect is called converse piezoelectric effect. When a piezoelectric material is placed in an electric field, or when charges are applied by external means to its faces, the material exhibits strain, i.e. the shape of the crystal changes. When the direction of the applied electric field is reversed, the direction of the resulting strain is reversed. This is called the *converse piezoelectric effect*. So, an applied electric field on the piezoelectric element induces strain.

The converse piezoelectric effect is described by the following equations:

$$S_j = d_{ij} E_i \tag{7}$$

$$S_j = g_{ij} P_i \tag{8}$$

$$T_j = -e_{ij} E_i \tag{9}$$

$$T_j = -h_{ij} P_i \tag{10}$$

where P_i and E_i are electrical polarization and electric field correspondingly, T_j is a tensor of mechanical stress and S_j is a tensor of strain, coefficients d_{ij}, $e_{ij,}$ $g_{ij,}$ h_{ij} are piezoelectric coefficients.

Converse effect: convert electrical energy into mechanical (Lippman from thermodynamic principles, Curie experimentally in 1881)

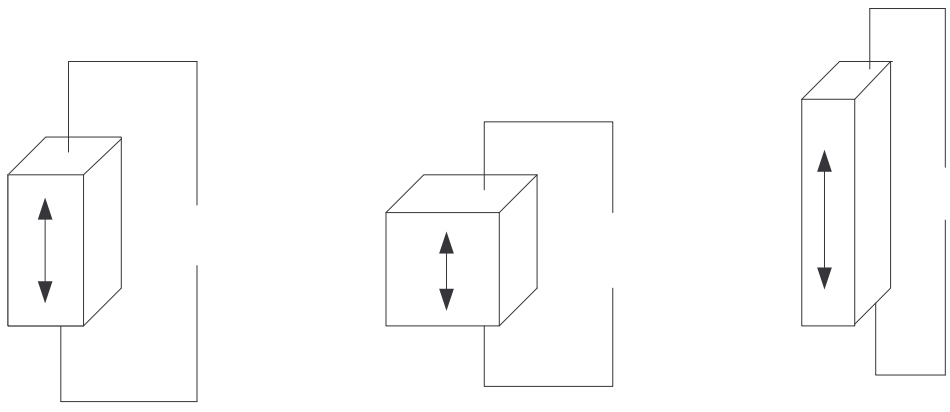

Figure 2. Converse piezoelectric effect

1.4. Main Coefficients and Directions

The piezoelectric properties of the investigated samples depend on the direction of polarization. To identify directions of the crystal, three axes: 1, 2, 3 corresponding to usual right-hand orthogonal set are used to describe monoclinic system. The axes 4, 5, 6 identify rotations (shear). The polar, or 3 axis, is taken parallel to the direction of polarization within the crystal. The direction of polarization (axis 3), parallel or antiparallel to axis z is established during the poling process by a strong electrical field applied between two electrodes.

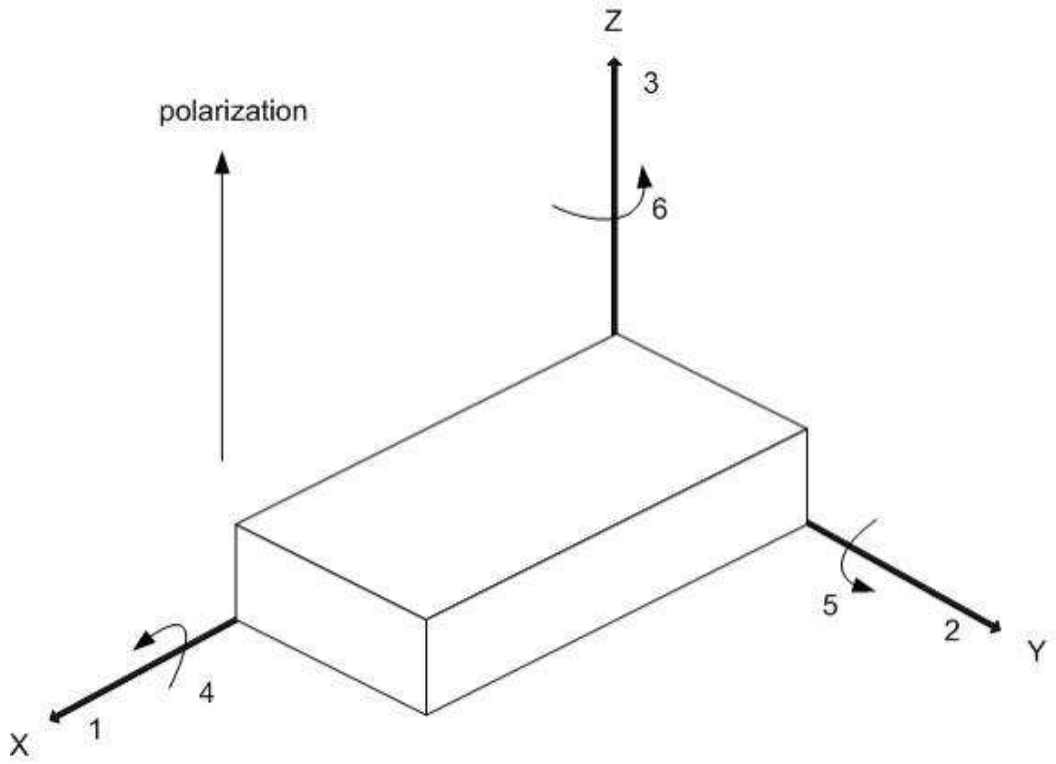

Figure 3. Orthogonal axis set of the sample. The third (z axis) is the poling direction

Piezoelectric materials are characterized by the piezoelectric tensor. The tensor components are often referred to as piezoelectric coefficients. These piezoelectric coefficients are often presented as constants, but their values are not invariable. These coefficients describe material properties under definite conditions only. They vary with temperature, pressure, electric field, and form factor, mechanical and electrical boundary conditions… Piezoelectric tensor is a third rank tensor that is symmetric in two of its components and can therefore be contracted by Voigt's notation. Voigt notation usually refers to the procedure for writing a symmetric tensor in column

matrix form. When the tensors are written in indicial notation, the difference between the Voigt and tensor form of second order tensors is indicated by the number of subscripts and the letter used. We use subscripts beginning with letters *i* to *q* for tensors, and subscripts *a* to *g* for Voigt matrix indices. For a second order, symmetric tensor such as the strain ε_{ij} the correspondence between the tensor indices and the row numbers are identical, but the shear strains, i.e. those with indices that are not equal, are multiplied by 2. Thus the Voigt rule for the strains is

$$\varepsilon = \begin{bmatrix} \varepsilon_{11} & \varepsilon_{12} \\ \varepsilon_{21} & \varepsilon_{22} \end{bmatrix} \rightarrow \begin{Bmatrix} \varepsilon_{11} \\ \varepsilon_{22} \\ 2\varepsilon_{12} \end{Bmatrix} = \begin{Bmatrix} \varepsilon_1 \\ \varepsilon_2 \\ \varepsilon_3 \end{Bmatrix} = \{\varepsilon\}$$

Piezoelectric coefficients usually have some subscripts. The subscripts describe the relationship of the property to the poling axis. Piezoelectric coefficients with double subscripts link electrical and mechanical quantities. The first subscript gives the direction of the electrical field associated with the voltage applied, or the charge produced. The second subscript gives the direction of the mechanical stress or strain. So, the first subscript position identifies the direction of the action; the second identifies the direction of the response. Several material constants may be written with a "superscript" which specifies either a mechanical or electrical boundary condition. The superscripts are T, E, D, and S, signifying:

T – corresponds to *constant stress* = mechanically free
E – corresponds to *constant field* = short circuit
D – corresponds to *constant electrical displacement* = open circuit
S – corresponds to *constant strain* = mechanically clamped

1.4.1. Piezoelectric Coefficient d_{ij}

These piezoelectric constants are relating mechanical strain produced by an applied electric field: strain developed [m/m] per unit of electric field strength applied [V/m], Eq.11 or charge density developed [C/m^2] per given stress [N/m^2], Eq.12. They indicate polarization generated per unit of mechanical stress (T) applied to a piezoelectric material or, alternatively, the mechanical strain (S) experienced by a piezoelectric material per unit of electric field applied:

$$S_j = d_{ij} E_i \tag{11}$$

$$\sigma_i = d_{ij} T_j \tag{12}$$

where σ_i is surface charge density of the crystal.

The piezoelectric coefficients d_{ij} are called *strain coefficients* [m/V] or *charge output coefficients* [C/N] or simply *piezoelectric charge coefficients*. The first subscript *(i)* of the coefficient d_{ij} corresponds to the direction of generated polarization when the electric field is zero or, alternatively, it is the direction of the applied field strength. The second subscript *(j)* gives the direction of the applied stress or the induced strain, respectively.

d_{33}

Indicates that piezoelectric induced strain, or applied stress, is in the direction 3

Indicates that electrodes are perpendicular to axis 3

d_h

Hydrostatic stress, indicates that stress is applied equally in 1, 2 and 3 directions, and that electrodes are perpendicular to axis 3

C*harge output coefficients* [C/N]: when the applied force is distributed over an area which is fully covered by electrodes, the coefficient may be expressed in terms of charge per unit force, coulombs per newton. To express the d_{ij} constants in such a view is useful when charge generators are contemplated, for example *accelerometers*.

Let's note that large values of d_{ij} constants are related to large mechanical displacements which are usually sought in motional transducer devices. Therefore, piezoelectric the charge coefficient d_{ij} is an important indicator of a material's suitability for strain-dependent (actuator) applications.

1.4.2. Piezoelectric Coefficient g_{ij}

These piezoelectric constants are relating electric field produced by a mechanical stress: open-circuit electric field developed [V/m] per applied mechanical stress [N/m^2], Eq.(13) or strain developed [m/m] per applied charge density [C/m^2]. Eq.(14). They indicate the electric field generated by a piezoelectric material per unit of mechanical stress applied or, alternatively, is the mechanical strain experienced by a piezoelectric material per unit of electric displacement applied:

$$E_i = g_{ij} T_j \tag{13}$$

$$S_j = g_{ij} \sigma_i \tag{14}$$

where σ_i is surface charge density of the crystal.

These coefficients are usually called v*oltage coefficients* or *field output coefficients* or simply the *"g" coefficients.* Although, the *g* coefficients are called voltage coefficients, it is correct to say that g_{ij} is the ratio of strain developed over the applied charge density. In general voltage coefficients have different values depending on the orientation used. Numerical subscripts are used to specify the directional properties. Direction 3 is considered to be the direction along which the sample has been polarized and directions 1 and 2 are the other perpendicular dimensions. The first subscript *(i)* of the coefficient g_{ij} gives the direction of the generated electric field in the material, or the direction of the applied electric displacement. The second subscript *(j)* corresponds to the direction of the applied stress or the induced strain, respectively.

g_{31} — *Indicates that the applied stress or piezoelectric induced strain is in direction 1*

Indicates that electrodes are perpendicular to axis 3

g_{15} — *Indicates that the applied stress or piezoelectric induced strain is in shear around axis 2*

Indicates that electrodes are perpendicular to axis 1

Please note that high values of g_{ij} coefficients are related to large voltage output. Therefore, piezoelectric voltage coefficient g_{ij} is an important value for assessing a material's suitability for sensing sought after for sensor applications.

1.4.3. Electromechanical Coupling Factor k_{ij}

These coefficients describe the ability of piezoelectric element to convert electrical energy into mechanical and vice versa. They are called *electromechanical coupling coefficients* k_{ij}. The squared value k^2 is the ratio of mechanical or electrical energy stored (E_1) to electrical or mechanical energy applied (E_2):

$$k^2 = \frac{E_1}{E_2} \tag{15}$$

Since this coefficient is the energy ratios, it is dimensionless.

The first subscript *(i)* of the coefficient k_{ij} denotes the direction along which the electrodes are applied; the second subscript *(j)* denotes the direction along which the mechanical energy is applied, or developed.

k_{15}
- *Indicates that stress or strain is in shear around axis 2*
- *Indicates that electrodes are perpendicular to axis 1*

k_p
- *Planar, is used only for thin discs. It indicates electrodes perpendicular to axis 3 and stress or strain equal in all directions perpendicular to*

k_{33}
- *Indicates that stress or strain is in shear around axis 3*
- *Indicates that electrodes are perpendicular to axis 3*

k_t
- *Indicates that stress or strain is in shear around axis 3 and electrodes are perpendicular to axis 3, (thin disc, surface dimensions large relative to thickness; $k_t < k_{33}$)*

Values of coefficient k_{ij} vary between 0,05 – 0,94. High values of coupling factor k are good for efficient energy conversion, but factor k does not account for dielectric losses or mechanical losses.

1.4.4. Elastic Compliance s_{ij}

This coefficient indicates the strain produced in the piezoelectric material per unit of applied stress.

$$S_i = s_{ij} T_j \tag{16}$$

For the 11 and 33 directions, it is the reciprocal of the modulus of elasticity (Young's modulus, Y). Also, double subscripts are used to describe the relationships between mechanical or electrical parameters. s^D is the compliance under a constant electric displacement; s^E is the compliance under a constant electric field.

S^D_{11}
- *Constant dielectric displacement (electrode circuit open)*
- *Indicates, that strain and stress are in direction 1*

S^E_{36}
- *Constant electric field (electrodes connected together)*
- *Indicated that mechanical stress is in shear around axis 3*
- *Indicates that strain is in direction of axis 3*

Young's Modulus

Young modulus Y indicates an elasticity of the material. It is determined as a ratio of the stress applied to the material and the value of the resulting strain in the same direction. The elasticity is different in the 3 direction from that is in the 1 or 2 directions.

Y^{E}_{33} stress and strain are in the 3 direction, electric field (E) is constant; Y^{D}_{33} stress and strain are in the 3 direction, dielectric displacement (D) is constant. The effective Young's Modulus with electrodes short circuited is lower than with the electrodes open circuited.
In SI units, *Young modulus is measured in* newtons per square meter (N/m^2).

1.4.5. Dielectric Coefficient ε_{ij}

Another important tensor is the *dielectric coefficient* ε_{ij} or *permittivity. Its* coefficients indicate the dielectric displacement per unit of electric field, in other words, the ability of the material to polarize in an external field.

$$D_i = \varepsilon_{ij} E_i \tag{17}$$

ε^T is a dielectric permittivity at constant stress ε^S is a dielectric permittivity at constant strain. In SI units, the permittivity is measured in farads per meter (F/m).

ε^{T}_{33}

Dielectric permittivity at constant stress

Electrical polarization and electric field are in direction 3

ε^{S}_{11}

Dielectric permittivity at constant strain

Dielectric displacement and electric field are in direction 1

Relative Dielectric Coefficient or Relative Permittivity

The r*elative dielectric constant K* or ε_r is the ratio of the permittivity of the material ε to the permittivity of the free space ε_0. Permittivity of the free space is $\varepsilon_0 = 8{,}85 \cdot 10^{-12}$ *F/m.* Since relative dielectric constant is permittivity ratios, it is dimensionless.

$$\varepsilon_r = \frac{\varepsilon}{\varepsilon_0} \tag{18}$$

The dielectric constant is an important value for capacitors design. If you place the material with a high dielectric constant in an electric field, the magnitude of that field will be measurably reduced within the volume of the dielectric. This fact is commonly used to increase the capacitance of a particular capacitor design.

The dielectric constant is an important value for capacitors design. If you place the material with a high dielectric constant in an electric field, the magnitude of that field will be measurably reduced within the volume of the dielectric. This fact is commonly used to increase the capacitance of a particular capacitor design.

Dielectric constant will exhibit some kind of anomaly at the transition temperature. Generally, any kind of phase transition in dielectrics is accompanied by an anomaly of the dielectric constant. A ferroelectric transition, being generally a transition from a polar into a non-polar phase, is no exception in this rule. In some ferroelectrics, the temperature dependence of the dielectric constant above the transition temperature can be described by the simple law, called the Curie-Weiss law:

$$\varepsilon = \varepsilon_0 + \frac{C}{T - T_0} \tag{19}$$

where the temperature-independent part ε_0 can often be neglected, C is the Curie constant and T_0 is the Curie-Weiss temperature. It is advisable, in general, to distinguish between this Curie-Weiss temperature T_0 and the Curie temperature (phase transition temperature) T_C. In certain ferroelectrics which undergo a second order phase transition the Curie-Weiss temperature T_0 practically coincides with the transition temperature T_C, but in others, which undergo a transition of the first order, it does not.

1.4.6. Dielectric Dissipation Factor tanδ

Another important coefficient is *the dielectric dissipation factor or the dielectric loss factor* tanδ. It is defined as tangent of the dielectric loss angle or the ratio of the power loss in a dielectric material to the total power transmitted through the dielectric. It is dimensionless and expressed in percents.

$$\tan\delta = \frac{\varepsilon''}{\varepsilon'} \tag{20}$$

When comparing similar dielectric material, lower values of the dielectric dissipation factor usually indicate better quality capacitors as tanδ quantifies AC losses that also lead to

heating of the sample with subsequent fatigue and possible failure.

1.5. Phenomenology of Phase Transitions in Ferroelectrics

In thermodynamics, phase transition or phase change is the transformation of a thermodynamic system from one phase to another. The first attempt at classifying phase transitions was the Ehrenfest classification scheme. Under this scheme, phase transitions were labelled by the lowest derivative of the free energy that is discontinuous at the transition.

Let us examine the dielectric behavior of the crystal when it undergoes a ferroelectric transition. To simplify the treatment, we are going to deal only with the free energy.

Based on the phase transition theory of Ginsburg-Landau we can develop a phenomenological theory of ferroelectricity by expanding the free energy in powers of the electric displacement D as an order parameter. The most convenient thermodynamic potential to use is the elastic Gibbs energy per unit volume

$$G_1 = U - TS - X_i x_i \tag{21}$$

with its corresponding differential

$$dG = -SdT - x_i dX_i + EdD \tag{22}$$

where x_i and X_i are the components of the strain and stress tensors respectively, and E is the Maxwell electric field.

Using the relation

$$D = \varepsilon_0 E + P \tag{23}$$

also E and P could be used as conjugate variables but it seems more natural to use E and D, since D is the variable that enters the thermodynamic work function. Suppose first that the stress is zero and that the non-polar phase is centrosymmetric, the free energy can be written in the polynomial form

$$G_1 = \frac{\alpha}{2} D^2 + \frac{\beta}{4} D^4 + \frac{\gamma}{6} D^6 \tag{24}$$

In general, α, β and γ are temperature dependent but in most cases β and γ can be assumed independent of temperature. The order of the transition depends on the sign of β, and for reasons of stability γ has to be positive in either case.

1.5.1. Second-Order Phase Transitions

In the case of a second-order phase transition, the parameter β (eq.24) is a positive constant.

Figure 4 shows the shape of G_1 versus D for different values of α. If α is positive, there is only one stable state with D = 0 (P = 0), corresponding to the non-polar paraelectric phase. When α is negative, the curve has two minima corresponding to a stable ferroelectric state with non-zero spontaneous displacement $D = \pm D_s$ ($P = \pm P_s$); i.e. the crystal will undergo a ferroelectric *second-order phase transition*. Second-order phase transitions have a discontinuity in a second derivative of the free energy.

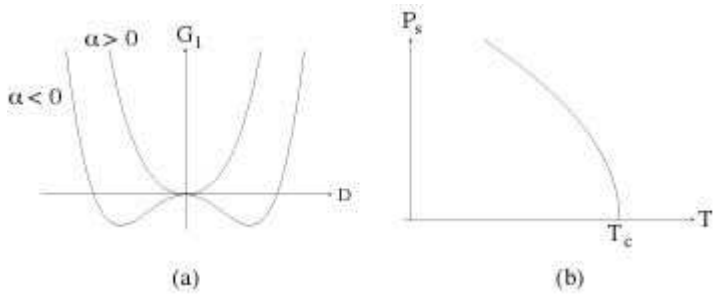

Figure 4. a) Temperature dependence of the free energy versus electric displacement D and (b) of the spontaneous polarization P_s near a second-order phase transition. The parameter α is proportional to $T-T_0$.

Coefficient α can be expressed as the first order term of a Taylor series in $(T-T_0)$:

$$\alpha = \alpha_0 (T - T_0) \tag{25}$$

where $\alpha_0 > 0$ and T_0 is called the Curie-Weiss temperature.

Among other things, the order of the ferroelectric transition is determined by the way in which the polarization goes from the value zero to a finite value, whether the onset of P_s is continuous or discontinuous. In the case of second order transition, the polarization P_s is continuous (Figure 4b).

The temperature dependence of P_s below T_C is given by the minima of equation 24:

$$E = \frac{dG_1}{dD} = \alpha P_s + \beta P_s^3 = 0 \tag{26}$$

$$P_s^2 = \frac{\alpha_0 (T_0 - T)}{\beta} \tag{27}$$

where the term with coefficient γ is small and has been neglected. Note that in this case $T_0 = T_C$

is the transition temperature which is not correct in the case of first-order phase transitions as will be shown in the next paragraph.

1.5.2. First-Order Phase Transitions

Consider coefficient β to be negative in equation 24. In this case the potential G_1 can develop two equal minima, one for D = 0 (P = 0) and the other for non-zero values $D = \pm D_c$ ($P = \pm P_c$) at the same temperature. The stable state of the crystal at transition temperature will jump from one with P = 0 to another with $P = P_0$ discontinuously; this kind of the transition is a *first-order phase transition* (Figure 5). First-order phase transitions exhibit a discontinuity in the first derivative of the free energy with a thermodynamic variable.

Using the basic Devonshire assumption (eq. 25) the free energy can be written as

$$G_1 = \frac{\alpha_0}{2}(T - T_0)D^2 + \frac{\beta}{4}D^4 + \frac{\gamma}{6}D^6 \tag{28}$$

and its first derivative (the dielectric equation of state)

$$E = \alpha_0(T - T_0)D + \beta D^3 + \gamma D^5 \tag{29}$$

A zero-field first-order transition takes place when G_1 and its first derivative are both zero

$$\frac{\alpha_0}{2}(T - T_0) + \frac{\beta}{4}P_s^2 + \frac{\gamma}{6}P_s^4 = 0 \tag{30}$$

$$\alpha_0(T - T_0) + \beta P_s^2 + \gamma P_s^4 = 0 \tag{31}$$

The transition temperature could be found by eliminating P_s:

$$T_C = T_0 + \frac{3}{16}\frac{\beta^2}{\alpha_0 \gamma} \tag{32}$$

Note that T_C is greater than the Curie-Weiss temperature T_0. At T_C the system undergoes a transition between absolutely stable states, but the non-polar phase remains metastable down to

T_0 and the polar metastable phase can exist up to a temperature

$$T_1 = T_0 + [(\beta^2)/4\alpha_0\gamma)] \tag{33}$$

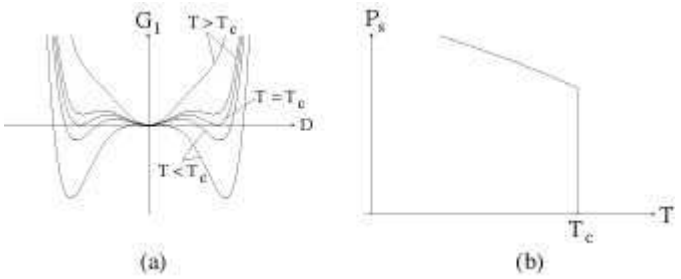

Figure 5. Temperature dependence of (a) the free energy versus electric displacement D and (b) of the spontaneous polarization P_s near a first-order phase transition. The parameter α is proportional to $T-T_0$.

At $T = T_C$ the polarization assumes the finite value

$$P_C^2 = -\frac{3\beta}{4\gamma} \tag{34}$$

Experimentally, it is often difficult to establish whether or not the polarization or other quantities is discontinuous at the transition temperature. For this reason, it has been suggested that a better definition of a first order transition is coexistence of two equilibrium at the transition temperature, so that a definite phase boundary if formed. This definition is also subject to experimental limitations [1].

1.5.3. Phase Transition in $Sn_2P_2S_6$ Crystal

Dielectric studies of the phase transition in $Sn_2P_2S_6$ single crystal are presented in [19], where the temperature dependences of a dielectric permittivity (ε') Figure 6a and dielectric loss (ε'') Figure 6b along the direction approximately perpendicular to a (110) at several frequencies are presented.

We decided to include some figures from this work [19] for $Sn_2P_2S_6$ (x=0) crystal in order to the following comparison with our measurements of $Sn_2P_2(Se_xS_{1-x})_6$ for x=0.05, x=0.10 and x=0.15.

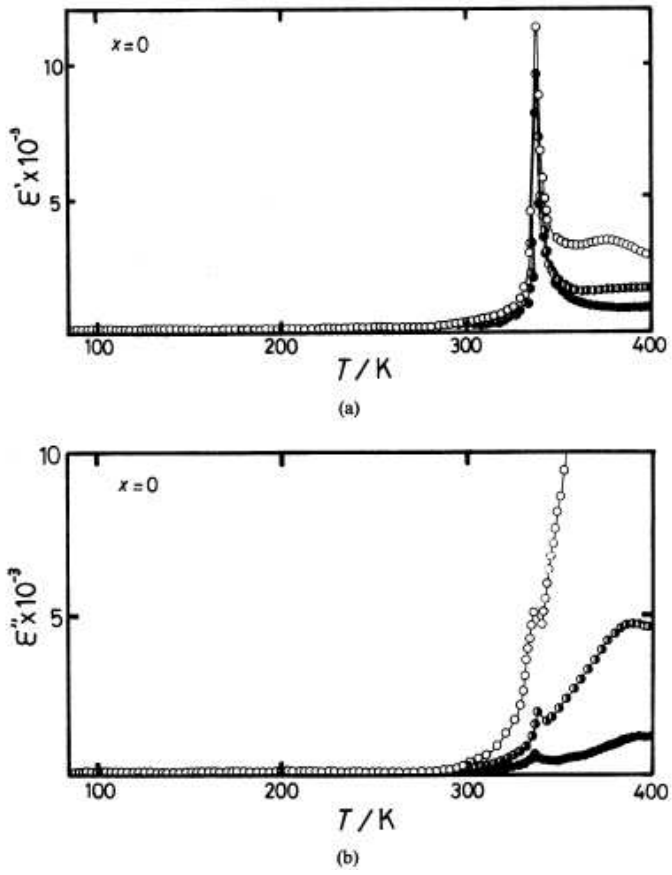

Figure 6. Temperature dependence of (a) dielectric permittivity ε' and (b) dielectric loss ε'' of $Sn_2P_2S_6$ (x=0) single crystal at 1 kHz, 10 kHz and 100 kHz[19]

As can be extracted from Figure 6, the ferroelectric-paraelectric phase transition in $Sn_2P_2S_6$ occurs at 339 K [19]. Reciprocal dielectric permittivity versus temperature at frequency 100 kHz is shown in Figure 7 [19].

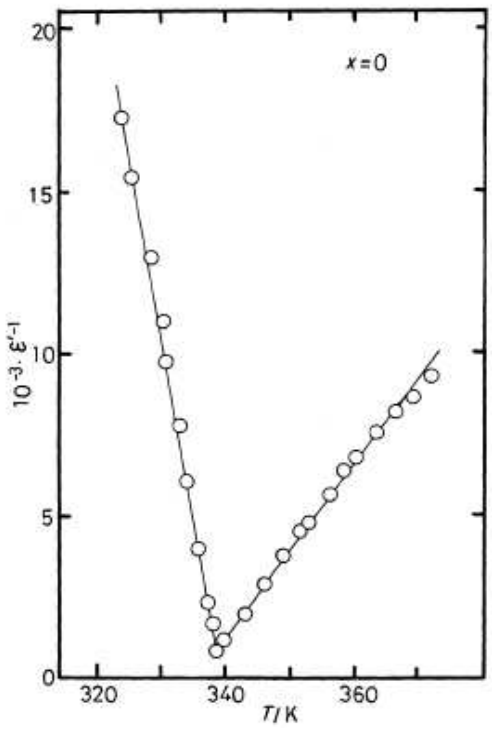

Figure 7. Temperature dependence of reciprocal dielectric constant $\varepsilon^{|-1}$ of $Sn_2P_2S_6$ (x=0) at 100 kHz [19]

The reciprocal dielectric permittivity ε'^{-1} (Figure 7) obeys the Curie-Weiss law (19) both above and below the ferroelectric-paraelectric phase transition temperature T_C. The Curie constants obtained for ferroelectric and paraelectric phases are 22000 and -87000 respectively. The Curie temperature is $T_C = 339$ K. From these results we categorize the crystal as a proper ferroelectric in which the order parameter is the spontaneous polarization [19].

In ref. [20] pressure investigations of dielectric and piezoelectric properties of $Sn_2P_2S_6$ crystals are presented. Dependences of the dielectric permittivity (ε) and the piezoelectric hydrostatic coefficient (d_h) versus pressure are studied. It is determined, that $Sn_2P_2S_6$ single crystal has following piezoelectric quantity criteria: tan δ = 0.007, ε = 310 for f = 10 kHz, $d_h = 252$ pC/N, $g_h = 0.092$ Vm/N at temperature T = 295 K [20].

Chapter 2

2. MATERIALS AND APPLICATIONS

This chapter consists of three paragraphs. In the first paragraph the possible applications of the piezoelectric materials are described. The second paragraph presents one of the classifications of the ferroelectric materials. The main and the most used piezoelectric materials and their properties are reported in the third paragraph.

2.1. Applications

Crystals studied in the early period included quartz, tourmaline and Rochelle salt only became technically important 50 years after the discovery of piezoelectricity. Piezoelectric quartz crystals found some use in electrostatic measurements in connection with studies of radioactivity by Pierre and Marie Curie. The first step towards an engineering application was taken about 1916 in France by Paul Langevin, who constructed an underwater ultrasonic source of a piezoelectric quartz element sandwiched between steel plates; this device was used for submarine detection. During World War I the frequency control by quartz crystals was invented. The closely related use of piezoelectric crystals in wave filters for multi-channel telephony was largely developed in Bell Telephone laboratories beginning about 1925. Yet, another result of the search for ultrasonic generation in 1917 – 1918 was the observation of the exceptionally high dielectric constant and dielectric hysteresis in Rochelle salt. This behavior was soon recognized to be a dielectric analogue to ferromagnetism. Since Rochelle salt is known in Europe as Seignette salt, after its discoverer P. Seignette, the phenomenon was termed Seignette electricity by Russian researchers. After 1945, the term ferroelectricity was generally accepted. The growth of these applications came about largely through the efforts of the Brush Development Company in Cleveland, beginning in 1930. Extensive studies were undertaken un the early 1940s to find a water soluble crystals which would approach Rochelle salt in piezo electric effect without its dielectric anomalies and limiting temperature range. These efforts were partly successful, as indicated by the introduction of ammonium dihydrogen phosphate, primary for sonar applications. Major progress came, however, from an unexpected direction. About 1940, a dielectric constant in excess of 1 000 was found in a refractory material, barium titanate ($BaTiO_3$). The ferroelectric nature of this compound was recognized by Arthur von Hippel and co-workers at Massachusetts Institute of Technology. This discovery opened the way for the

development of piezoelectric elements comparable with Rochelle salt in sensitivity and with quartz in chemical stability. Ceramics preparation methods made possible shapes and sizes which were unattainable with single crystals. Barium titanate is ferroelectric and piezoelectric only below 120°C. This limitation of the temperature was overcome in the 1950s by the discovery of a piezoelectric effects in ceramic lead metaniobate $PbNb_2O_6$, and lead titanate zirconate, $Pb(Ti,Zr)O_3$, which were usable at least to 250°C. By the late 1950s barium titanate and the newer ceramics were dominant in the electro-acoustic field in United States, and novel applications as electric circuit elements were indicated. For frequency control and highly sensitive electric wave filters, quartz crystals remained unchallenged; the dependence on high quality natural quartz crystals, a near-monopoly of Brazil, was alleviated by the development of and industrial process for growing quartz crystals, and crystals of this type became commercially available in 1958.

In present time, the piezoelectric effect is often encountered in daily life. For example, in simple gas lighter, a piezoelement is used, where a small pressure on it generates an electric potential high enough to create a spark. Most electronic alarm clocks use piezoelectric ceramics because it is more compact and more efficient. In addition to such simple applications, piezo technology has recently established itself in the automotive branch. Piezo – driven injection valves in diesel engines require much lower transition times than conventional electromagnetic valves, providing quieter operation and lower emissions.

Table III. Partial List of Ferroelectric Crystals in Chronological Order of Their Discovery [1]

Name and chemical formula	Curie temperature, T_C, (°C)	Spontaneous Polarization P_S, (10^{-6}C/cm^2)	Year in which reported
Rochelle (Seignette) salt $NaKC_4H_4O_6 \cdot 4H_2O$	+23	0,25	1921
Lithium ammonium tartrate $Li(NH_4)C_4H_4O_6 \cdot H_2O$	-170	0,20	1951
Potassium di-hydrogen phosphate KH_2PO_4	-150	4,0	1935
Potassium di-deuterium phosphate KD_2PO_4	-60	5,5	1942
Potassium di-hydrogen arsenate KH_2AsO_4	-177	5,0	1938
Barium titanate $BaTiO_3$	+120	26,0	1945
Lead titanate $PbTiO_3$	+490	>50	1950
Potassium niobate $KNbO_3$	+415	30	1951
Potassium tantalate $KTaO_3$	-260	?	1951
Cadmium (pyro) niobate $Cd_2Nb_2O_7$	-85	~10	1952
Lead (meta) niobate $PbNb_2O_6$	+570	?	1953
Guanidinium aluminium sulfate hexahydrate $C(NH_2)_3Al(SO_4)_2 \cdot 6H_2O$	-	0.35	1955
Methylammonium aluminium alum $CH_3NH_3Al(SO_4)_2 \cdot 12H_2O$	-96	1.0	1956
Ammonium sulfate $(NH_4)_2SO_4$	-50	0.25	1956
Tri-glicine sulfate $(NH_2CH_2COOH)_2 \cdot H_2SO_4$	+49	2.8	1956
Colemanite $CaB_3O_4(OH)_3 \ H_2O$	-7	0.65	1956
Dicalcium strontium propionate $Ca_2Sr(CH_3CH_2COO)_6$	+8	0.3	1957
Lithium acid selenite $LiH_3(SeO_3)_2$	-	10,0	1959
Sodium nitrite $NaNO_2$	+160	7,0	1958

The applications of piezoelectricity transcend the borders of various fields and directly improve our daily life. Piezoelectricity is used much more widely than radioactivity, although it is not as well known. Main fields of applications are described below.

2.1.1. Piezo Sensors (generators)

For over the past 50 years piezoelectric sensors have proven to be a versatile tool for the measurement of various processes. Today they are used for the determination of pressure, acceleration, strain or force in quality assurance, process control and development across many different industries.

Depending on the way a piezoelectric material is cut, three main types of operations can be distinguished: transversal, longitudinal, shear (Figure 8).

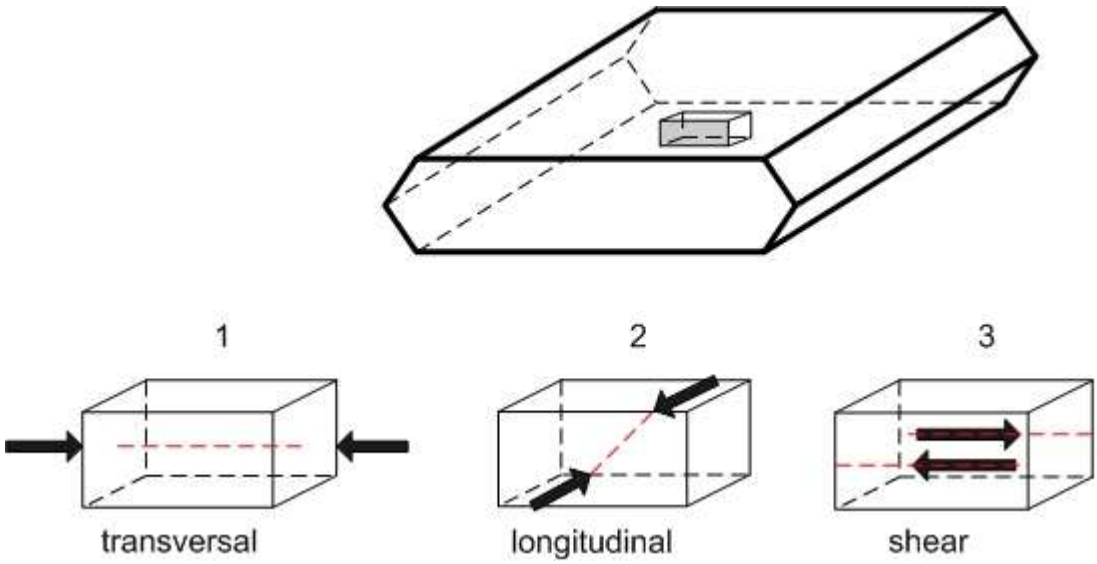

Figure 8. Three main types of operations on the sensing element

A sensor converts a physical parameter, such as acceleration or pressure, into an electrical signal. In other words, when a mechanical stress is applied to a single sheet of piezoelement in the longitudinal direction (parallel to polarization) (Figure 9 a), a voltage is generated which tries to return the piece to its original thickness. Similarly, when a stress is applied to a sheet in a transverse direction (perpendicular to polarization) (Figure 9 b), a voltage is generated which tries to return the piece to its original length and width. In some sensors the physical parameter acts directly on the piezoelectric element; in other devices an acoustical signal establishes vibrations in the element and the vibrations are, in turn, converted into an electrical signal. Often, the system provides a visual, audible, or physical response to the input from the sensor - automobile seatbelts lock in response to a rapid deceleration, for example.

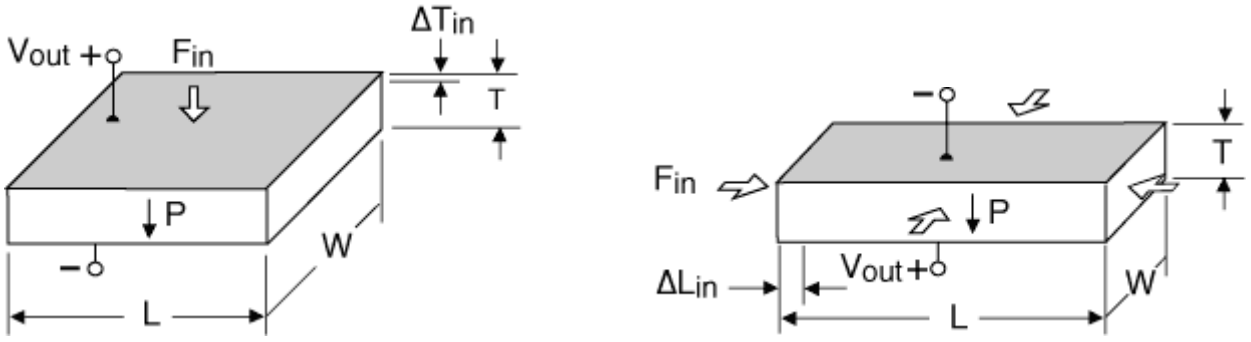

a) **b)**

Figure 9. a) Single layer longitudinal (d_{33}) generator compressed from the top and bottom; b) Single layer transversal (d_{31}) generator compressed from the sides

Depending on the number of piezo layers that may be stacked on top of one another there are several types of piezo generators: single layer (sheets and plates), two-layer (benders and extenders) and multi-layer generators (stacks).

2.1.2. Piezo Actuators (motors)

A piezoelectric actuator converts an electrical signal into a physical displacement. When an electric field having the same polarity and orientation as the original polarization field is placed across the thickness of a single sheet of piezoelement, the piece expands in the thickness or "longitudinal" direction (i.e. along the axis of polarization). At the same time, the sheet contracts in the "transverse" direction (i.e. perpendicular to the axis of polarization). When the field is reversed, the motions are reversed.

Piezoelectric actuators are also used to control hydraulic valves, act as small-volume pumps or special-purpose motors, and in other applications. Piezoelectric motors are unaffected by energy efficiency losses that limit the miniaturization of electromagnetic motors, and have been constructed to sizes of less than 1 cm^3. A potentially important additional advantage to piezoelectric motors is the absence of electromagnetic noise.

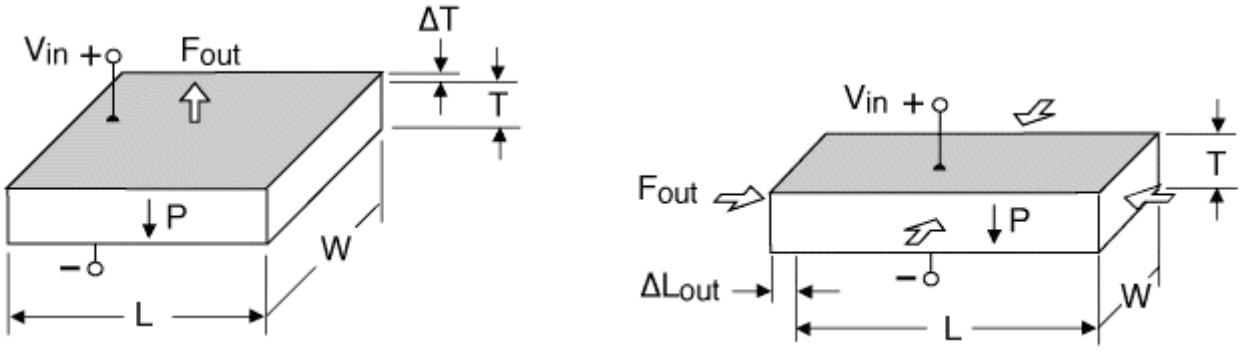

a) **b)**

Figure 10. a) Single layer longitudinal (d_{33}) motor getting thicker; b) Single layer transversal (d_{31}) motor with sides contracting

The rise of piezoelectric technology is directly related to a set of inherent advantages. The high modulus of elasticity of many piezoelectric materials is comparable to that of metals and goes up to 10^5 N/mm^2. Even thought piezo sensors are electromechanical systems that react on compression, the sensing elements show almost zero deflection. This is the reason why piezoelectric sensors are so rugged, have an extremely high natural frequency and an excellent linearity over a wide amplitude range. Additionally, piezoelectric technology is insensitive to electromagnetic fields and radiation, enabling measurements under harsh conditions. Some materials used, especially gallium phosphate or tourmaline, have an extreme stability over temperature enabling sensors to have a working temperature range of 1000 °C.

2.1.3. Piezo Transducers

Devices, translating electric energy into mechanical energy and vice versa are known as electromechanical transducers. Piezoelectric transducers that generate audible sounds provide significant advantages, relative to alternative electromagnetic devices – they are compact, simple, and highly reliable, and comparably low energy consumption can produce a high level of sound. These characteristics are ideally matched to the needs of battery-powered equipment.

Since the piezoelectric effect is reversible, a transducer can both generate an ultrasound signal from electrical energy and convert incoming sound into an electrical signal. Some devices designed for measuring distances, flow rates, or fluid levels incorporate a single piezoelectric transducer in the signal sending and receiving roles, other designs incorporate two transducers

and separate these roles.

Piezoelectric transducers are also used to generate ultrasonic vibrations for cleaning, atomizing liquids, drilling or milling ceramics or other difficult materials, welding plastics, medical diagnostics, or for other purposes. Ultrasonic cleaning devices, operating at frequencies from 10 kHz to 100 kHz have been particularly successful.

Table IV. Applications by Piezo Effect

<table>
<tr><th>Direct piezo effect</th><th>Converse piezo effect</th><th>Both effects</th></tr>
<tr><td>Mechano – electrical</td><td>Electro – mechanical</td><td rowspan="4"></td></tr>
<tr><td>• Accelerometers
• Lighters
• Piezo keyboards
• Generators
etc.</td><td>• Actuators
• Micro- and nanopositioning
• Laser tuning
• Micro pumps
• Active vibration damping
etc.</td></tr>
<tr><td>Acousto – electrical</td><td>Electro – acoustical</td></tr>
<tr><td>• Acoustic and ultrasonic receivers
• Noise analysis
• Acoustic emission spectroscopy
etc.</td><td>• Signal generator (buzzer)
• High voltage sources (transformers)
• Delay lines
• High powered ultrasonic generators
etc.</td><td>• Level measurement
• Flow-rate measurement
• Object recognizing
• Medical diagnostics
• Materials testing
• Sonar and echo sounders
• Adaptive structures
etc.</td></tr>
</table>

2.2. Classification of Ferroelectric Materials

Ferroelectric crystals belong to that part of the pyroelectric family for which the direction of the spontaneous polarization can be reversed by application of an electric field. Dielectric measurements can also be conducted below the coercive field where we do not see a difference in polarization. The coercive field, of a ferromagnetic material is the intensity of the applied magnetic field required to reduce the magnetization of that material to zero after the magnetization of the sample has been driven to saturation. The coercive field is usually measured in ampere per meter units

With an increasing number of ferroelectric materials and with respect to their properties, various classifications were proposed. As indicated in *Table III*, from the chemical point of view, representative ferroelectrics are found among the tartrates, phosphates, arsenates, double oxides, sulphates, borates, propionates, nitrates, nitrites, etc. The symmetries of the non-polar phases vary from cubic to tetragonal, orthorhombic and monoclinic, and the Curie temperature ranges from approximately 10 K, for potassium tantalate, and to about 840 K for lead metaniobate. The values of the spontaneous polarization vary from the order of 10^{-7} C/cm^2 to about 10^{-4}C/cm^2.

The following is the summary of the criteria according to which the various classifications of the ferroelectric materials have been proposed [1]:

(I) Crystal – chemical classification. In accordance to this classification, ferroelectric materials may be divided into two groups. The first group includes hydrogen – bonded crystals, such as KH_2PO_4, Rochelle salt, tri-glycine sulphate, etc. The second group includes the double oxides, such as $BaTiO_3$, $KNbO_3$, $Cd_2Nb_2O_7$, $PbNb_2O_6$, $PbTa_2O_6$, etc.

(II) Classification according to the number of possible directions of the spontaneous polarization. Ferroelectric materials are divided into two groups. The first group, were ferroelectrics, which can polarize only along one axis belong, such as Rochelle salt, KH_2PO_4, colemanite, $PbTa_2O_6$, etc. And a second group, including crystals which can polarize along several axes that are crystallography equivalent in the non-polar phase, such as $BaTiO_3$, $Cd_2Nb_2O_7$, the ferroelectric alums, etc. This classification may be particularly useful for study of the ferroelectric domains.

(III) Classification according to the existence of a centre of symmetry in the point

group of the non-polar phase. Here, the first group characterized by a non-polar phase which is piezoelectric (non-centrosymmetrical), such as Rochelle salt, KH_2PO_4, and isomorphous compounds. And the second group is characterized by a centrosymmetrical non-polar phase, such as $BaTiO_3$, $Cd_2Nb_2O_7$, tri-glycine sulphate, etc. This classification may be particularly useful for the thermodynamic treatment of the ferroelectric transitions.

(IV) Classification according to the nature of the phase change occurring at Curie point. A first group of ferroelectrics undergo a transition of the order-disorder type, as KH_2PO_4, tri-glycine sulphate and probably some of the alums. A second group of compounds undergo a transition of a displacive type, such as that of $BaTiO_3$ and most of the double oxide ferroelectrics.

It is evident that the four classifications, described above, do not coincide with each other. Each one is useful only when discussing a particular aspect of the ferroelectric phenomenon, but consistent classification of all ferroelectrics appears hardly possible at the present stage.

2.3. Main Piezo Materials and Their Properties

Single crystals and piezoceramic materials are still subject of current research of the piezoelectric elements. In most applications for piezoelectric materials there is continuous demand for further improvement of their performance: larger coefficients, higher temperature tolerance, longer lifetime, etc. An expanding variety of single crystals is being developed for acoustical, optical, wireless communication, and other applications.

The most common piezoelectric materials technically used are quartz, tourmaline, gallium phosphate, lithium tantalate , lead magnesium niobate / lead titanate (PMN-PT), lead zirconate niobate / lead titanate (PZN-PT), lithium niobate ($LiNbO_3$), lithium tetraborate ($Li_2B_4O_7$), barium titanate $BaTiO_3$…

Depending on the specific application, the set of material properties of interest differs to a large extent. Therefore, a general comparison can only be a high level listing of properties.

2.3.1. Quartz, Gallium Phosphate, Aluminium Phosphate

Even though quartz is the most common mineral found on earth, a few million tons are still synthetically produced annually.

Quartz (SiO_2) has a comparably high mechanical strength of 2 - 3 GPa, is almost insoluble in water and is highly resistant against most acids and alkali. Its melting point is 1710°C. It combines a great number of such important properties as a very small temperature coefficient, high mechanical and chemical stability and very small mechanical losses. Applications for quartz crystals include timing mechanisms for watches and clocks and delay lines for electrical circuits. α-Quartz is widely used for resonators filters and frequency control. Aluminium and Gallium Phosphates *($AlPO_4$, $GaPO_4$)* are promising candidates for replacing α-Quartz.

Gallium phosphate ($GaPO_4$) shares many positive features of quartz. For example this crystal has high mechanical strength, but outperforms it with respect to many interesting properties, in particular with a higher electro-mechanical coupling and its greater piezoelectric sensitivity at temperatures up to 970°C. $GaPO_4$ has many advantages over quartz for technical applications, like a higher electromechanical coupling coefficient in resonators. Contrary to quartz, $GaPO_4$ is not found in nature. Also therefore, a hydrothermal process must be used to synthesize the crystal.

Table V. α - Quartz (SiO_2), Gallium Phosphate ($GaPO_4$) and Aluminium Phosphate ($AlPO_4$) Properties

	Symbol	Dimension	Quartz[1,3,4,5]	$GaPO_4$[2]	$AlPO_4$[3,5]
Electrical Properties *Relative Dielectric Const. at 1kHz*	ε_{11}^{T}	1	4,52	6,1	6,05
	ε_{33}^{T}	1	4,68	6,6	
	ε_{11}^{S}	1	4,5	5,8	
	ε_{33}^{S}	1	4,6	6,6	
Electromechanical Properties	k_{11}	%	9,8		5.1
Coupling factors	k_{26}	%	13,7		23
Coupling factor for BAW	k_{emc}	%	7,0		
Q factor for BAW	Q	10^3	100		
Coupling coeff. for SAW	K^2	%	0,16/0,11		
Piezoelectric charge coefficient	d_{11}	10^{-12} C/N	- 2,3	4,5	3,3
	d_{14}	10^{-12} C/N	- 0,67	1,9	1,5
Piezoelectric strain coefficient	e_{11}	C/m^2	0,171		
	e_{14}	C/m^2	- 0,0436		

[1] BA. Auld "Acoustic Fields and Waves in Solids" Vol. 1 John Wiley and Sons, New York (1973)
[2] www. gapo4.com
[3] CS. Brown, RC. Kell, R. Taylor, and LA. Thomas, The Institution of Electrical Engineers 3798, 99-113 Jan. (1962)
[4] www.cardley-crystals.com
[5] Landolt-Borstein, Vol. 11, New Series Group 3 Springer-Verlaf Heidelberg New-York (1979)

2.3.2. Lithium Niobate, Lithium Tantalate and Lithium Tetraborate

Lithium niobate ($LiNbO_3$) is commercially available and widely used for its good electro-optical, photo-elastic and non linear properties. $LiNbO_3$ is a candidate for very high temperature applications.

Applications for these single-crystal materials include actuators and diagnostic and therapeutic medical devices. A useful combination of piezoelectric and electro-optic properties makes lithium niobate crystals very useful for surface acoustic wave (SAW) devices and electro-optical applications. A SAW chip made from a lithium tetraborate crystal can be significantly smaller than its lithium niobate or quartz counterpart. Other applications for lithium tetraborate

crystals include bulk acoustic wave (BAW) devices, pagers, cordless and cellular telephones, and data communication devices.

Table VI. Lithium Niobate (LN), Lithium Tantalate and Lithium Tetraborate Properties $LiNbO_3$ (LN), $LiTaO_3$ (LT), $Li_2B_4O_7$ (LBO)

	Symbol	Dimension	LN[1,6]	LT[1,4,5,6]	LBO[2,4] Czochralski	LBO[3,4] Bridgman	LBO[5] Commercial
Electrical Properties *Relative Dielectric Const. at 1kHz*	ε_{11}^T	1	85,2	53,6	9,33	9,33	8,5
	ε_{33}^T	1	28,7	43,4	9,93	10,1	8,2
	ε_{11}^S	1	44,3	42,6	8,9	8,91	
	ε_{33}^S	1	27,9	42,8	8,07	8,07	
Curie temperature	T_c	°C	1133	604	Melt.917	Melt.917	Melt.917
Electromechanical Properties *Coupling factors*	k_{22}	%	32				
	k_{31}	%	2,3	-5		0,21	
	k_{33}	%	47	18		0,42	
	k_{15}	%	68	44		0,27	
	k_{24}	%	60	38			
Coupling factor for BAW	k_{emc}	%		47	24	24	
Q factor for BAW	Q	10^3		2	10	10	
Coupling coeff. for SAW	K^2	%	5,55/11,3/17,2	5/7,6/0,75	1/1,2	1/1,2	0,7-1,6
Piezoelectric charge coefficients	d_{22}	10^{-12} C/N	20,8	7,5/24			
	d_{31}	10^{-12} C/N	- 0,85	- 3	- 2,58	- 2,63	
	d_{33}	10^{-12} C/N	6	5,7/8	19,4	19,5	19,4
	d_{15}	10^{-12} C/N	69,2	26,4	8,07	8,19	8,07
Piezoelectric strain coefficient	e_{15}	C/m^2	3,7	2,63			
	e_{22}	C/m^2	2,5	1,84			
	e_{31}	C/m^2	0,23	- 0,11			
	e_{33}	C/m^2	1,33	1,93			

[1] www.roditi.com SingleCrystal
[2] T. Shiosaki, M. Adachi, A. Kawabata, Proc. 1986 Int. Symp. Appl. of Ferro., 455-464 (1986)
[3] S. Fan, Proc. 1993 IEEE Int. Freq. Contr. Symp. 353-358, (1993)
[4] www.cardley-crystals.com
[5] www.sinocera.net [6] Landolt-Borstein, Vol. 11, New Series Group 3 Springer-Verlaf Heidelberg New-York (1979)

2.3.3. Tourmaline, Lithium Sulfate, TGS

Tourmaline is a mineral stone known for a very long time. From a chemical point of view, tourmaline is a complex aluminium-borosilicate (Na, Ca) $(Mg, Fe)_3 B_3 Al_6Si_6 (O,OH,F)_{31}$, sometimes containing Li, Mn, Ti, Fe or Cr. These elements contribute, in a large extent, to the changing colors of tourmalines, by allowing for ion charge transfers. Tourmaline has a high mechanical stability and has similar resistance, as quartz does, to many acids and alkaline solutions. Very pure tourmalines can be used beyond 900°C, the actual technical limit is 750 - 780 °C. Additionally tourmaline shows significant pyroelectricity.

The disadvantage of Lithium Sulfate and Tourmaline is their solubility in water.

Table VII. Lithium Sulfate (LS) Li_2SO_4-H_2O, TGS $(C_2H_5NO_2)_3$-H_2SO_4 and Tourmaline (TO) $(Na,Ca)(Mg,Fe)_3B_3.Al_6Si_6(O,OH,F)_{31}$ Properties

	Symbol	Dimension	LS[1]	TGS[1]	TO[1]
Electrical Properties *Relative Dielectric Const. at 1kHz*	ε_{11}^T	1	5,6	8,6	8,2
	ε_{22}^T	1	10,3	43	
	ε_{33}^T	1	6,5	5,7	7,5
	ε_{13}^T	1	0,07	0,53	
Electromechanical Properties *Coupling factors*	k_t	%	30		
Piezoelectric charge coefficients	d_{21}	10^{-12} C/N	0	23,5	
	d_{22}	10^{-12} C/N	16,2	7,9	- 0,23
	d_{23}	10^{-12} C/N	- 1,3	25,3	
	d_{14}	10^{-12} C/N	- 1	2,7	
	d_{16}	10^{-12} C/N	- 2,5	- 4,5	
	d_{25}	10^{-12} C/N	6,6	24,3	0,24
	d_{34}	10^{-12} C/N	- 4	- 3,2	
	d_{36}	10^{-12} C/N	3,8	2,8	1,92
	d_{15}	10^{-12} C/N			3,68

[1] Landolt-Borstein, Vol. 11, New Series Group 3 Springer-Verlaf Heidelberg New-York (1979)

2.3.4. Barium Titanate and Barium Zirconate

Barium Titanate ($BaTiO_3$) and related compounds including lead titanate $PbTiO_3$, calcium titanate $CaTiO_3$ belong to a simple structure type, the perovskite type, which is a cubic and has a centre of symmetry in the high temperature phase. This cubic symmetry for barium titanate (BT) is found above 120°C; below this temperature BT is tetragonal with a polar symmetry, class 4mm. The transition from cubic to tetragonal near 120°C is a Curie point with a peak dielectric constant as high as 10 000. Below this temperature a BT crystals is found to consist of domains having electrical polarity in different directions but always parallel to a cube axis. Each of these domains is a true tetragonal piezoelectric crystal having definite piezoelectric coefficients. Due to forces acting between the crystals, the electric polarization of the ceramic is more stable than that of the single crystals. BT and ceramics thus became the major practical piezoelectric materials.

$BaTiO_3$ single crystals have a relatively high shear piezoelectric coefficient d_{15}=587 pC/N. By using engineered domain configurations some properties can be strongly enhanced: d_{31}=180 pC/N and k_{31}= 41,4% for a poling direction <111> and a 3 domain configuration. The main drawback of BT is its low Curie temperature. From the literature we can find the following values of d_{33} coefficient for $BaTi_{0.92}Zr_{0.08}O_3$ for poling directions <110> d_{33}=440 pC/N and <001> d_{33}=850 pC/N.

As a piezoelectric material, barium titanate was largely replaced by lead zirconate titanate, also known as PZT. Polycrystalline barium titanate exhibits normal semiconducting behavior as a function of temperature, that is, there is a negative coefficient of resistivity. This is manifest in the sample resistance decreasing slowly with increasing temperature. However, when it is processed as a polycrystalline sample, a dramatic change in the sample conductivity is observed, characterized by a positive temperature coefficient of resistivity, making it a useful material for thermistors and self-regulating electric heating systems. The nature of this PTCR (positive temperature coefficient of resistivity) effect occurs in the same temperature range where the sample undergoes a structural phase transition from a tetrahedral to a cubic unit cell and from a ferroelectric phase to a paraelectric phase. However, the phase transition also occurs in the single crystal sample where no PTCR effect is observed.

Table VIII. Barium Titanate (BT) $BaTiO_3$ Properties

	Symbol	Dimension	BT[1]	BT[2] Tetragonal Single domain
Electrical Properties *Relative Dielectric Const. at 1kHz*	ε_{11}^T	1	2920	4400
	ε_{33}^T	1	168	129
	ε_{11}^S	1	1970	2200
	ε_{33}^S	1	109	56
Curie temperature	$T_c >$	°C	135	120
Electromechanical Properties *Coupling factors*	k_{31}	%	31,5	36,3
	k_{33}	%	56	56
	k_{15}	%	57	
Piezoelectric charge coefficients	d_{31}	10^{-12} C/N	- 34,7	
	d_{33}	10^{-12} C/N	85,7	90
	d_{15}	10^{-12} C/N	587	

[1] Landolt-Borstein, Vol. 11, New Series Group 3 Springer-Verlaf Heidelberg New-York (1979)
[2] M. Zgonik, P. Bernasconi, M. Duelli, R. Schlesser, P. Gunter, MH. Garret, D. Ritz. Y. Zhu and X. Wu, Phys. Rev. B. 50, 5941, (1994)

2.3.5. Potassium Niobate

Potassium Niobate ($KNbO_3$) is a perovskite type negative biaxial crystal and can provide extremely high values of the electromechanical coupling coefficient. These single crystals have a high shear coupling factor $k_{15} = 88,3\%$ and a piezoelectric coefficient $d_{15} = 250$ pC/N. For poling in <001> direction and 50 μm domain size high electromechanical transverse coefficients: $d_{31} = 66,4$ pC/N and $k_{31} = 32,3$ % are reported. Among their advantages are high Curie temperature and mechanical quality factors. They are candidates for BAW and SAW applications.

Table IX. Potassium Niobate (KN) $KNbO_3$ Properties

	Symbol	Dimension	KT[1]	KT[2]
Electrical Properties *Relative dielectric constant at 1kHz*	ε_{11}^T	1	160	150
	ε_{22}^T	1	1000	985
	ε_{33}^T	1	55	44
	ε_{11}^S	1	37	
	ε_{22}^S	1	780	
	ε_{33}^S	1	24	
Curie temperature	$T_c >$	°C	435	
Electromechanical Properties *Coupling factors*	k_{15}	%	88,2	
	k_{24}	%	46	
Piezoelectric charge coefficients	d_{31}	10^{-12} C/N		9,8
	d_{32}	10^{-12} C/N		- 19,5
	d_{33}	10^{-12} C/N		29,3
	d_{15}	10^{-12} C/N	215	156
	d_{24}	10^{-12} C/N	159	206

[1]E. Wiesendanger, Ferroelectrics, 16, 263- 281, (1974) and [1]Landolt-Borstein, Vol. 11; New series Group 3 Springer-Verlag Heidelberg New York (1979)
[2]M. Zgonik, R. Schlesser, I. Biaggio, E. Voit, J. Tscherry and P. Gunter, J. Appl. Phys., 74, 1287-1297, (1993)

2.3.6. Bismuth Titanate

Bismuth titanate (sillenite) belongs to the group of sillenite structure-based ceramics ($Bi_{12}MO_2$ where M=Si, Ge, Ti). It has a very high Curie temperature and operating temperatures of up to 550°C. The materials exhibit a low dielectric constant, low dielectric loss and properties stable up to very high temperatures. Bismuth titanate is used in high temperature applications such as pressure sensors and accelerometers.

The composition $(1-x)(Na_{0.5}Bi_{0.5})TiO_3$-$xBaTiO_3$ (NBBT) with x = 0,055 presents a high piezoelectric charge coefficient $d_{33} = 450$ pC/N and a high permittivity in <100> poling direction.

Table X. Bismuth Titanate (NBT) $(Na_{0,5}Bi_{0,5})TiO_3$ and $(1-x)(Na_{0,5}Bi_{0,5})TiO_3$-$xBaTiO_3$ (NBBT) Properties

	Symbol	Dimension	NBT[1,2,3,4]	NBBT[1,3] x=0,055
Electrical Properties *Relative dielectric constant at 1kHz*	ε_{11}^T	1		
	ε_{33}^T	1	300-500	1500-2000
	ε_{11}^S	1		
	ε_{33}^S	1	240	
Curie temperature	$T_c >$	°C	260	
Electromechanical Properties *Coupling factors*	k_{33}	%	40	
	k_{31}	%	10	
	k_t	%	42	
Piezoelectric charge coefficients	$- d_{31}$	10^{-12} C/N	- 15	
	d_{33}	10^{-12} C/N	70 - 120	450

[1] JK. Lee, K.S. Hong, Piezoelectric Single Crystals and their Application, Ed. S. Trolier-McKinstry, LE. Cross and Y. Yamashita, pp. 396-415, (2004)
[2] Y. Hosono, K. Harada and Y. Yamashita, Jap. J. Appl. Phys. 40 pp. 5722-5726 (2001)
[3] Y. Chiang, GW. Farrey and AN. Soukholak, Appl. Phys. Letters 73 25 pp. 3683-3685 (1998)
[4] Landolt-Borstein, Vol. 11, New Series Group 3 Springer-Verlaf Heidelberg New-York (1979)

2.3.7. Langasite type single crystals

Langasite: CGG *($Ca_3Ga_2Ge_4O_{14}$)* had been developed to comprise an entire group of crystal materials with at least 40 members. The different crystals are obtained by variations of the cations of CGG. The main materials are LGS (langasite), LGG (lanthan gallium germanate), LGT (lanthan gallium tantalate), LGN (lanthan gallium niobate) and SGG (strontium gallium germanate). A general property of this group is the high temperature stability, which is much higher compared to quartz. Langasite has 3~4 times larger electro-mechanical coupling coefficient than quartz, better frequency-temperature characteristics and smaller equivalent series resistance. Langasite is used for high volume BAW and SAW applications due to its high coupling and its availability in large dimensions and also these crystals may found applications in the mobile digital communication field.

Table XI. Langasite Type Single Crystals Properties $La_3Ga_5SiO_{14}$ (LGS), $Ca_3NbGa_3Si_2O_{14}$ (CNGS), $La_3Ta_{0,5}Ga_{5,5}O_{14}$ (LGT), $La_3Nb_{0,5}Ga_{5,5}O_{14}$ (LGN)

	Symbol	Dimension	LGS[1,3,4,6,9] Y-cut	CNGS[2]	LGT[1,3,5,8]	LGN[1,3,7]
Electrical Properties *Relative dielectric constant at 1kHz*	ε_{11}^{T}	1	18,99	17,8	19,9	20,7
	ε_{33}^{T}	1	50,44	27,9	77,2	79
	ε_{11}^{S}	1	18,9	16,9	19,1	
	ε_{33}^{S}	1	50,44	27,9	77,2	
Melting point	$T_m >$	°C	1400		1450	1450
Electromechanical Properties *Coupling factors*	k_{12}	%		10,9		
	k_{25}	%		17,3		
	k_{26}	%	16	11,9		
Coupling factor for BAW	k_{emc}	%	15,8			
Q factor for BAW	Q	10^3	50			
Coupling coeff. for SAW	K^2	%	0,32		0,7	
Piezoelectric charge coefficients	d_{11}, d_{111}	10^{-12} C/N	6,25	- 4,09	7,39	7,06/7,41
	d_{14}, d_{123}	10^{-12} C/N	- 3,65	10,7	- 2,81	- 2,95/- 6,16
Piezoelectric strain coefficients	e_{11}	C/m^2	- 0,4365	- 0,335	- 0,456	-0,45/-0,51
	e_{14}	C/m^2	0,092-0,15	0,439	0,094	0,06/0,11

[1] J. Stade, L. Mohaty, M. Hengst, RB. Heimann, Cryst. Res. Technol. 37, 10, pp.1113-1120 (2002)
[2] T. Karaki, R. Sato, M. Adachi, J. Kushibiki and M. Arakawa, Jap. J. Appl. Phys. 43, 9B, pp. 6721-6724 (2004)
[3] www.piezotech.com
[4] www.cradley-crystals.com
[5] J. Schreuer, IEEE Trans. Ultra. Ferro. Freq. Contr. 49, 11, pp. 1474-1479 (2002)
[6] J. Kosinski, R. Pastore, E. Bigler, M. Pereira da Cunha, D. Malocha, J. Detaint, 2001 IEEE Int. Freq. Contr. Symp. And PDA Exhib. (2001)
[7] J. Bohm, E. Chilla, C. Flannery, HJ. Frohlich, T. Hauke, RB. Heimann, M. Hengst, U. Straube, J. Crystal Growth, 216, pp. 293-298 (2000)
[8] M. Pereira da Cunha, DC. Malocha, EL. Adler, KJ. Casey, IEEE UFFC 49, 9, pp. 1291-1299 (2002)
[9] http://www.americanpiezo.com/products_services/crystals/langasite.html

2.3.8. Rochelle salt, ADP, KDP

These water soluble crystals, which do not possess the stability of quartz, are no longer used as piezoelectric resonators. However, *Potassium Dihydrogen Phosphate (KDP)* is known for its non-linear optical properties. It is therefore used in optical modulators and for non-linear optics.

Also to be noted, Deuterated Potassium Dihydrogen Phosphate (DKDP) which exhibits slightly different properties. Deuterated KDP is almost always used in nonlinear frequency conversion of laser light.

Rochelle salt $KNaC_4H_4O_6{\cdot}4H_2O$ produces a comparatively large voltage upon compression and was used in early crystal microphones. Piezoelectric coefficients are the following: (d_{21} = 7.0(6) × 10^{-10} CN^{-1}, d_{22} = 2.2(9) × 10^{-9} CN^{-1}, d_{23} = 2.1(9) × 10^{-9} CN^{-1} and d_{25} = 3.7(8) × 10^{-11} CN^{-1} *E* parallel to the [0 1 0] direction (the *b*-axis) [4].

Table XII. Rochelle salt (RS), ADP and KDP Properties
$NaKC_4H_4O_6$-$4H_2O$ (RS), $(NH_4)H_2PO_4$ (ADP), KH_2PO_4 (KDP)

	Symbol	Dimension	RS[1]	ADP[1]	KDP[1]
Electrical Properties *Relative dielectric constant at 1kHz*	ε_{11}^T	1	320	55,8	43,2
	ε_{22}^T	1	9,3		
	ε_{33}^T	1	9,5	15,3	20,8
Curie temperature	T_C	°C	24/-18	-125	-150
Electromechanical Properties *Coupling factors*	k_{14}	%	88	0,6	0,8
	k_{25}	%	27,9		
	k_{36}	%	11,1	33	12,1
Piezoelectric charge coefficients	d_{14}	10^{-12} C/N	530	1,76	1,28
	d_{25}	10^{-12} C/N	- 56		
	d_{36}	10^{-12} C/N	13,1	48,31	20,9

[1] Landolt-Borstein, Vol. 11, New Series Group 3 Springer-Verlag Heidelberg, New-York (1979)

Chapter 3

3. INVESTIGATED SAMPLES

This chapter consists of four paragraphs which give a brief introduction to the investigated samples. The crystal structure, crystal growth and main physical properties are described in paragraphs below.

3.1. The Crystal Family $Sn_2P_2(Se_x S_{1-x})_6$

The $Sn_2P_2S_6$ compound is a member of the large isomorphous $(Pb_xSn_{1-x})_2P_2(S_ySe_{1-y})_6$ family of uniaxial displacive ferroelectrics [9]. The (x, y, T)-phase diagram of this monoclinic family exhibits a ferroelectric (x<0.4) and a paraelectric phase, and for y<0.72 an incommensurate phase [5].

$Sn_2P_2S_6$ is a ferroelectric compound which exhibits strong piezoelectric effect, combining large photorefractive constants with a fast holographic response, a large pyroelectric coefficient and bulk piezo-modulus, which make them promising materials for optical and acoustical applications. At the p-T phase diagram of these crystals the line of policritical points – the Lifshitz points is realized. The $Sn_2P_2S_6$ is a proper ferroelectric; at atmospheric pressure it undergoes a second-order phase transition at T=337 K from the high-temperature centrosymmetric (space group $P2_1/n$) to the low-temperature ferroelectric modification (space group Pn) [6]. The Lifshitz point is realized at p_{LP} = 0.18 GPa and T_{LP} = 295 K. An increase of Se concentration leads to the shift of the LP towards the region of lower pressure [7].

Pure $Sn_2P_2Se_6$ at room temperature is in paraelectric phase with the centrosymmetric space group $P2_1/c$. It is one of the proper ferroelectrics that show the presence of an incommensurately modulated phase, intermediate between the paraelectric and ferroelectric phases. The temperature range of the stability of this incommensurate phase is (193-220 K) [10]. The high temperature phase has the symmetry $P2_1/c$ and the low temperature phase has Pc symmetry [8]. At T = 221 K and atmospheric pressure a second-order phase transition occurs. At T = 193 K there is a first-order lock-in transition to a proper ferroelectric phase with space group P_c.

3.2. Crystal Growth

In 1970, the growth of $Sn_2P_2S_6$ crystals was firstly described by Nitsche et.al, where a possibility of growing crystals of the metal-phosphorus-sulfur family ($Me_2P_2S_6$) by a vapor transport technique using pure iodine was reported. At the beginning of the growing process, the constituting elements and the transporter were sealed into quartz ampoules and then brought to reaction at 650-700°C. The ampoule was placed in the hot spot of a horizontal temperature gradient, while the crystal grows in the cold end (ca 20°C colder) by chemical transport. A possible reaction for this transport is:

$$2(SnI_2)_{gas} + 0.5(P_4)_{gas} + 3(S_2)_{gas} \rightarrow (Sn_2P_2S_6)_{solid} + 2(I_2)_{gas}$$

The average growth time was of order of 100 hours.

Nowadays, also other transporters are used: SnI_2, SnI_4 and $SnCl_2$ [9. 10]. The description of the room-temperature synthesis of $Sn_2P_2S_6$ crystals is described in [11]:

$$2SnCl_2 + Li_4P_2S_6 \rightarrow Sn_2P_2S_6 + 4LiCl$$

With SnI_4 or I_2 yellow-colored crystals are obtained, recently a light-brown colored $Sn_2P_2S_6$ sample was grown using SnI_2 [12].

3.3. Crystal Structure

At room temperature $Sn_2P_2S_6$ crystal has a ferroelectric monoclinic structure with point group *m*.

The primitive cell of the $Sn_2P_2S_6$ is shown in Figure 11. In according to [13] vector *b* is perpendicular to the mirror plane, $c < a$, $\beta > 90°$ and $\alpha = \gamma = 90°$. Values of the translation vectors are the following: $a = 9{,}375\ \text{Å}$, $b = 7{,}488\ \text{Å}$, $c = 6{,}512\ \text{Å}$, the angle β=91.15° [14]. And in accordance to [11]: $a = 9{,}37(7)\ \text{Å}$, $b = 7{,}450(1)\ \text{Å}$, $c = 6{,}51(5)\ \text{Å}$, β=91,(1)°. The crystal axis *b* is perpendicular to the plane of Figure 11. At room temperature the atoms of the unit cell have a space group P_n.

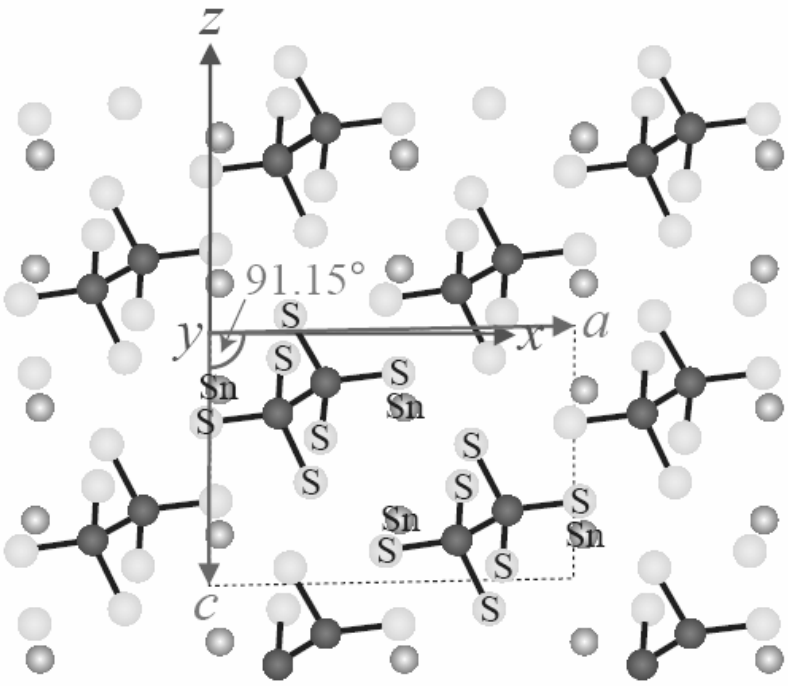

Figure 11. The Fragment of the Crystal Structure of $Sn_2P_2S_6$

The elementary cell has two P_2S_6 units. The whole structure shows pseudo symmetry through a pseudo twist axis in direction [010]. The P_2S_6 unit is settled by two distorted trigonal PS_3 prisms which are related together through a P-P bond. The bases are rotated so that the whole symmetry is *3m*. The two Sn^{2+} cations are connected to the $(P_2S_6)^{4-}$ complex by ionic bonds. The coordinate system $\vec{a}, \vec{b}, \vec{c}$ is a right handed Cartesian x, y, z system. According to the standard of piezoelectric materials the y-axis is perpendicular to the symmetry plane (y k b), the z-axis is chosen parallel to the crystal c-axis and the x-axis perpendicular to y and z.

For $Sn_2P_2Se_6$ the primitive cell is shown in Figure 12. Values of the translation vectors are the following [10]: a = 6,8145 Å , b = 7,7170 Å , c = 11,692 Å , the angle β=124,594°. There are 20 atoms in the unit cell. As a whole, the group may be seen as a distorted trigonal antiprism, with monoclinic *2/m* symmetry.

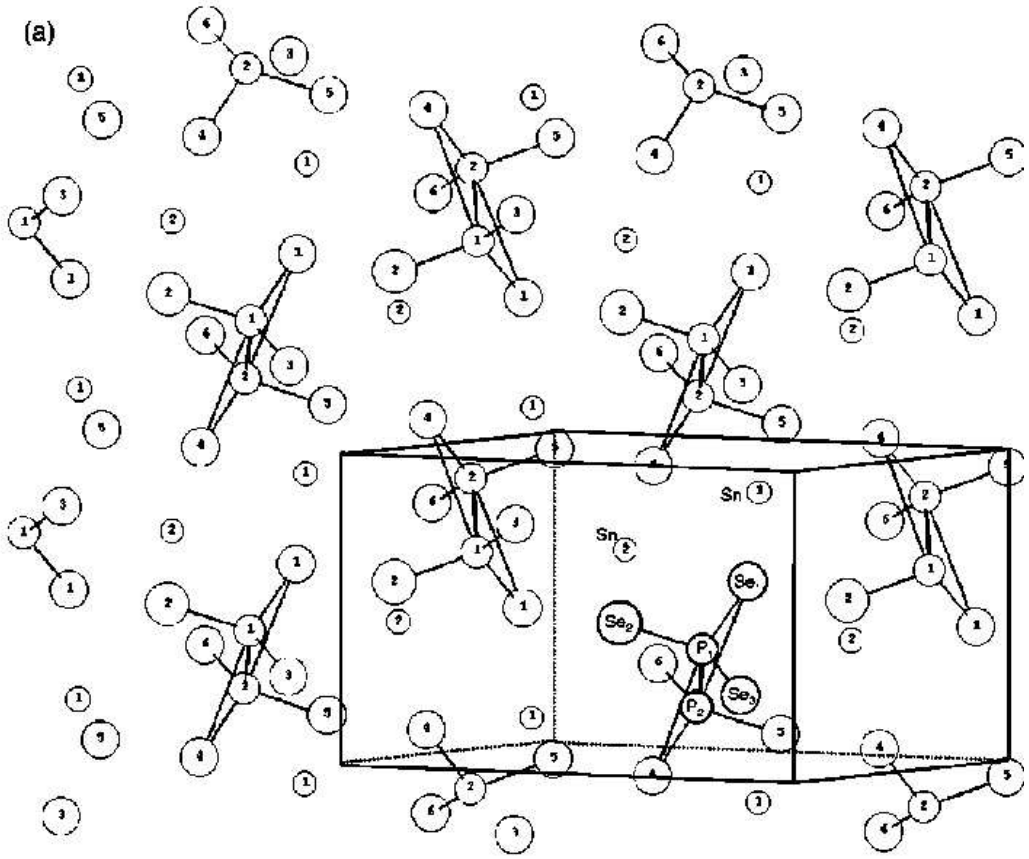

Figure 12. The Fragment of the Crystal Structure of $Sn_2P_2Se_6$

With respect to basic chemical arguments and geometrical consideration, the structure may be seen as built of P_2Se_6 anionic groups and Sn cations. Within the P_2Se_6 group, each P atom is fourfold coordinated (one P atom and three Se atoms). A distance of 2.225 Å separates the two P atoms. The Se atoms are disposed at the apices of a basal triangle. The P-Se bond distance ranges between 2.18 and 2.20 Å. As a whole the group may be seen as a distorted trigonal antiprism, with monoclinic2/*m* symmetry. The P_2Se_6 units are arranged along chains parallel to [010]. Two consecutive chains are in an antisymmetrical relationship. The Sn atoms lie between these P_2Se_6 units, surrounded by eight Se atoms at distances of 2.9 Å up to 3.6 Å, suggesting possible ionic-type bonds. They ensure the in-chain connections and the further binding of these chains in directions parallel to [100], [001], and [101], [10].

3.4. Main Physical Properties

In literature you may found the following experimental data: the phase transition analysis [8], the Raman study [9], the first principles study [10], pressure behavior in the vicinity of Lifshitz point [15], thermal measurements [16], spontaneous polarization [17] etc. The piezoelectric quantity criteria for $Sn_2P_2S_6$ (SPS) are the following: $\tan\delta = 0.005$, $\varepsilon = 280$ at f=100 kHz, d_h=320 pC/N, $g_h = 0.145$ Vm/N. From literature, the value of spontaneous polarization P_s is 14 $\mu C/cm^2$ at 20°C [14].

For piezoelectric or any other applications, SPS crystals should be poled, because grown crystals are usually poly domain. Polarization is realized by heating of the sample over the phase transition temperature and then slowly cooling to the room temperature under an applied electric field. During heating, polarization decreases up to critical temperature where it goes to zero following the square root dependence typical for second order phase transition.

Table XIII. An Overview of the Physical Properties of $Sn_2P_2S_6$

Density	ρ	$3{,}54\ 10^3$	kg/m^3
Curie temperature	T_C	337	K
Spontaneous polarization	P_S	14	$\mu C/cm^2$
Unit cell	a	9,375	$\mathring{A}$
	b	7,488	$\mathring{A}$
	c	6,513	$\mathring{A}$
	β	91,15	°
Dielectric constant	ε_{11}	230 - 300	
Piezoelectric coefficients	d_{1111}	244	pC/N
	d^S_{122}	37	pC/N
	d^S_{133}	40	pC/N
	d^S_{311}	38	pC/N
	d^S_{322}	13,9	pC/N
	d_h	320	pC/N
	g_h	0.145	Vm/N
Elastic constant	C_{1111}	$4{,}2\ .\ 10^{10}$	N/m^2

Chapter 4

4. MEASUREMENTS AND RESULTS

This chapter consists of three paragraphs where the results of the investigations are reported. The first paragraph dealt with an experiment description. In the second paragraph the results and discussion of the frequency measurements are described. The third paragraph contains the results and analysis of the temperature investigations.

4.1. Experiment Description

Single crystals of $Sn_2P_2(Se_xS_{1-x})_6$ family with concentration of selenium x = 5 %, x = 10 % and x = 15 % are investigated. Samples are grown by the standard chemical vapor transport reactions in Institute for Solid State Physics and Chemistry of Uzhgorod National University. Crystals were oriented using XRD and special plates were cut. In our notation, the direction of spontaneous polarization P_s is close to the direction of the plates, the X-axis. Then, crystals were polished and the Au thin film electrodes were applied on their surfaces by magnetron sputtering. Also, thin Ag wires were applied on the Au electrodes using Degussa's paste to avoid squeezing of the crystal during the measurements. Using these wires the sample was soldered to the crystal-holder of the special chamber for further investigations.

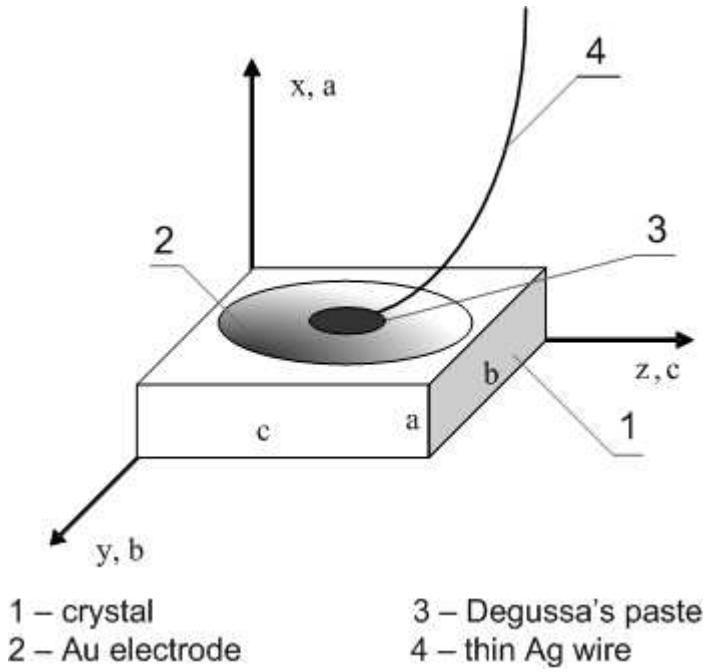

Figure 13. Model of the investigated sample

4.1.1. Frequency-dependent measurements

At the beginning, the frequency measurements of the $Sn_2P_2(Se_{0.05}S_{0.95})_6$, $Sn_2P_2(Se_{0.10}S_{0.90})_6$ and $Sn_2P_2(Se_{0.15}S_{0.85})_6$ crystals were made. Frequency investigations of the capacity phase and the other parameters were realized by an *HP 4192A* impedance analyzer and were registered by a PC *HpVee* program. The scheme is shown in Figure 14. Results are analyzed using a special scientific graphing and analysis software *OriginPro*.

The HP 4192A LF impedance analyzer performs both network analysis and impedance analysis of the basic electronic components. Variable measuring frequency 5 Hz to 13 MHz, frequency accuracy 5ppm, sweep mode: linear or logarithmic (frequency only).

HpVee for Windows is a data program that can control and communicate with a piece of test equipment over a General Purpose Interface Bus (GPIB, also known as HPIB or IEEE 488) cable. The data software allows for electronic capture of data from an experiment, thereby allowing more flexible and powerful data analysis. It also helps to automate experimentation and to speed up analysis. The HpVee program for our frequency measurements was programmed for sweep mode logarithmic to capture capacity, impedance and phase depending on the frequency.

During the measurements, the investigated sample is soldered to the crystal-holder and placed into the small closed chamber to avoid illumination of the sample (see Figure 14, Figure 15). Investigations are realized in air and silicone oil medium, to compare if there is any difference of properties depending on the characteristics of the medium. Measurements are realized in the interval of frequencies from 50 Hz to 13 MHz.

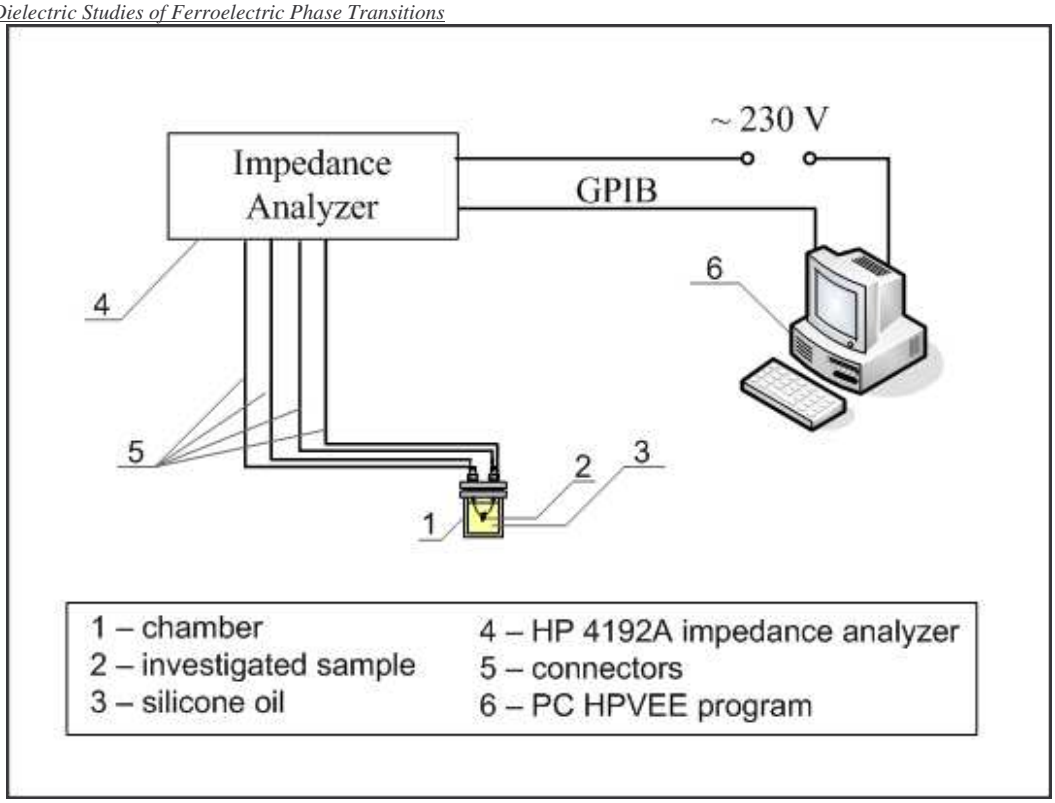

Figure 14. Scheme of the frequency measurements

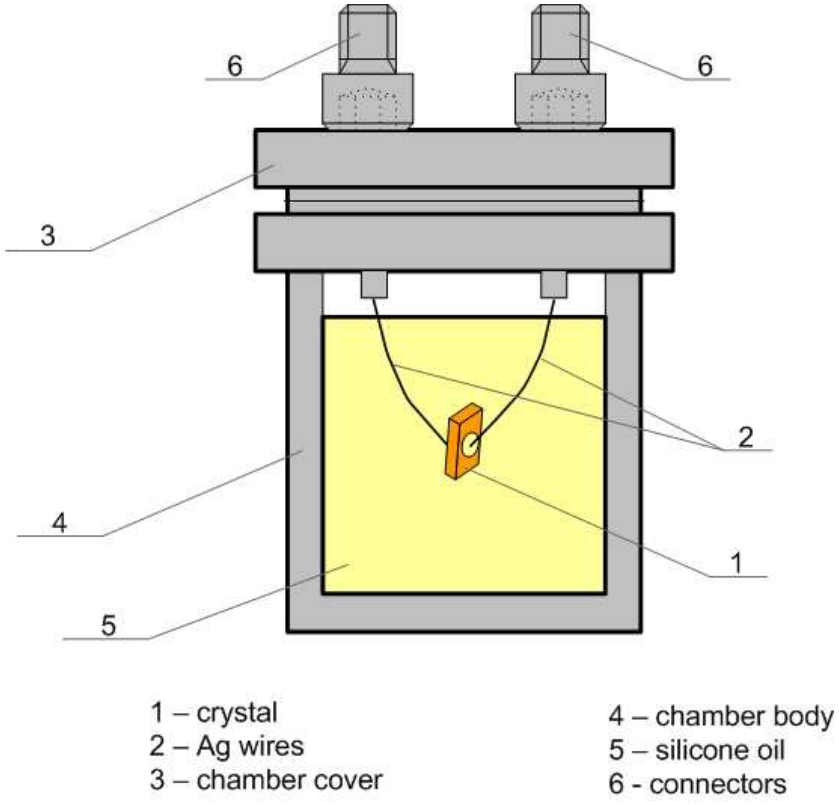

Figure 15. Detail of the chamber with crystal inside

4.1.2. Temperature-dependent measurements

The second step of our investigations, were temperature measurements of the dielectric properties of the crystals. These measurements were realized using the *HP 4276A LCZ meter* and also were controlled by the *HpVee* PC program for temperature measurements, the scheme is shown in Figure 16; results were registered on PC and also analyzed using the scientific software *OriginPro.*

The *HP 4276A LCZ meter* is a general purpose impedance measuring device designed to measure circuit components using frequency and dc bias conditions identical to those of the intended application. Test frequencies: 100 Hz - 20 kHz, capacity range: 1 pF – 10 mF.

Our HpVee program for temperature measurements was programmed to capture capacity and automatically calculate the dielectric permittivity, dielectric loss and conductivity, depending on the electrode surfaces and thickness of the investigated sample (geometry factor).

During the experiment the sample is soldered to the crystal-holder and placed into the small closed chamber to prevent illumination, the chamber is filled with silicone oil. Temperature measurements are realized by automatic heating the chamber with a sample (with step ~ 0.5°C per minute) over the phase transition temperature and then slow spontaneous cooling to the room temperature. Measurements are realized in the interval of temperatures from the room temperature ~295 K to ~353 K for $Sn_2P_2(Se_{0.05}S_{0.95})_6$ and $Sn_2P_2(Se_{0.10}S_{0.90})_6$ crystals. And in the interval from ~253 K to 353 K for $Sn_2P_2(Se_{0.15}S_{0.85})_6$ crystal, because after measurements in the first temperature range we observed that for this sample the phase transition temperature is lower than the room temperature, therefore the temperature interval for $Sn_2P_2(Se_{0.15}S_{0.85})_6$ is a little different than for previous samples. Also, for this sample we used a special liquid-nitrogen refrigerating system to cool it down to ~253 K.

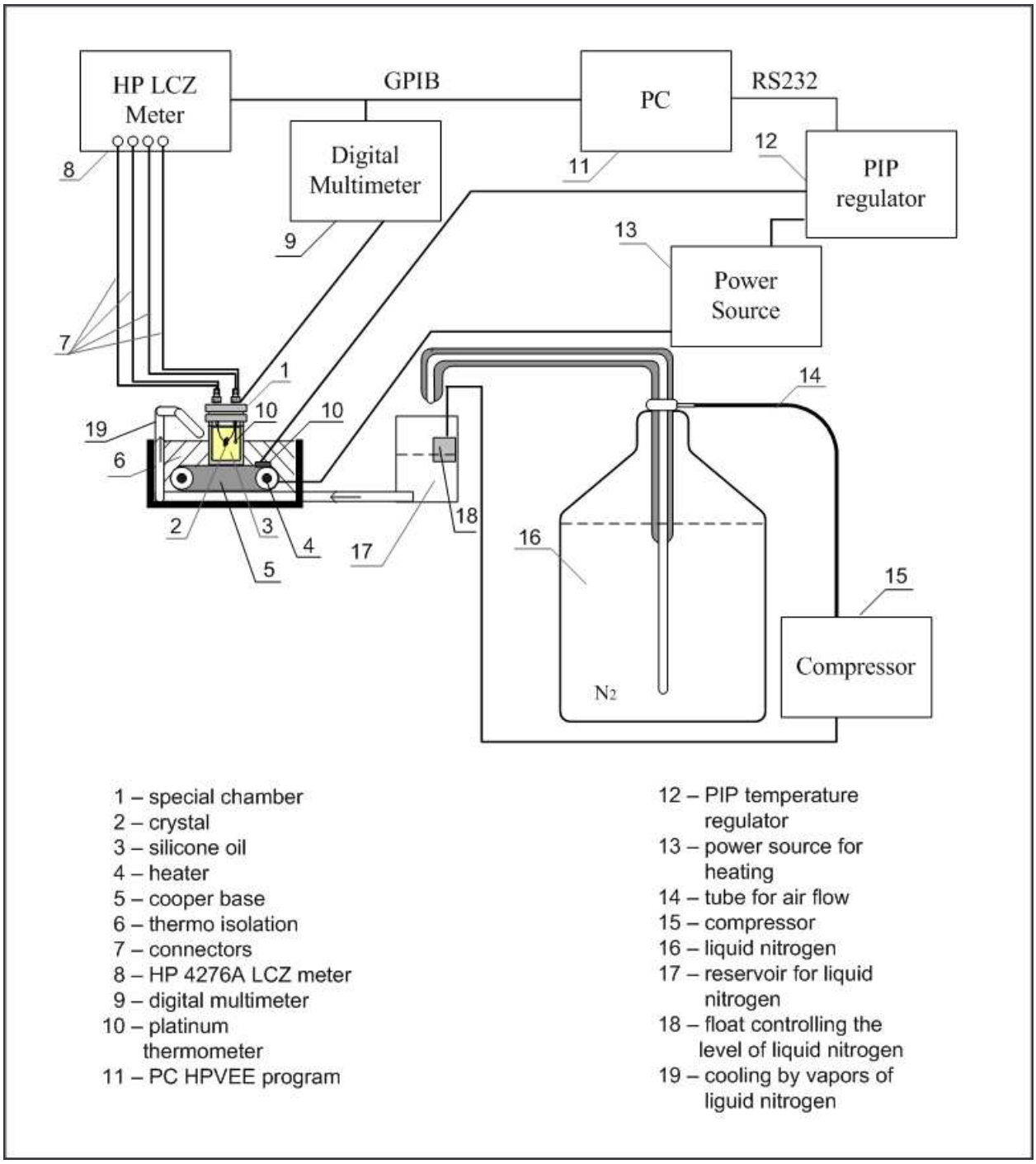

Figure 16. Scheme of the temperature measurements

4.2. Results of Frequency-depend Measurements

Frequency-dependent measurements of the capacity, phase, impedance and dielectric dissipation factor of $Sn_2P_2(Se_{0.05}S_{0.95})_6$, $Sn_2P_2(Se_{0.10}S_{0.90})_6$ and $Sn_2P_2(Se_{0.15}S_{0.85})_6$ are made. The measurements were realized in the frequency range of 50 Hz to 13 MHz in air and silicone oil medium.

It's known, that the capacity (C) of a plane condenser is expressed by the following equation:

$$C=\frac{\varepsilon_0\varepsilon' S}{d} \tag{35}$$

where ($\varepsilon^{|}$) is a dielectric permittivity, $\varepsilon_0 = 8.85\ 10^{-12}$ F/m, (d) is thickness of the sample and (S) is an electrode's area.

Using measured values of the capacity, frequency dependences of the dielectric permittivity ($\varepsilon^{|}$) of $Sn_2P_2(Se_{0.05}S_{0.95})_6$ (x=0.05) are calculated:

$$\varepsilon'=\frac{Cd}{\varepsilon_0 S} \tag{36}$$

where an electrode's area $S=\frac{\pi d^2}{4}$ (d is a diameter), therefore we have a samples with Au circle electrodes on the larger faces.

Using measured values of the dielectric dissipation factor (tanδ) and calculated frequency dependences of the dielectric permittivity ($\varepsilon^{|}$) dependences of the dielectric loss ($\varepsilon^{||}$) as a function of frequency are calculated.

$$\varepsilon''=\varepsilon'\cdot tg\delta=\varepsilon'\cdot D \tag{37}$$

Obtained results for each sample are presented below.

4.2.1. $Sn_2P_2(Se_{0.05}S_{0.95})_6$ (x=0.05) single crystal

Frequency measurements of $Sn_2P_2(Se_{0.05}S_{0.95})_6$ (x=0.05) are made. Dependences of the capacity, the dielectric dissipation factor, phase and impedance as a function of frequency are shown in Figure 17.

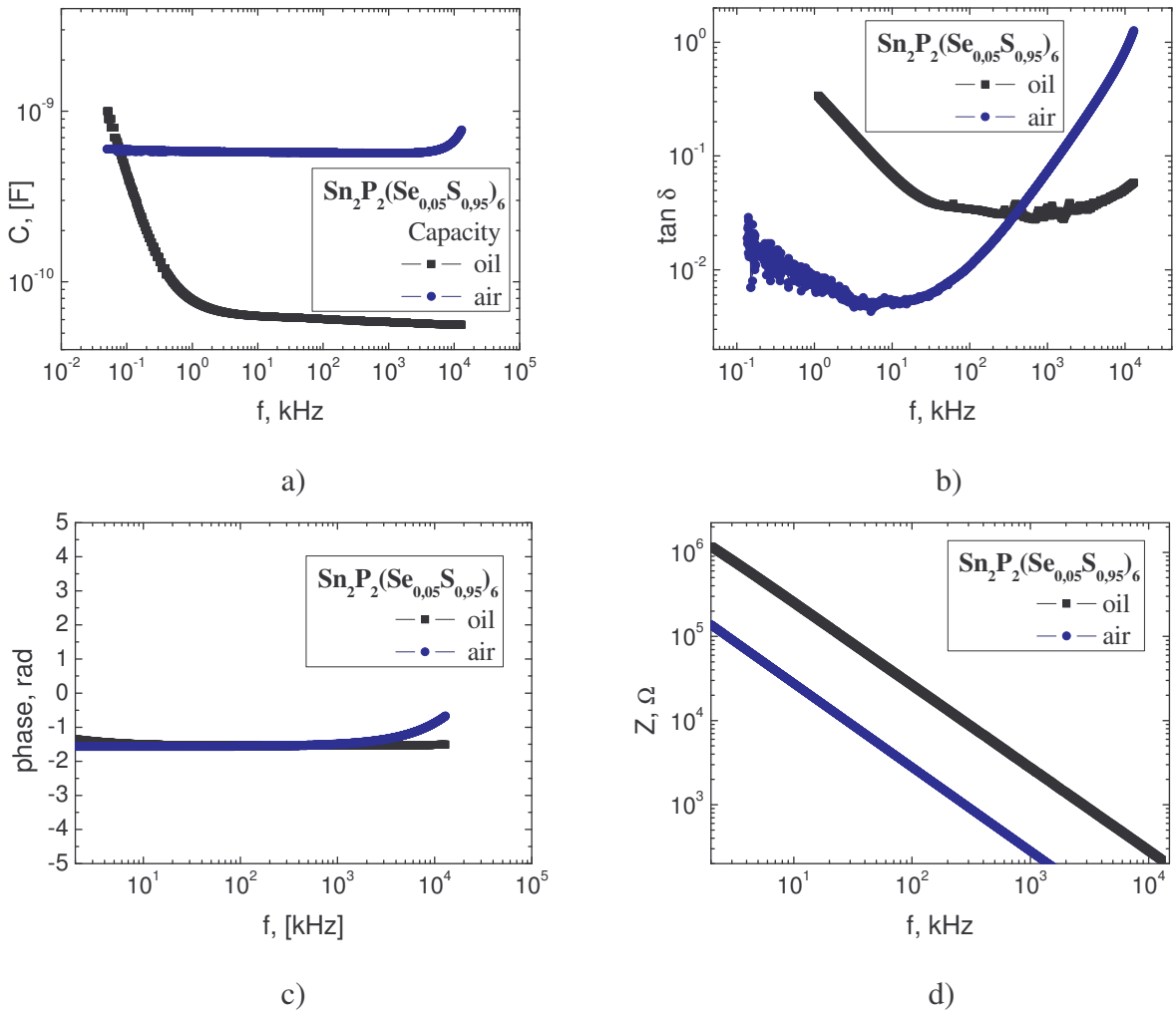

Figure 17. Frequency dependences of a) capacity, b) dissipation factor, c) phase and d) impedance of $Sn_2P_2(Se_{0.05}S_{0.95})_6$ (x=0.05) in air and silicone oil medium

As it's seen from Figure 17 there is a difference between measured values in air and silicone oil medium for $Sn_2P_2(Se_{0.05}S_{0.95})_6$ crystal.

Capacity (C) of $Sn_2P_2(Se_{0.05}S_{0.95})_6$ crystal, measured in silicone oil medium (black curves a) initially falls sharply as the frequency increases and then saturates to some value (~ 0.056 nF), instead of the capacity measured in air medium (Figure 17a). Capacity measured in air medium saturates to the value ~ 0.570 nF almost in the entire interval of

investigated frequencies. Capacity values of the sample in air are larger then in silicone oil medium; the ratio of the capacity in air to silicone oil medium is close to 10:1, starting from frequency 1 kHz.

Figure 17b shows dependences of the dielectric dissipation factor (tanδ) as a function of frequency. It is found that (tanδ) initially decreases with increase frequency, attains a minimum and again starts to increase further frequency increased for both silicone oil and air medium. In the range of frequencies from 50 Hz to 400 kHz the values of (tanδ) in air medium are less than in silicone oil medium, and starting from 400 kHz it is vice versa. At frequency 400 kHz the value of (tan δ) in air and silicone oil medium is the same tanδ=0,0317.

Using the experimental values of the capacity and impedance, frequency dependences of the dielectric permittivity, dielectric loss and resistance of $Sn_2P_2(Se_{0.05}S_{0.95})_6$ (x=0.05) were calculated. These dependences are shown below.

Dielectric permittivity mainly depends on the capacity (Eq.36), because thickness of the sample and the electrode's area are constants for the same sample. Therefore, the frequency dependences of the dielectric permittivity behave almost the same way as the capacity-frequency dependences. The dielectric permittivity values of $Sn_2P_2(Se_{0.05}S_{0.95})_6$ in air are larger than in silicone oil medium, the ratio of the permittivity in air to silicone oil medium is close to 14:1, starting from frequency 1 kHz.

Obtained values for $Sn_2P_2(Se_{0.05}S_{0.90})_6$ (x=0.05) at f = 100 kHz are the following: $C_{air} = 571.00$ pF and $C_{oil} = 60.37$ pF; $\tan\delta_{air} = 0.011$ and $\tan\delta_{oil} = 0.034$; $\varepsilon'_{air} = 11826$ and $\varepsilon'_{oil} = 631$; $\varepsilon''_{air} = 128$ and $\varepsilon''_{oil} = 22$.

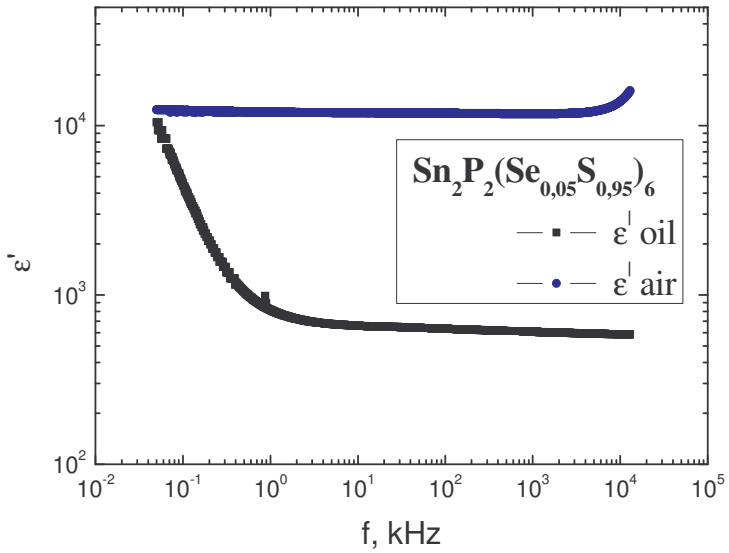

a)

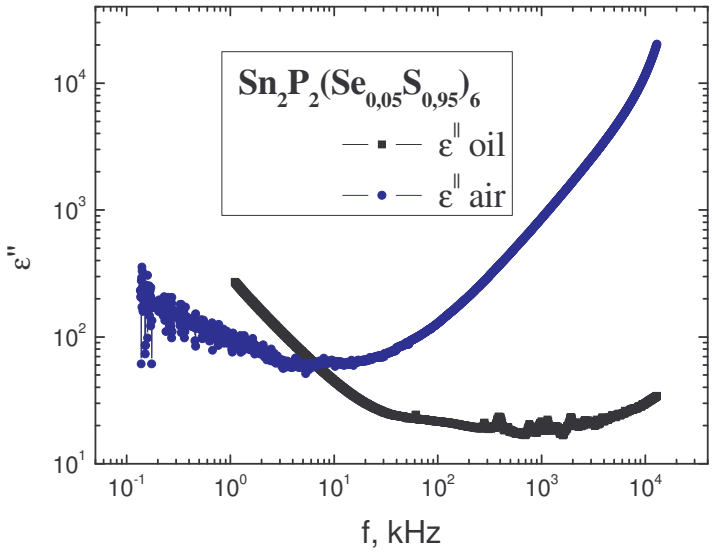

b)

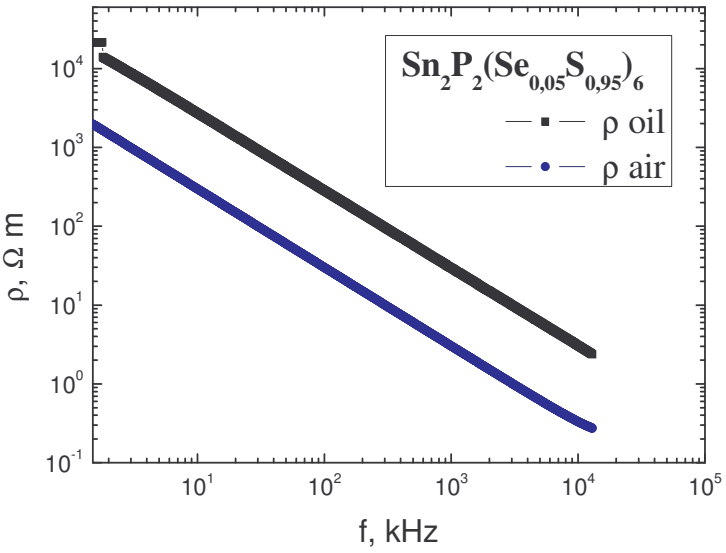

c)

Figure 18. Frequency dependences of the a) dielectric permittivity, b) dielectric loss and c) resistance of $Sn_2P_2(Se_{0.05}S_{0.95})_6$ (x=0.05) in air and silicone oil medium

4.2.2. $Sn_2P_2(Se_{0.10}S_{0.90})_6$ (x = 0.10) single crystal

Investigations of $Sn_2P_2(Se_{0.10}S_{0.90})_6$ (x=0.10) single crystal are realized the same way as for x=0.05. Frequency dependences of measured values are shown in Figure 19.

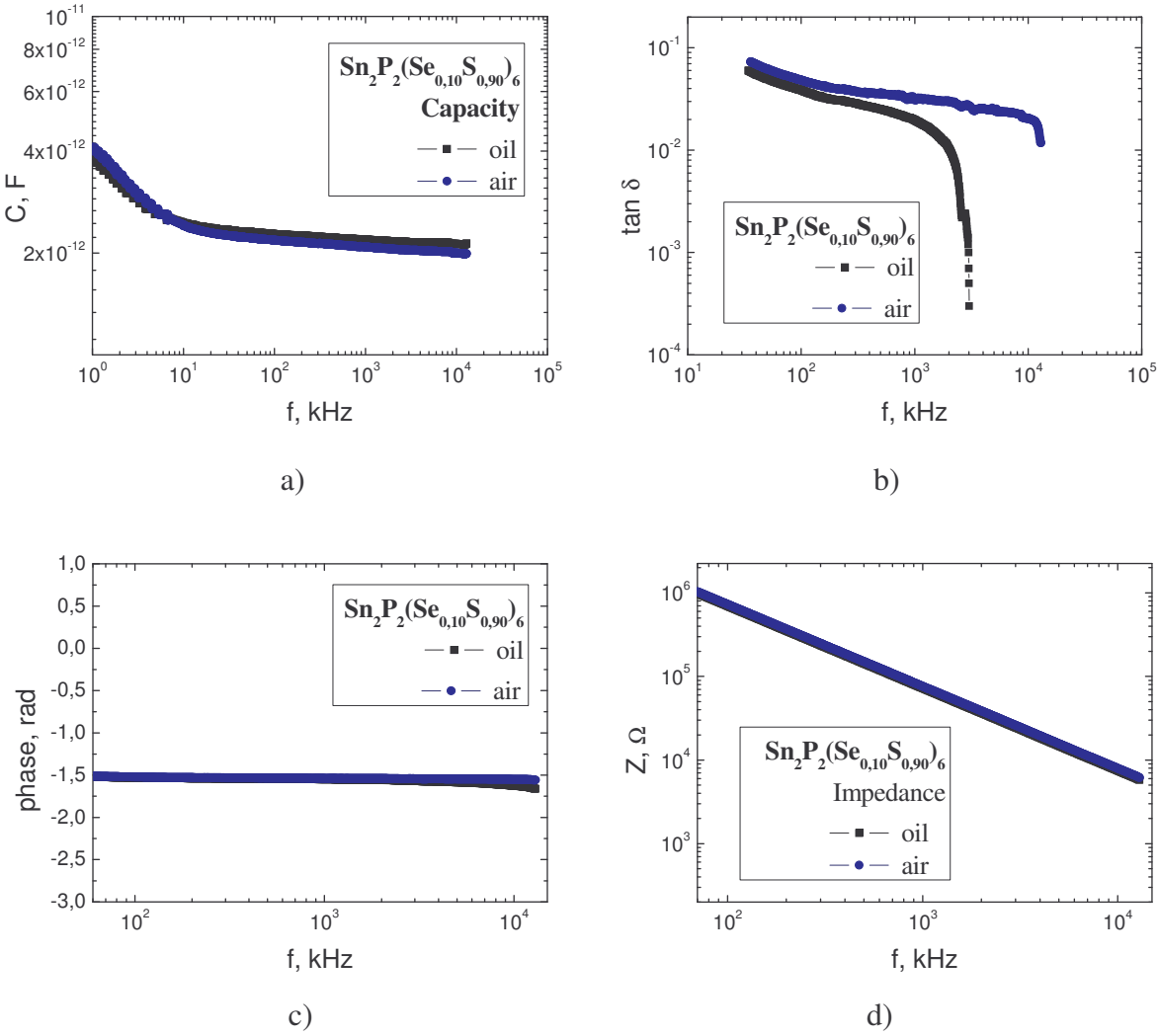

Figure 19. Frequency dependences of a) capacity, b) dissipation factor, c) phase and d) impedance of $Sn_2P_2(Se_{0.10}S_{0.90})_6$ (x=0.10) in air and silicone oil medium

As it's seen from Figure 19 there is no significant difference between the values measured in air and silicone oil medium for $Sn_2P_2(Se_{0.10}S_{0.90})_6$ crystal.

It is obtained that the capacity (C) of $Sn_2P_2(Se_{0.10}S_{0.90})_6$ crystal falls slightly as the frequency increases (Figure 19a) and saturates to the some value both in air and silicone oil

medium. Values of the capacity in silicone oil and air medium are almost the same.

Figure 19b shows the dielectric dissipation factor dependences versus frequency. It is found, that this sample has quite high values of (tanδ) in both air and silicone oil medium. The dielectric dissipation factor sharply falls with increase frequency.

Using experimental values shown in Figure 19, the frequency dependences of the dielectric permittivity, dielectric loss and resistance of $Sn_2P_2(Se_{0.10}S_{0.90})_6$ (x=0.10) are calculated. Obtained dependences are shown in Figure 20.

Frequency dependences of the dielectric permittivity and the dielectric loss behave the same way as the dependences of the capacity and the dielectric dissipation factor, respectively.

Obtained values for $Sn_2P_2(Se_{0.10}S_{0.90})_6$ (x=0.10) at f = 100 kHz are the following: $C_{air} = 2.18$ pF and $C_{oil} = 2.28$ pF; $\tan\delta_{air} = 0.049$ and $\tan\delta_{oil} = 0.039$; $\varepsilon'_{air} = 22$ and $\varepsilon'_{oil} = 23$; $\varepsilon''_{air} = 1.05$ and $\varepsilon''_{oil} = 0.87$

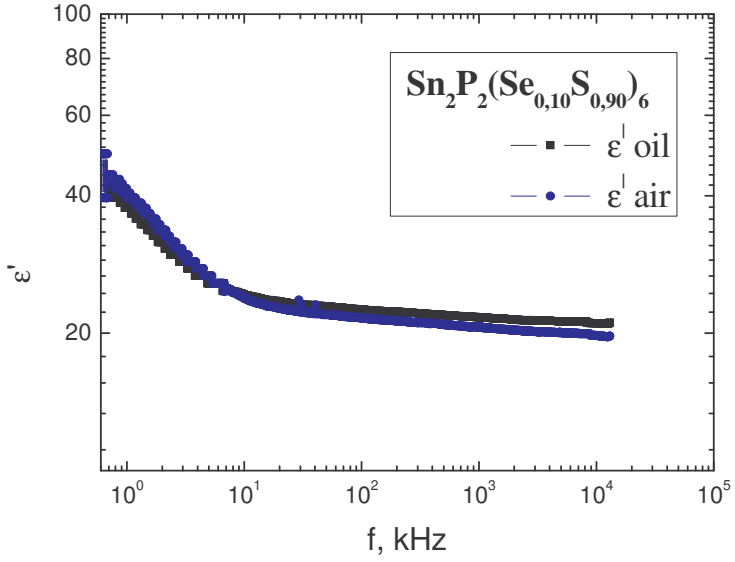

a)

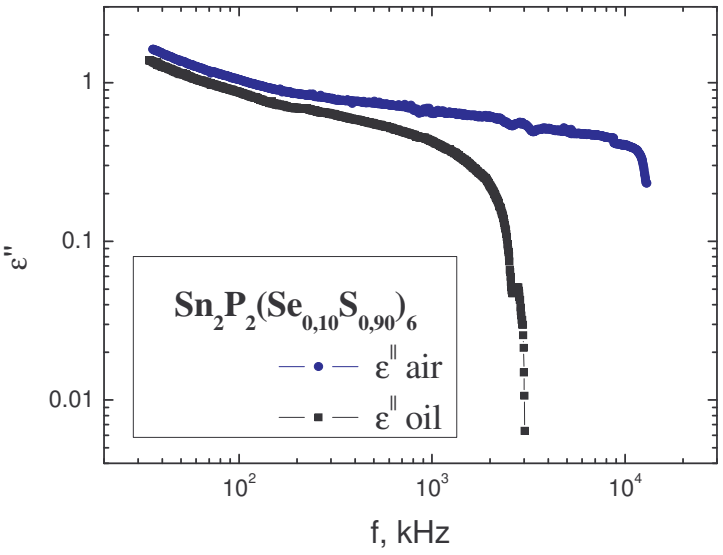

b)

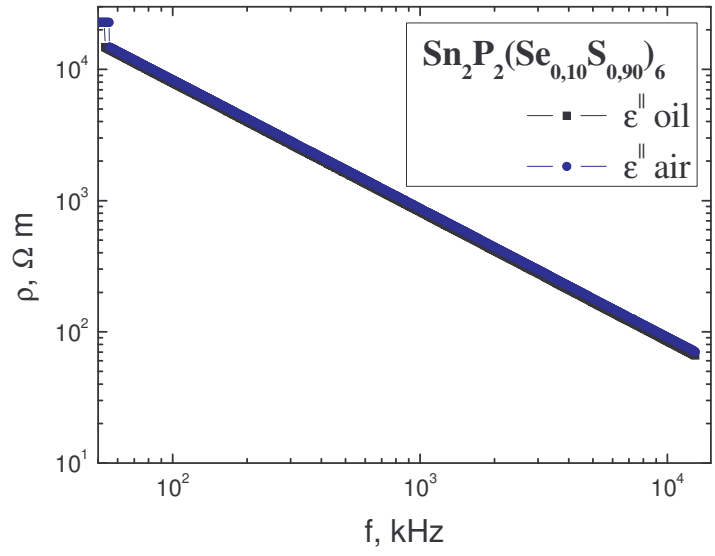

c)

Figure 20. Frequency dependences of the a) dielectric permittivity, b) dielectric loss and c) resistance of $Sn_2P_2(Se_{0.10}S_{0.90})_6$ (x=0.10) in air and silicone oil medium

4.2.3. $Sn_2P_2(Se_{0.15}S_{0.85})_6$ (x=0.15) single crystal

Frequency-depend measurements of $Sn_2P_2(Se_{0.15}S_{0.85})_6$ (x=0.15) are carried out the same way as for previous two samples. Dependences of the capacity, dielectric dissipation factor, phase and impedance are shown in Figure 21.

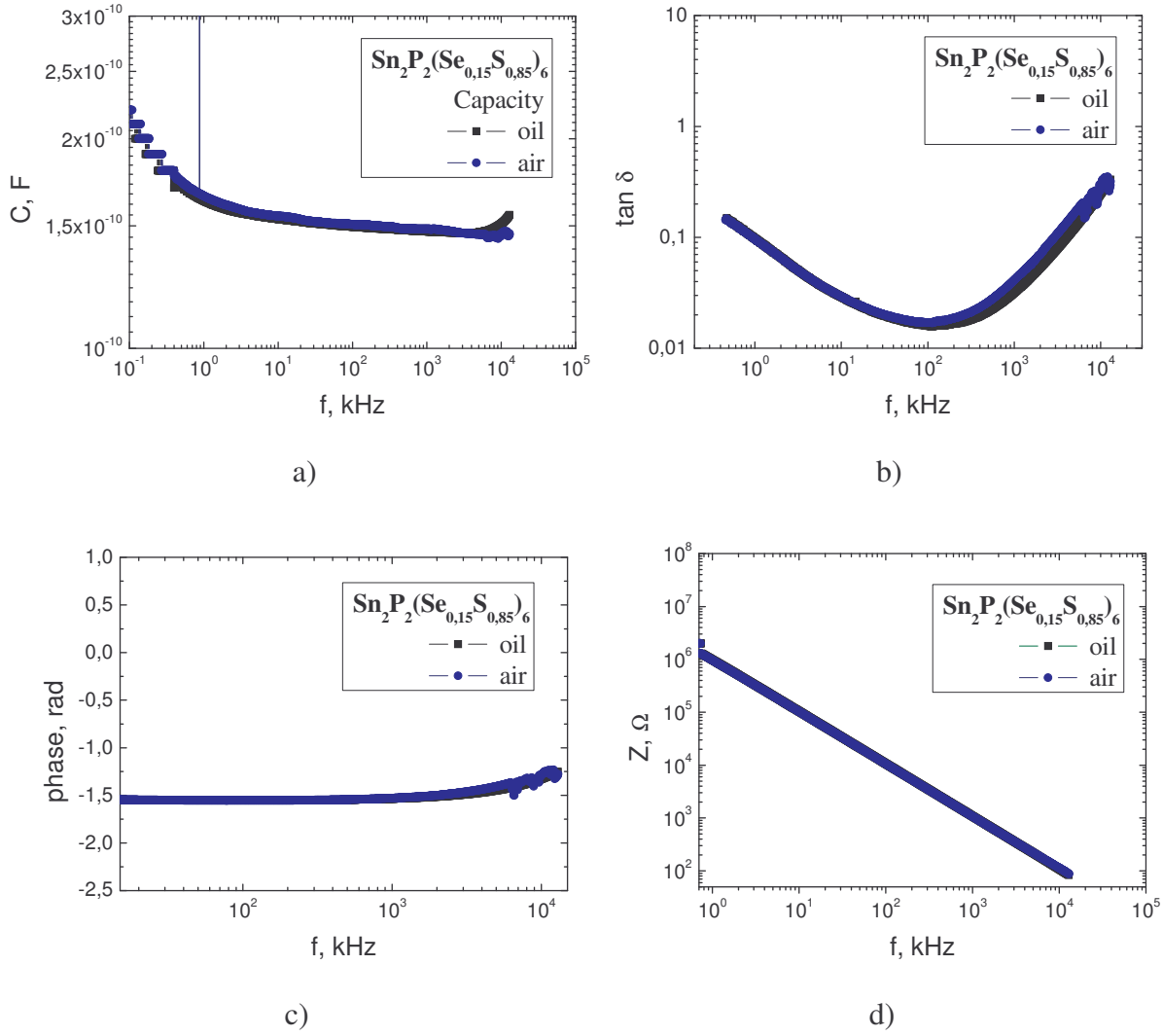

Figure 21. Frequency dependences of a) capacity, b) dissipation factor, c) phase and d) impedance of $Sn_2P_2(Se_{0.15}S_{0.85})_6$ (x=0.15) in air and silicone oil medium

As it's seen from Figure 21 there is no significant difference between the values measured in air and silicone oil medium for $Sn_2P_2(Se_{0.15}S_{0.90})_6$ crystal.

It is obtained that the capacity (C) of $Sn_2P_2(Se_{0.10}S_{0.90})_6$ crystal falls slightly as the frequency increases (Figure 21a) and saturates to the value ~ C = 0.15 nF both in air and silicone

oil medium. Frequency dependences of the dielectric dissipation factor are shown in Fig.21b.

It is found that (tanδ) of $Sn_2P_2(Se_{0.15}S_{0.85})_6$ initially decreases with increase frequency, attains a minimum and again starts to increase further frequency increased for both silicone oil and air medium. Values of (tanδ) in air and silicone oil medium are almost the same.

Calculated frequency dependences of the dielectric permittivity, dielectric loss and the resistance of $Sn_2P_2(Se_{015}S_{0.85})_6$ (x=0.15) are shown in Figure 22.

Frequency dependences of the dielectric permittivity, expectedly, behave the same way as the frequency dependences of the capacity. And frequency dependences of the dielectric loss as the dielectric dissipation factor initially decreases with increase frequency, attains a minimum and again starts to increase with a frequency.

Obtained values for $Sn_2P_2(Se_{0.15}S_{0.90})_6$ (x=0.15) at f = 100 kHz are the following: $C_{air} = 150.69$ pF and $C_{oil} = 149.44$ pF; $tan\delta_{air} = 0.017$ and $tan\delta_{oil} = 0.016$; $\varepsilon^{|}_{air} = 3121$ and $\varepsilon^{|}_{oil} = 3095$; $\varepsilon^{||}_{air} = 53$ and $\varepsilon^{||}_{oil} = 49$.

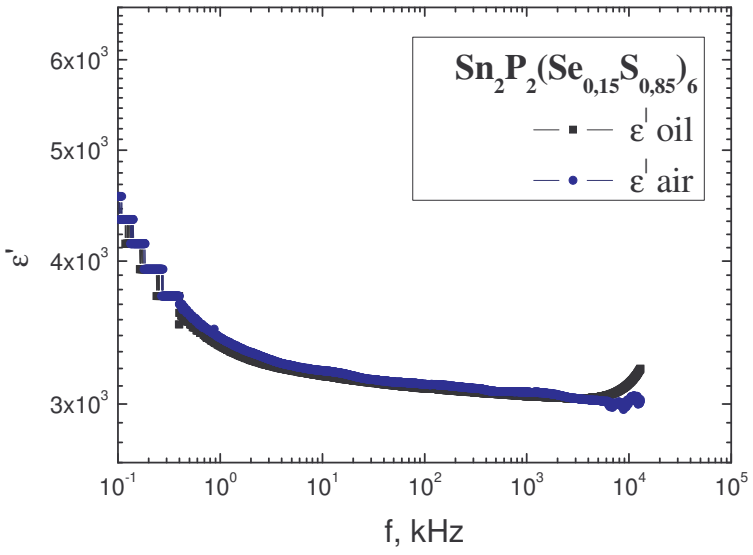

a)

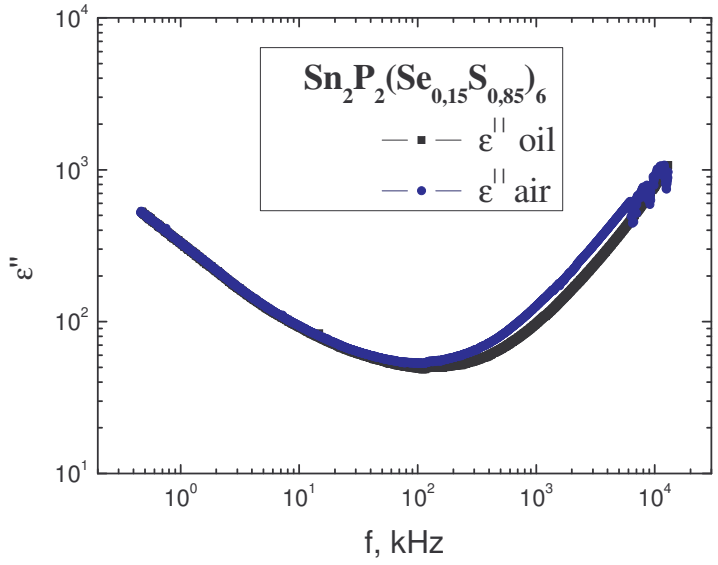

b)

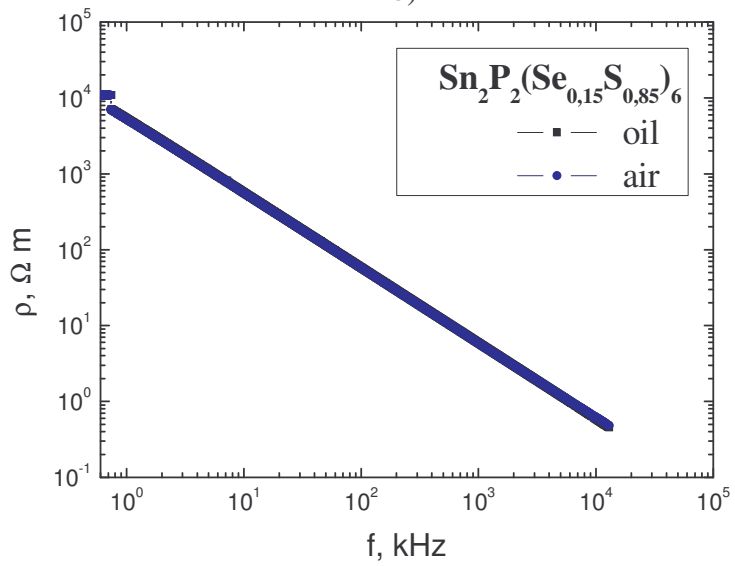

c)

Figure 22. Frequency dependences of the a) dielectric permittivity, b) dielectric loss and c) resistance of $Sn_2P_2(Se_{0.15}S_{0.85})_6$ (x=0.15) in air and silicone oil medium

4.3. Results of Temperature-depend Measurements

Temperature investigations of the dielectric permittivity (ε'), dielectric loss (ε''), capacity (C) and conductivity (σ) for $Sn_2P_2(S_{1-x}Se_x)_6$ single crystals for x = 0.05, x = 0.10 and x = 0.15 concentration of selenium (Se) at frequencies f = 1 kHz, f = 5 kHz and f = 10 kHz are made. Results of the investigations are presented below.

4.3.1. $Sn_2P_2(Se_{0.05}S_{0.95})_6$ (x=0.05) single crystal

Temperature investigations of the dielectric permittivity (ε'), dielectric loss (ε''), capacity (C) and conductivity (σ) of $Sn_2P_2(Se_{0.05}S_{0.95})_6$ single crystal at several frequencies are made. Measurements were realized by heating the sample in oil medium from ~ 293 K over the phase transition temperature T_C to ~ 353 K and slow cooling to room temperature.

Temperature dependences of dielectric permittivity (ε') at frequencies f = 1 kHz (A), f = 5 kHz (B) and f = 10 kHz (C) for heating and cooling modes are shown in Figure 23.

Form Figure 23 1 it is seen, that at a definite temperature (T) there is a jump of the dielectric permittivity (ε'). The ferroelectric-paraelectric phase transition is observed at $T_{0,h}$ = 332.62 K (heating mode) and the paraelectric-ferroelectric phase transition is observed at $T_{0,c}$ = 329.10 K (cooling mode), Figure 23. The discrepancy of the phase transition temperatures in heating and cooling modes is intrinsic.

Temperature dependences of the dielectric loss (ε'') of $Sn_2P_2(Se_{0.05}S_{0.95})_6$ at frequencies f = 1 kHz (A), f = 5 kHz (B) and f = 10 kHz (C) for heating and cooling modes are shown in Figure 24. There is also clear jump of the (ε'') at the definite temperature in ferroelectric-paraelectric (heating mode) and paraelectric-ferroelectric (cooling mode) transitions, as it is seen in Figure 24.

Dependences of the dielectric permittivity jump (ε'_{max}) and the dielectric loss jump (ε''_{max}) versus frequency (f) in heating and cooling modes for $Sn_2P_2(Se_{0.05}S_{0.95})_6$ (x=0.05) are shown in Figure 25.

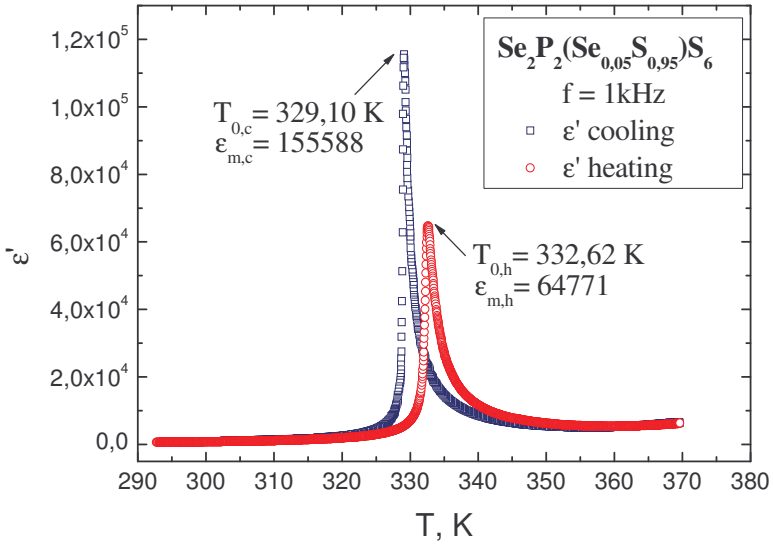

(A)

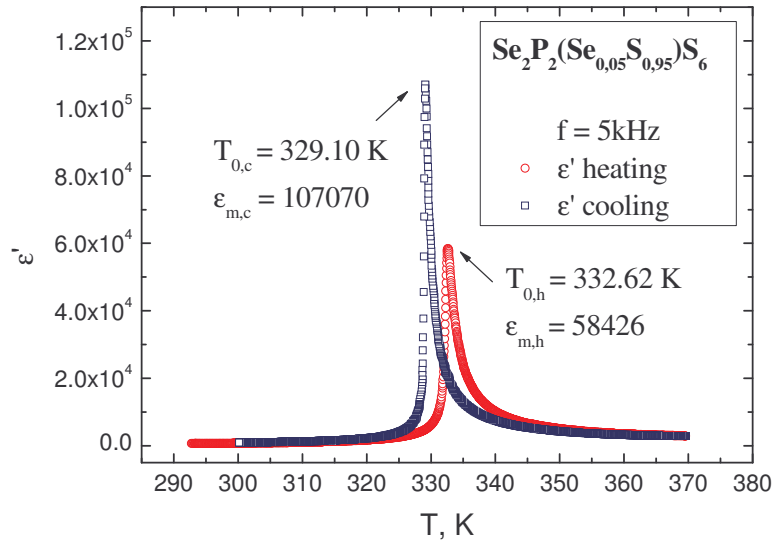

(B)

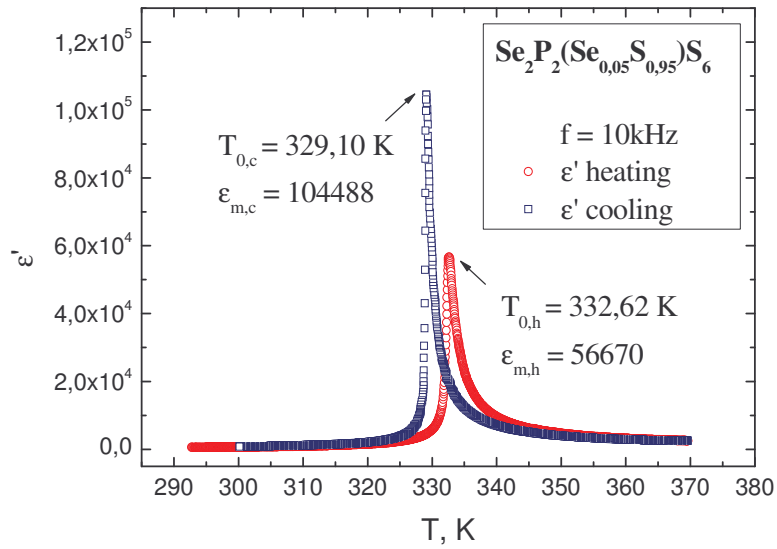

(C)

Figure 23. Temperature dependences of the dielectric permittivity (ε') of $Sn_2P_2(Se_{0.05}S_{0.95})_6$ (x=0.05) in heating and cooling modes at frequencies 1kHz (A), 5kHz (B) and 10kHz (C)

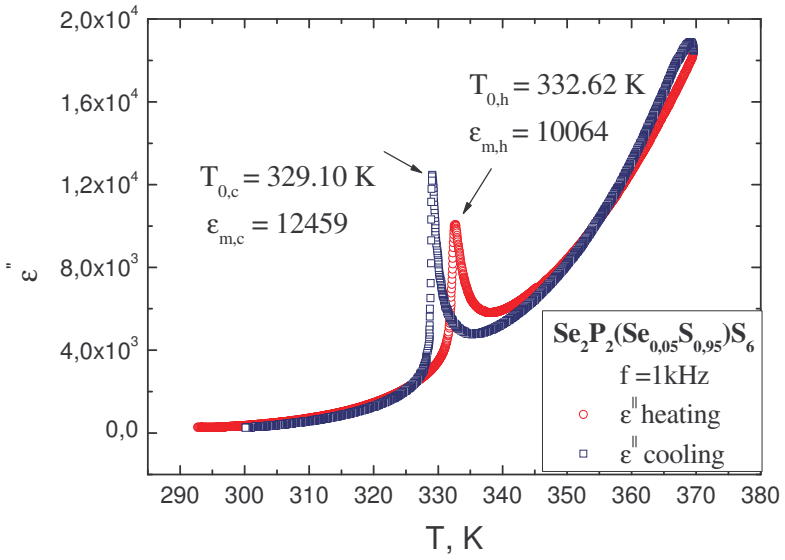

(A)

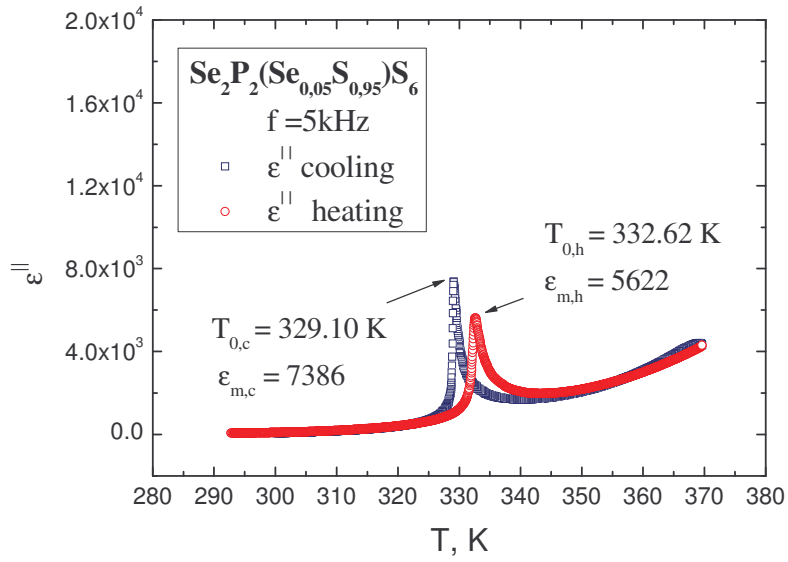

(B)

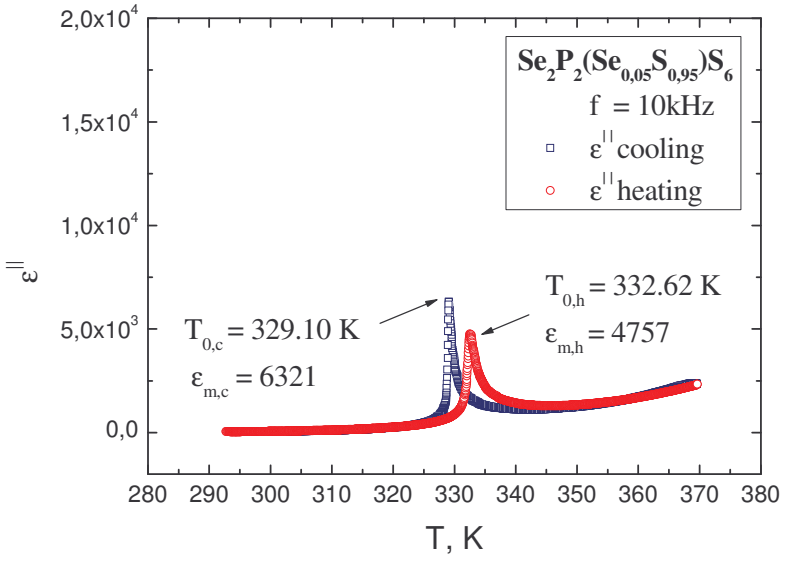

(C)

Figure 24. Temperature dependences of the dielectric loss (ε'') of $Sn_2P_2(Se_{0.05}S_{0.95})_6$ (x=0.05) in heating and cooling modes at frequencies f = 1 kHz (A), f = 5 kHz (B) and f = 10 kHz (C)

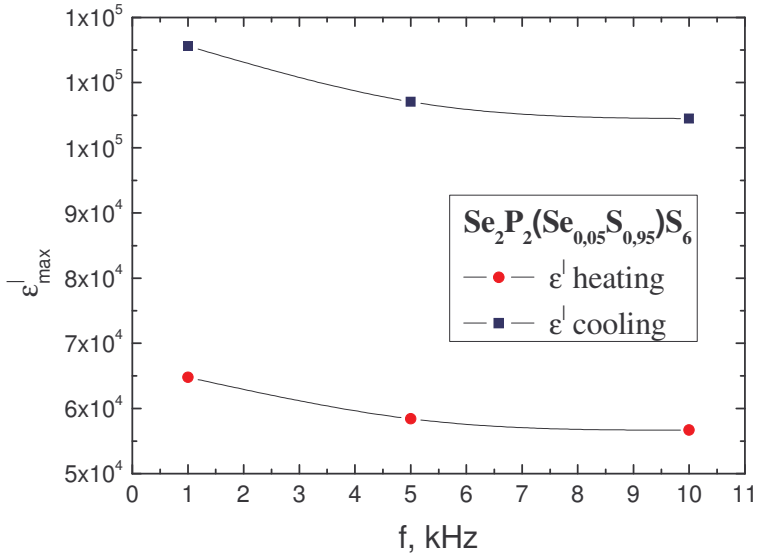

(a)

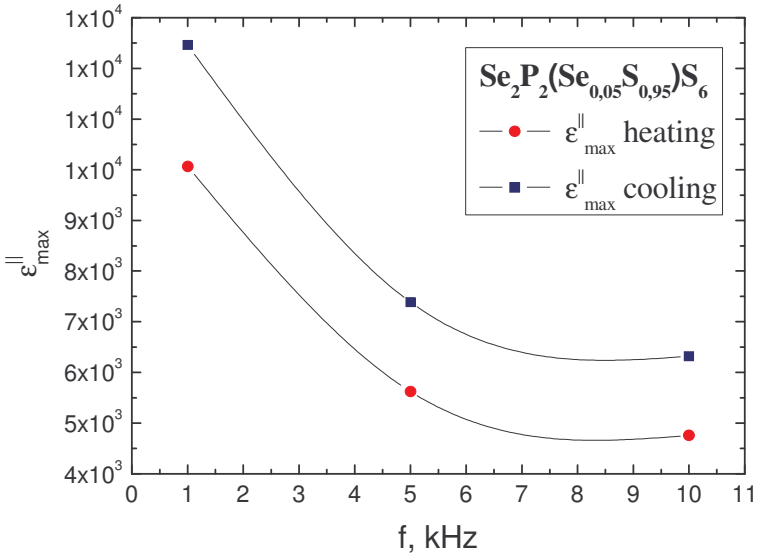

(b)

Figure 25. Dependences of (a) dielectric permittivity jump (ε'_{max}) and (b) dielectric loss jump (ε''_{max}) versus frequency (f) in heating and cooling modes for $Sn_2P_2(Se_{0.05}S_{0.95})_6$ (x=0.05)

From Figure 25 it is seen, that for $Sn_2P_2(Se_{0.05}S_{0.95})_6$ the jump of the dielectric permittivity (ε'_{max}) and the jump of the dielectric loss (ε''_{max}) at the ferroelectric-paraelectric phase transition (heating mode) and at the paraelectric-ferroelectric phase transition

(cooling mode) decrease with applied frequency (f). So, we may suppose, that at frequency f = 1 kHz they have more significant jumps than at higher frequencies.

Using the experimental temperature dependences of dielectric constant and dielectric loss of $Sn_2P_2(Se_{0.05}S_{0.95})_6$ the dielectric dissipation factor (tan δ) is calculated (Eq.20). Values of (tanδ) are usually determined at frequency 1 kHz. Figure 26 illustrates temperature dependence of (tanδ) at frequency 1 kHz.

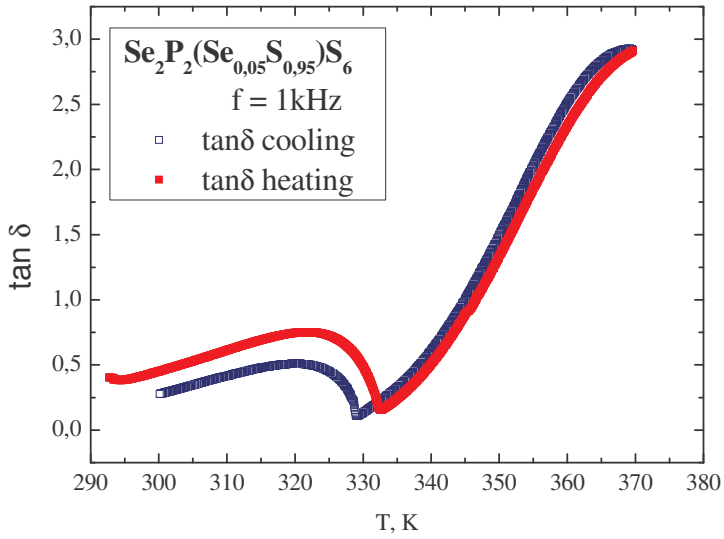

Figure 26. Temperature dependence of the dielectric dissipation factor (tanδ) for $Sn_2P_2(Se_{0.05}S_{0.95})_6$ (x=0,05) in cooling and heating mode, f = 1kHz

The value of the dielectric dissipation factor in cooling mode for $Sn_2P_2(Se_{0.05}S_{0.95})_6$ (x=0,05) at atmospheric pressure p = 100kPa, temperature T = 300 K and frequency f = 1 kHz, is tanδ = 0.277, and at the phase transition temperature tanδ = 0.107.

Figure 27 illustrates the temperature dependence of the conductivity of $Sn_2P_2(Se_{0.05}S_{0.95})_6$ at 1 kHz.

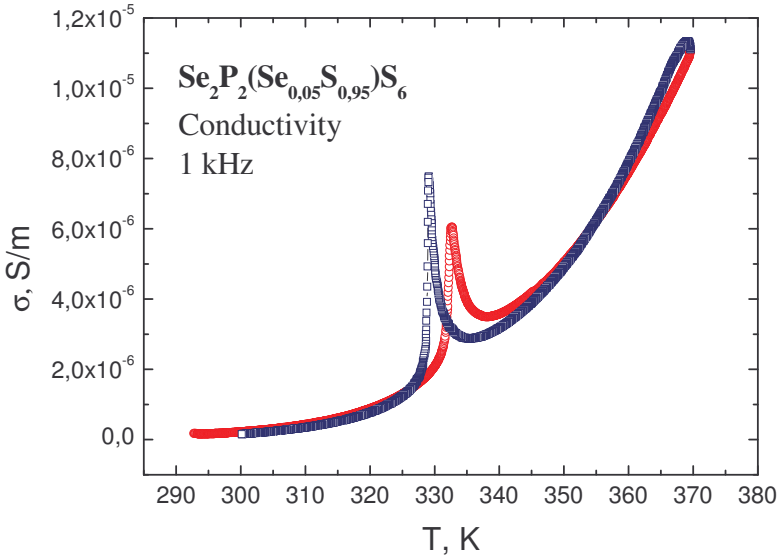

Figure 27. Temperature dependence of the conductivity of $Sn_2P_2(Se_{0.05}S_{0.95})_6$ in heating and cooling modes at 1 kHz

Also, the dependences of the reciprocal dielectric constant versus temperature are studied.

Plots of the reciprocal dielectric constant ($1/\varepsilon'$) versus temperature (T) at frequency f = 1 kHz for $Sn_2P_2(Se_{0.05}S_{0.95})_6$ single crystal are shown in Figure 28. The figure illustrates the temperature dependences of the reciprocal dielectric constant in heating and cooling modes.

No significant jump of the reciprocal dielectric constant is observed, what suggests that the phase transition in $Sn_2P_2(Se_{0.05}S_{0.95})_6$ may be second order. The ferroelectric-paraelectric phase transition is observed at $T_{0,h} = 332.62$ K (heating mode) and the paraelectric-ferroelectric phase transition is observed at $T_{0,c} = 329.10$ K (cooling mode).

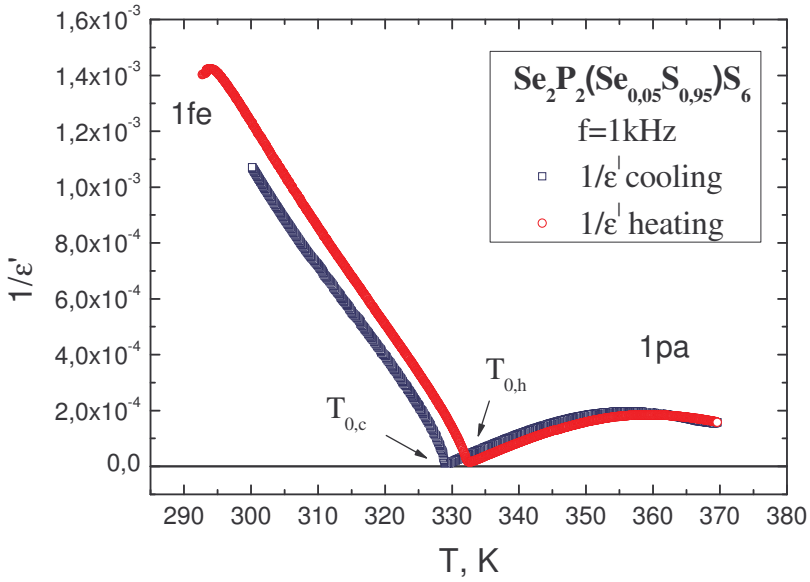

Figure 28. Temperature dependence of the reciprocal dielectric permittivity $1/\varepsilon'$ of $Sn_2P_2(Se_{0.05}S_{0.95})_6$ in heating and cooling modes at frequency 1kHz

For our further examinations, we considered only temperature dependence of the reciprocal dielectric constant at frequency 1 kHz in cooling mode. This dependence is shown in Figure 29.

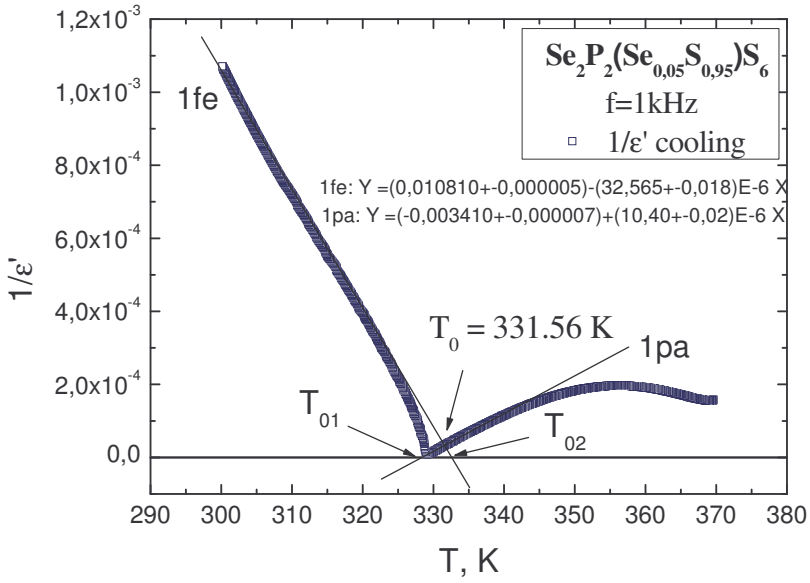

Figure 29. Temperature dependence of the reciprocal dielectric permittivity $1/\varepsilon'$ of $Sn_2P_2(Se_{0.05}S_{0.95})_6$ in cooling mode at frequency 1kHz

If we assume the existence of a second order phase transition in $Sn_2P_2(Se_{0.05}S_{0.95})_6$ then, the temperature dependence of the reciprocal dielectric constant should obey the Curie-Weiss law both above and below the phase transition temperature. On the basis of our measurements we see (Figure 29) that in the vicinity of the phase transition temperature at f = 1 kHz the values of the reciprocal dielectric constant slightly deviate from the Curie-Weiss law. At frequencies of 5 kHz and 10 kHz this deviation is also observed. This deviation makes us unsure about the type of the phase transition in $Sn_2P_2(Se_{0.05}S_{0.95})_6$. We supposed that investigated crystals of $Sn_2P_2(Se_xS_{1-x})_6$ family will behave like $Sn_2P_2S_6$ and the phase transition will be second-order (Figure 7), [19]. Let us examine the behavior of the crystal's properties in the vicinity of the phase transition temperature.

The temperature dependence of the reciprocal dielectric permittivity of $Sn_2P_2(Se_{0.05}S_{0.95})_6$ in the vicinity of the phase transition temperature T_0 in cooling mode at frequency 1 kHz is shown in Figure 30. The experimentally determined phase transition temperature is $T_{0,c} = 329.00$ K while the extrapolated phase transition temperature is $T_0 = T_C = 331.56$ K (see Figure 30).

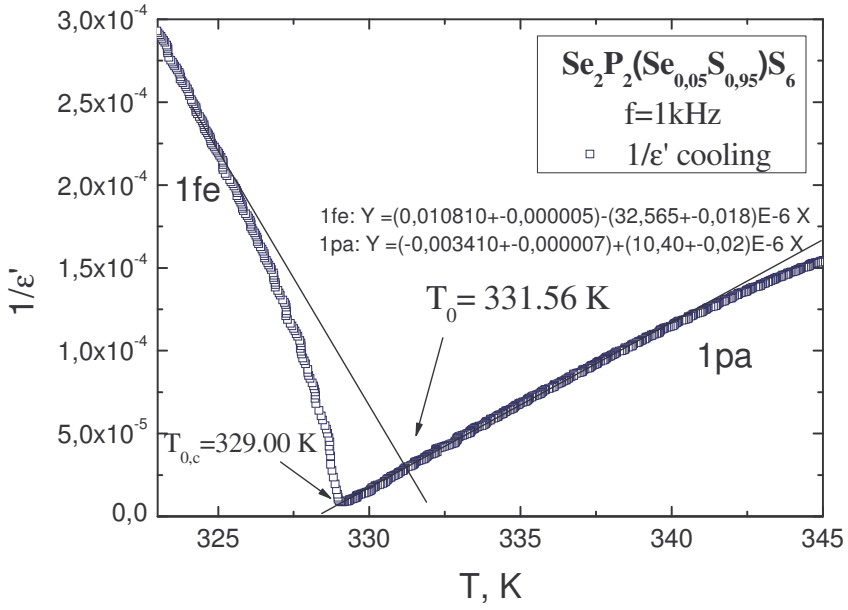

Figure 30. Temperature dependence of the reciprocal dielectric permittivity $1/\varepsilon'$ of $Sn_2P_2(Se_{0.05}\ S_{0.95})_6$ in the vicinity of the phase transition temperature T_0 in cooling mode at frequency 1kHz

Temperature dependences of the reciprocal dielectric permittivity in ferroelectric phase 1fe= $\varepsilon_{fe}^{-1}(T)$ and paraelectric phase 1pa= $\varepsilon_{pa}^{-1}(T)$ are described by the following equations

$$\varepsilon_{fe}^{-1}(T) = \frac{T_{02}}{C_{w,fe}} - \frac{1}{C_{w,fe}} \cdot T = (108{,}1 \pm 0{,}05) \cdot 10^{-4} - (32{,}56 \pm 0{,}18) \cdot 10^{-6} \cdot T \tag{38}$$

$$\varepsilon_{pa}^{-1}(T) = -\frac{T_{01}}{C_{w,pa}} + \frac{1}{C_{w,pa}} \cdot T = (-34{,}10 \pm 0{,}07) \cdot 10^{-4} + (10{,}40 \pm 0{,}02) \cdot 10^{-6} \cdot T \tag{39}$$

Using these equations the following parameters for $Sn_2P_2(Se_{0.05}S_{0.95})_6$ are obtained: Curie temperature (phase transition temperature) $T_0 = T_C = 331.56$ K, Curie-Weiss temperature T_{01}=327.88 K and T_{02}=332.00 K (Figure 29). In our case, the Curie-Weiss temperatures practically coincide with the phase transition temperature, what is obvious for the second-order phase transitions. Also, the Curie-Weiss temperature constants for the ferroelectric $C_{w,fe}$ and paraelectric $C_{w,pa}$ phases of $Sn_2P_2(Se_{0.05}S_{0.95})_6$ are calculated. The values are: $C_{w,fe}$ = - 30708 and $C_{w,pa}$ = 96154. Ratio $\left|C_{w,pa} / C_{w,fe}\right|$ = 3,10. These values indicate a second order phase transition in $Sn_2P_2(Se_{0.05}S_{0.95})_6$ at temperature $T_C = 331.56$ K and atmospheric pressure.

4.3.2. $Sn_2P_2(Se_{0.10}S_{0.90})_6$ (x=0.10) single crystal

Temperature investigations of $Sn_2P_2(Se_{0.10}S_{0.90})_6$ (x=0.10) single crystal at frequencies 1 kHz, 5 kHz and 10 kHz are performed. Investigations were realized by heating the sample from ~ 295 K over the phase transition temperature T_C to ~ 353 K with a subsequent slow cooling to room temperature.

The temperature dependences of the dielectric permittivity (ε') of $Sn_2P_2(Se_{0.10}S_{0.90})_6$ crystal at frequency f = 1 kHz for heating and cooling modes are shown in Figure 31.

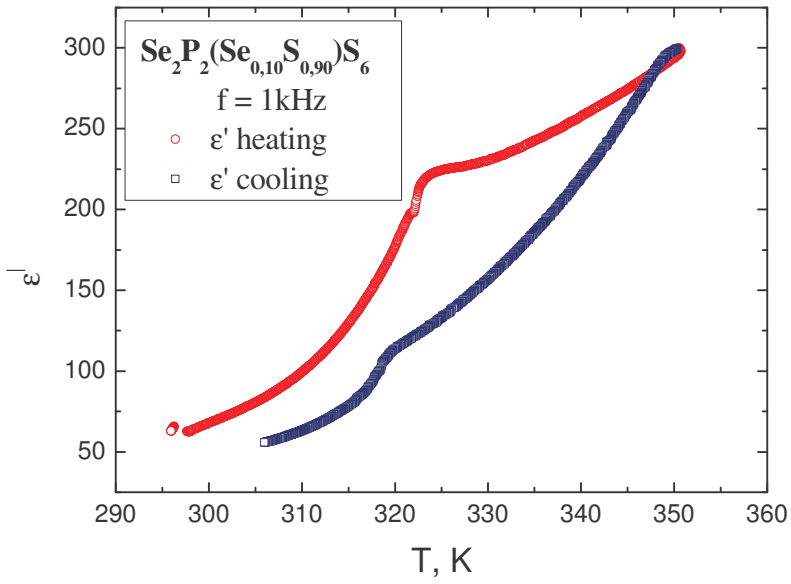

Figure 31. Temperature dependences of the dielectric constant (ε') of $Sn_2P_2(Se_{0.10}S_{0.90})_6$ (x=0.10) in heating and cooling modes at frequency 1kHz

From Figure 31 it is seen, that there is no significant jump of the dielectric permittivity (ε') in the vicinity of the phase transition temperature. The ferroelectric-paraelectric phase transition is observed at $T_{0,h} = 322.61$ K (heating mode) and the paraelectric-ferroelectric phase transition is observed at $T_{0,c} = 319.55$ K (cooling mode).

Temperature dependences of the dielectric loss (ε'') of $Sn_2P_2(Se_{010}S_{0.90})_6$ at frequency f = 1 kHz for heating and cooling modes are shown in Fig. 32. As we see, in ferroelectric-paraelectric phase transition (heating mode) a jump of dielectric loss is observed, instead of cooling mode, where no significant jump was obtained.

Such a blurred behavior of $Sn_2P_2(Se_{0.10}S_{0.90})_6$ in the vicinity of the phase transition temperature may be caused by several reasons. Maybe it occurs because of the existence of a tricritical Lifshits point (TCLP) or an incommensurate phase (ICP). As it is known [17], on the p-T diagrams of $Sn_2P_2(Se_xS_{1-x})_6$ at different x from the interval of $0 \le x \le 0.13$ the TCP and TP take place which, with increasing concentration of x become closer and for x=(13±3)% the TCLP and an incommensurate phase are realized.

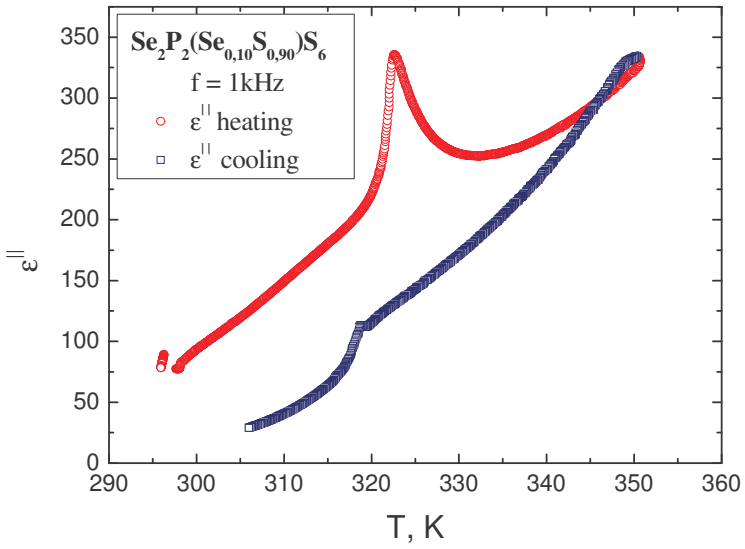

Figure 32. Temperature dependences of dielectric loss (ε'') of $Sn_2P_2(Se_{0.10}S_{0.90})_6$ (x=0.10) in heating and cooling modes at frequency f = 1 kHz

Besides, in the vicinity of the phase transition temperature, this sample has quite high values of the dielectric dissipation factor $\tan\delta \approx 1.06$ ($x = 0.10$), in comparison to $x = 0.05$ $\tan\delta \approx 0.11$ and $x = 0.15$ $\tan\delta \approx 0.07$, what is typical for relaxor type materials and needs a further study of this sample.

4.3.3. $Sn_2P_2(Se_{0.15}S_{0.85})_6$ (x=0.15) single crystal

Temperature investigations of the dielectric permittivity (ε'), dielectric loss (ε''), capacity (C) and conductivity (σ) of $Sn_2P_2(Se_{0.15}S_{0.85})_6$ (x=0.15) single crystal at several frequencies are made. Measurements were realized the same way as for x=0.05 and x=0.10 and in the same temperature interval, but as it was established, the phase transition temperature of this sample (x=0.15) is less than the room temperature. So, further measurements of $Sn_2P_2(Se_{0.15}S_{0.85})_6$ (x=0.15) are realized between ~ 253 K and ~ 353 K (heating mode) and ~353 K to ~ 221 K (cooling mode).

The experimental temperature dependences of the dielectric permittivity (ε') of $Sn_2P_2(Se_{0.15}S_{0.85})_6$ (x=0.15) at several frequencies in heating and cooling modes are shown in Figure 33**.**

Form Fig. 33 it can be seen, that at definite temperature (T) there is a jump of the dielectric permittivity (ε'). Therefore, $Sn_2P_2(Se_{0.15}S_{0.85})_6$ single crystal undergoes the ferroelectric-paraelectric phase transition at $T_{0,h}$ = 285.87 K (heating mode) and the paraelectric-ferroelectric phase transition at $T_{0,c}$ = 263.55 K (cooling mode)

Temperature dependences of the dielectric loss (ε'') of $Sn_2P_2(Se_{0.15}S_{0.85})_6$ at frequencies f = 1 kHz (A), f = 5 kHz (B) and f = 10 kHz (C) for heating and cooling modes are shown in Figure 34. There is also a clear jump of the (ε'') at definite temperature in ferroelectric-paraelectric (heating mode) and paraelectric-ferroelectric (cooling mode) transitions.

Dependences of the dielectric permittivity jump (ε'_{max}) and the dielectric loss jump (ε''_{max}) versus frequency (f) in heating and cooling modes for $Sn_2P_2(Se_{0.15}S_{0.85})_6$ (x=0.15) are shown in Figure 35.

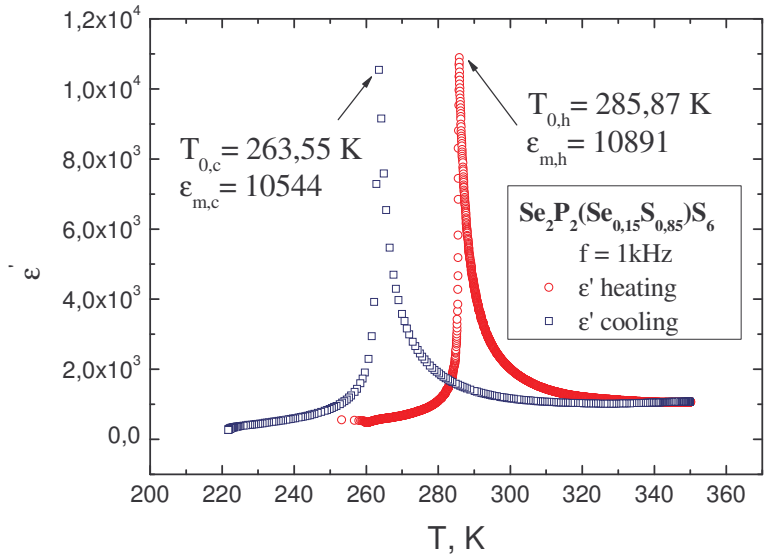

(A)

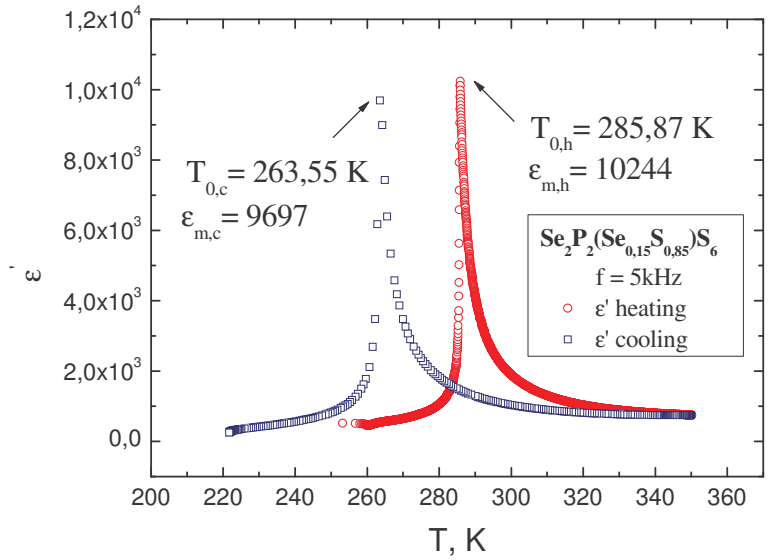

(B)

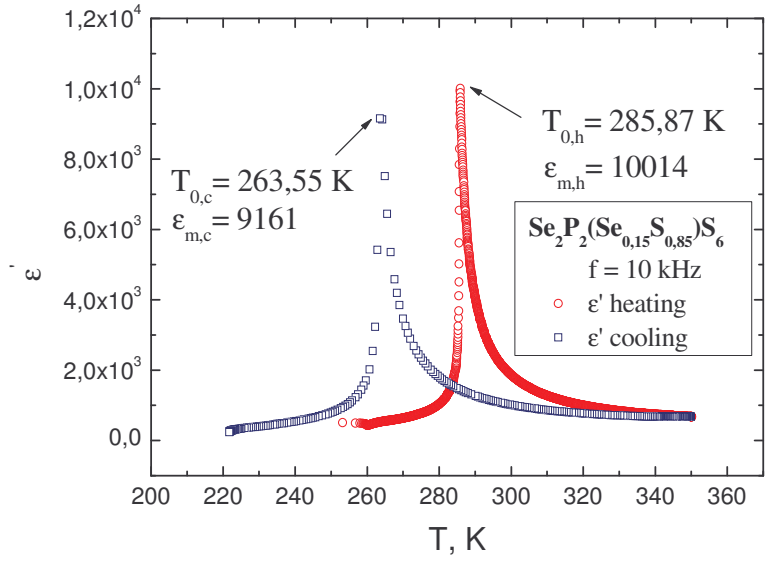

(C)

Figure 33. Temperature dependences of the dielectric constant (ε') of $Sn_2P_2(Se_{0.15}S_{0.85})_6$ (x=0.15) in heating and cooling modes at frequencies 1kHz (A), 5kHz (B) and 10kHz (C)

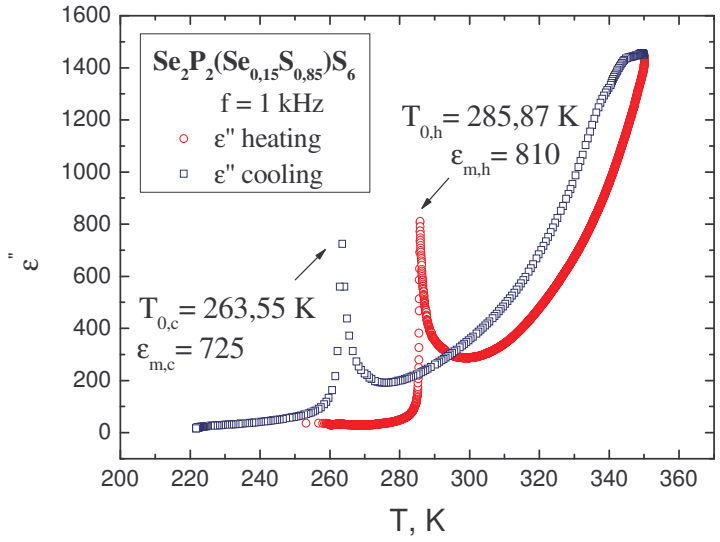

(A)

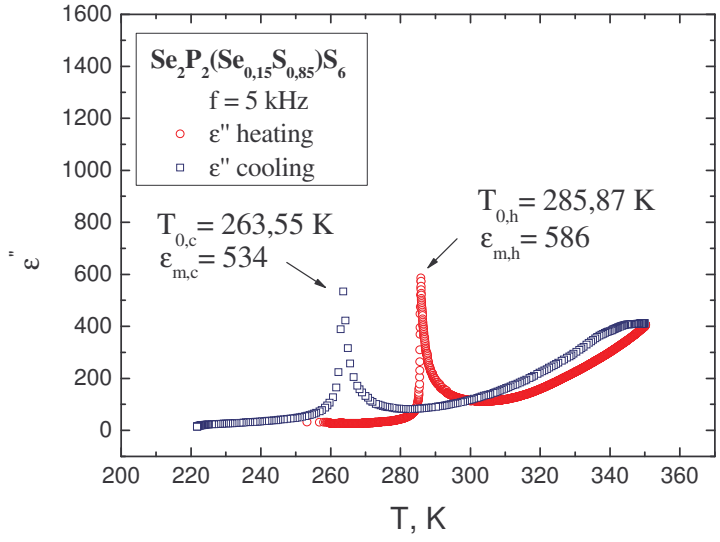

(B)

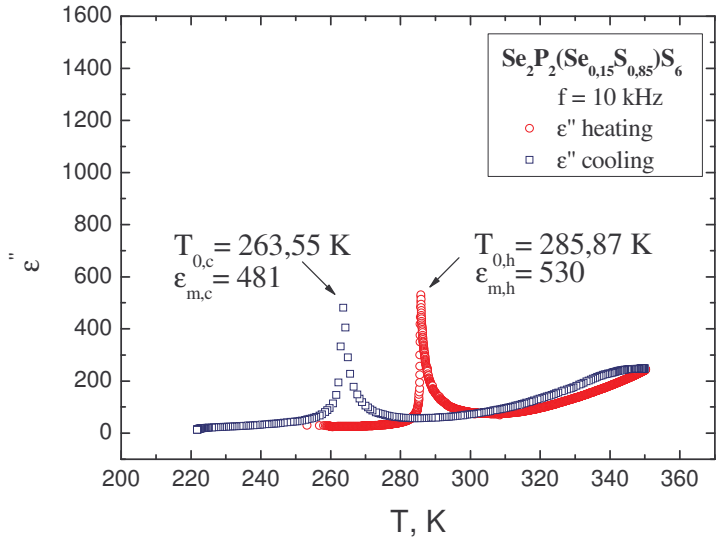

(C)

Figure 34. Temperature dependences of the dielectric loss (ε'') of $Sn_2P_2(Se_{0.15}S_{0.85})_6$ (x=0.15) in heating and cooling modes at frequencies f = 1 kHz (A), f = 5 kHz (B) and f = 10 kHz (C)

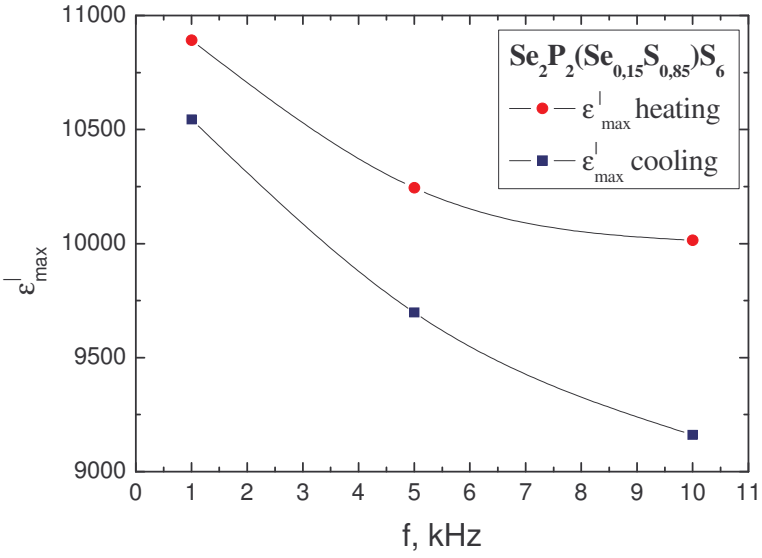

(a)

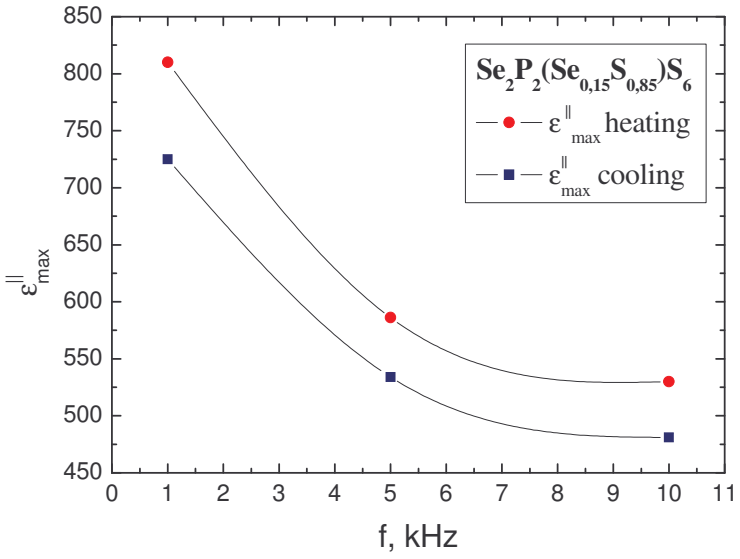

(b)

Figure 35. Dependences of (a) dielectric permittivity jump (ε'_{max}) and (b) dielectric loss jump (ε''_{max}) versus frequency (f) in heating and cooling modes for $Sn_2P_2(Se_{0.15}S_{0.85})_6$ (x=0.15)

From Fig. 35 it can be seen, that for $Sn_2P_2(Se_{0.15}S_{0.85})_6$ a jump of the dielectric permittivity (ε'_{max}) and a jump of the dielectric loss (ε''_{max}) at the ferroelectric-paraelectric phase transition (heating mode) and at paraelectric-ferroelectric phase transition

(cooling mode) decrease with applied frequency (f). So, we may suppose, that at frequency f = 1 kHz these variables have more significant jumps than at higher frequencies.

Figure 36 illustrates temperature dependence of (tanδ) of $Sn_2P_2(Se_{0.15}S_{0.85})_6$ at frequency 1 kHz.

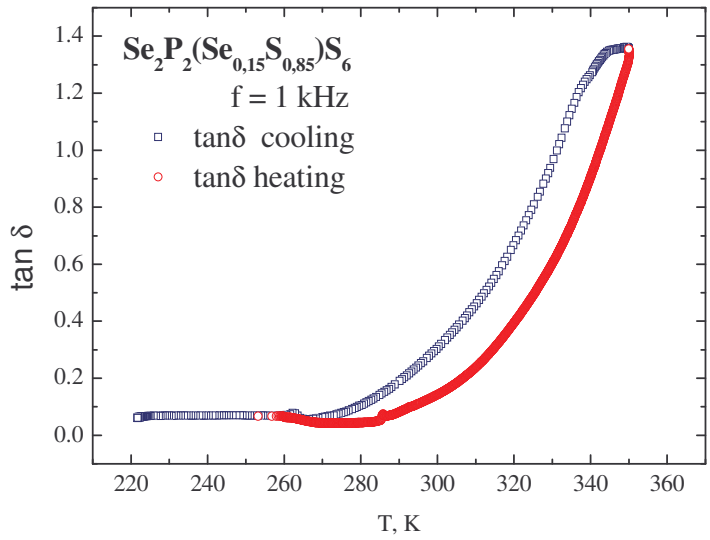

Figure 36. Temperature dependence of the dielectric dissipation factor (tanδ) for $Sn_2P_2(Se_{0.15}S_{0.85})_6$ (x=0,15) in cooling mode, f = 1 kHz

The experimental value of the dielectric dissipation factor in cooling mode for $Sn_2P_2(Se_{0.15}S_{0.85})_6$ (x=0,15) at atmospheric pressure p = 100kPa, temperature T = 300 K and frequency f = 1 kHz, is tanδ = 0.312, and at the phase transition temperature tanδ = 0.067.

Figure 37 illustrates the temperature dependence of the conductivity of $Sn_2P_2(Se_{0.15}S_{0.85})_6$ at frequency 1 kHz.

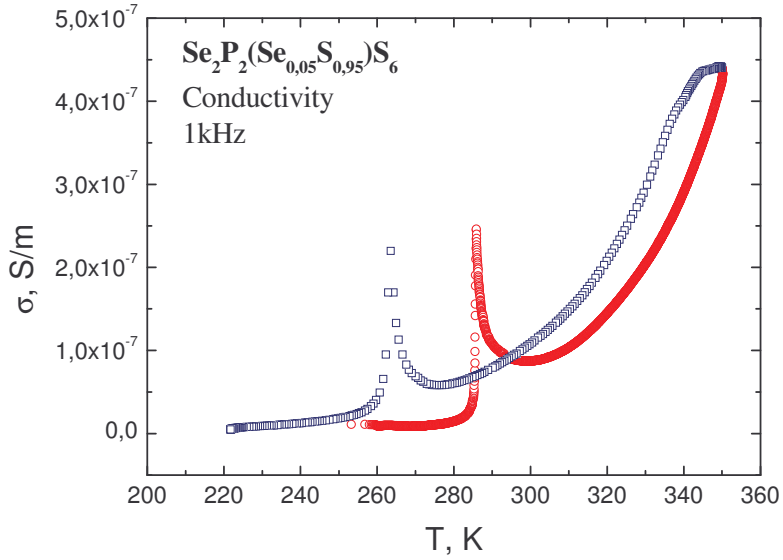

Figure 37. Temperature dependence of the conductivity of $Sn_2P_2(Se_{0.15}S_{0.85})_6$ in heating and cooling modes at 1 kHz

Dependences of the reciprocal dielectric constant versus temperature at several frequencies are investigated. Plots of the reciprocal dielectric constant ($1/\varepsilon'$) versus temperature (T) at frequency f =1 kHz for $Sn_2P_2(Se_{0.15}S_{0.85})_6$ single crystal are shown in Fig. 38. Figure 38 illustrates the temperature dependences of the reciprocal dielectric constant in heating and cooling modes.

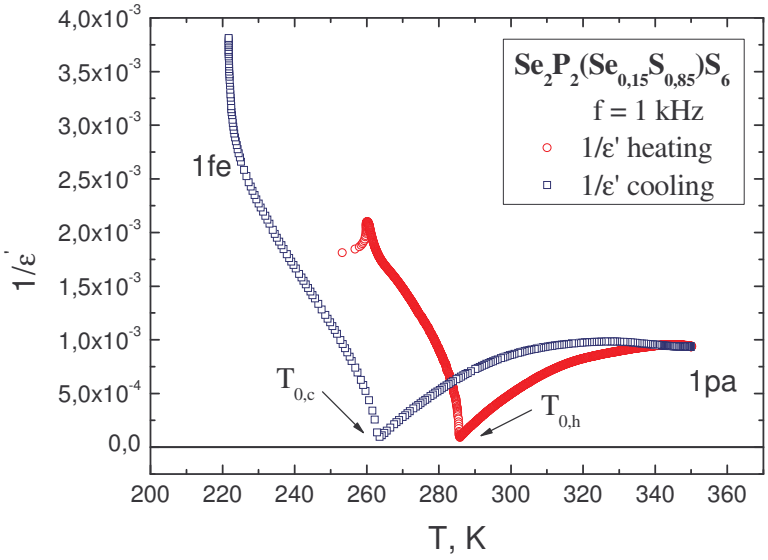

Figure 38. Temperature dependence of the reciprocal dielectric permittivity $1/\varepsilon'$ of $Sn_2P_2(Se_{0.15}S_{0.85})_6$ in heating and cooling modes at frequency 1kHz

As it can be seen, no significant jump of the reciprocal dielectric constant in the phase transition temperature is observed, it changes continuously, what suggests that the phase transition in $Sn_2P_2(Se_{0.15}S_{0.85})_6$ x=0.15, as in x=0.05 and 0.10 may be second order. At definite temperature and atmospheric pressure the crystal undergoes a ferroelectric phase transition. The transition from the ferroelectric to the paraelectric phase (heating mode) occurs at temperature $T_{0,h}$ = 285.87 K and the transition from the paraelectric to the ferroelectric phase (cooling mode) is observed at temperature $T_{0,c}$ = 263.55 K .

For our further phase transition study of $Sn_2P_2(Se_{0.15}S_{0.85})_6$ we considered only the temperature dependence of the reciprocal dielectric constant at frequency 1 kHz in cooling mode related to the paraelectric-ferroelectric phase transition. This dependence is shown in Fig. 39.

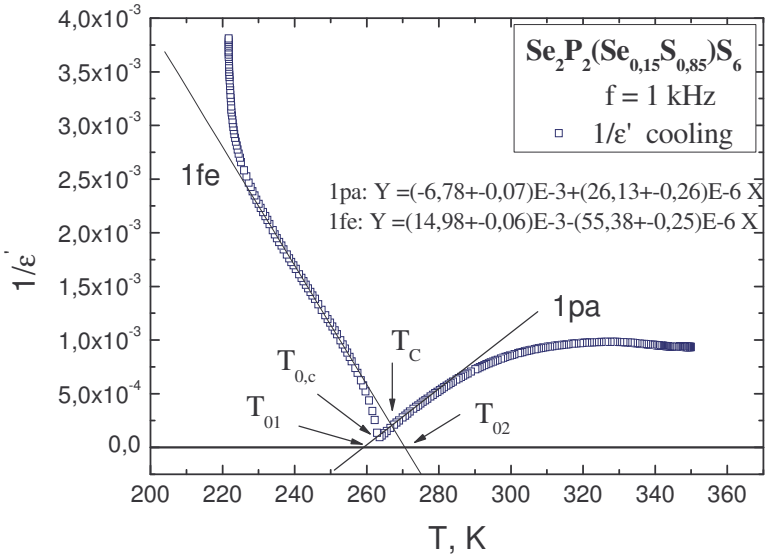

Figure 39. Temperature dependence of the reciprocal dielectric permittivity $1/\varepsilon'$ of $Sn_2P_2(Se_{0.15}S_{0.85})_6$ in cooling mode at frequency 1kHz

If we assume that the phase transition in $Sn_2P_2(Se_{0.15}S_{0.85})_6$ is second-order then the temperature dependence of the reciprocal dielectric constant should obey the Curie-Weiss law both above and below the phase transition temperature T_0. On the basis of our measurements we see that in the vicinity of the phase transition temperature T_0 at f = 1 kHz the values of the reciprocal dielectric constant a little deviate from the Curie-Weiss law (curve 1fe), as for sample with x=0.05. At frequencies of 5 kHz and 10 kHz this also occurs. This deviation makes us unsure about the type of the phase transition in $Sn_2P_2(Se_{0.15}S_{0.85})_6$, as in $Sn_2P_2(Se_{0.05}S_{0.95})_6$.

The temperature dependence of the reciprocal dielectric permittivity of $Sn_2P_2(Se_{0.15}S_{0.85})_6$ in the vicinity of the phase transition temperature T_0 in cooling mode at frequency 1 kHz is shown in Figure 40. The experimentally obtained phase transition temperature is $T_{0,c} = 263.55$ K and the extrapolated theoretical phase transition temperature is $T_0 = T_C = 267.09$ K.

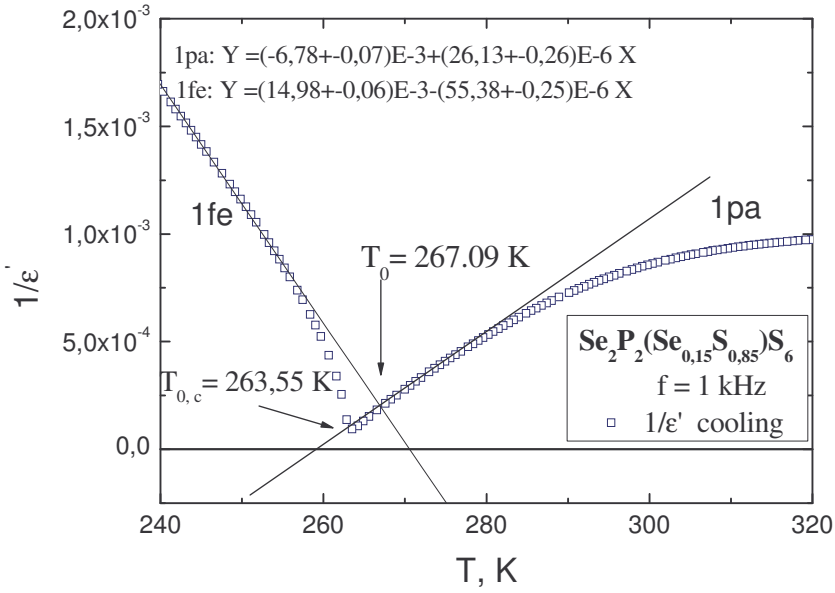

Figure 40. Temperature dependence of the reciprocal dielectric permittivity $1/\varepsilon'$ for $Sn_2P_2(Se_{0.15}S_{0.85})_6$ in the vicinity of the phase transition temperature T_0 in cooling mode at frequency 1kHz

Temperature dependences of the reciprocal dielectric permittivity in the ferroelectric phase 1fe= $\varepsilon_{fe}^{-1}(T)$ and the paraelectric phase 1pa= $\varepsilon_{pa}^{-1}(T)$ are described by the following equations (Fig. 40):

$$\varepsilon_{fe}^{-1}(T) = \frac{T_{02}}{C_{w,e}} - \frac{1}{C_{w,fe}} \cdot T = (14{,}98 \pm 0{,}06) \cdot 10^{-3} - (55{,}38 \pm 0{,}25) \cdot 10^{-6} \cdot T \qquad (40)$$

$$\varepsilon_{pa}^{-1}(T) = -\frac{T_{01}}{C_{w,pa}} + \frac{1}{C_{w,pa}} \cdot T = (-6{,}78 \pm 0{,}07) \cdot 10^{-3} + (26{,}13 \pm 0{,}26) \cdot 10^{-6} \cdot T \qquad (41)$$

Using these equations the following parameters for $Sn_2P_2(Se_{0.15}\ S_{0.85})_6$ are obtained: Curie temperature (phase transition temperature) $T_0 = T_C = 267.09$ K, Curie-Weiss temperature T_{01}=259.47 K and T_{02}= 270.49 K. Also, the Curie-Weiss temperature constants for the ferroelectric $C_{w,fe}$ and paraelectric $C_{w,pa}$ phases of $Sn_2P_2(Se_{0.15}S_{0.85})_6$ are calculated. The values are: $C_{w,fe}$ = -18057 and $C_{w,pa}$ = 38270. Ratio $\left|C_{w,pa} / C_{w,fe}\right|$ = 2.11. The experimental values indicate a second-order phase transition in $Sn_2P_2(Se_{0.15}S_{0.85})_6$ at a phase transition temperature $T_C = 267.09$ K and atmospheric pressure.

Conclusions

This work reports the investigations of the frequency and temperature depend measurements of the dielectric properties of $Sn_2P_2(Se_xS_{1-x})_6$ crystals.

Frequency measurements of $Sn_2P_2(Se_xS_{1-x})_6$ crystals with concentration of the selenium x=5%, x=10% and x=15% are made in air and silicone oil medium. It is found that the values of the capacity and accordingly the values of the dielectric permittivity falls slightly with increased frequency from 50 Hz to 13 MHz for crystals with x=10% and x=15% and for x=5% they fall sharply. Concerning air and silicone oil medium, there is almost no difference in measured values, except of crystal with x=5% of the selenium, where the values of the dielectric permittivity, capacity, dielectric loss and the dissipation factor are found to be higher in air medium. It is significant, that the obtained values of the dielectric dissipation factor for $Sn_2P_2(Se_{0.10}S_{0.90})_6$ are quite high $\tan\delta = 1.06$, in comparison with other two samples: $\tan\delta = 0.11$ for $Sn_2P_2(Se_{0.05}S_{0.95})_6$ and $\tan\delta = 0.07$ for $Sn_2P_2(Se_{0.15}S_{0.85})_6$.

Temperature investigations of the dielectric permittivity, dielectric loss, capacity and conductivity of $Sn_2P_2(Se_xS_{1-x})_6$ crystals at frequencies 1 kHz, 5 kHz and 10 kHz are performed. It was found that all of the three samples undergo a phase transition. The phase transition temperature T_C with increasing concentration of selenium decrease: $T_C = 331.56$ K (x = 5 %); $T_C = 321.08$ K (x = 10 %) and $T_C = 267.06$ K (x = 15 %). Also, the values of the dielectric permittivity and dielectric loss in the vicinity of the phase transition temperature decrease with increased concentration of the selenium. It is found that the values of the dielectric permittivity and dielectric loss in the vicinity of the phase transition temperature are also depending on the applied frequency. Jump of the dielectric permittivity and jump of the dielectric loss at the point of the phase transition temperature decrease with applied frequency and at frequency f = 1 kHz it is more significant than at higher frequencies.

Using experimental data, Curie-Weiss temperature constants for ferroelectric $C_{w,fe}$ and paraelectric $C_{w,pa}$ phases are calculated. For $Sn_2P_2(Se_{0.05}S_{0.95})_6$ (x = 5%) obtained values are following: $\left|C_{w,fe}\right| = 30708$ and $\left|C_{w,pa}\right| = 96154$. Ratio $\left|C_{w,pa}/C_{w,fe}\right| =$ 3,10. And for $Sn_2P_2(Se_{0.15}S_{0.85})_6$ (x = 15%): $\left|C_{w,fe}\right| = 18057$ and $\left|C_{w,pa}\right| = 38270$. Ratio $\left|C_{w,pa}/C_{w,fe}\right| = 2.11$. Obtained values are the evidence of the second order phase transition in studied crystals at corresponding temperature T_C and atmospheric pressure.

Literature

[1] Franco Jona and G.Shirane. Ferroelectric crystals. Oxford. New York. Pergamon Press, 1962.

[2] M.E. Lines, and A.M. Glass. Principles and Applications of Ferroelectrics and Related Materials. Clarendon Press. Oxford, 2001.

[3] W. Cady. Piezoelectricity. Izdatelstvo Inostrannoj Literatury. Moskva. 1949.

[4] Santos et al. *J. Phys.: Condens. Matter,* **13** pp. 10497-10505, 2001.

[5] Yu. M. Vysochanskii, M.M. Maior, V. M. Rizak, V. Yu. Slivka and M.M. Khoma, *Zh. Eksp. Teor. Fiz.* 95, 1355, 1989

[6] K. Z. Rushchanskii et. al. *Phys. Rev*. B **73,** 2006

[7] Slivka A. G., Gerzanich E. I. et al. *Ferroelectrics*, **103,** 1990

[8] K. Morija, H. Kuniyoshi, K. Tashita, Y. Ozaki, S. Yano, and T. Matsuo, *J. Phys. Soc. Jpn*. **67**, 3505, 1998

[9] P. H. M. van Loosdrecht, M.M. Maior et. al. *Phys. Rev*., **48,** 1993

[10] Razvan Caracas and Xavier Gonze. *Phys. Rev*., **66**, 104 106, 2002

[11] X. Bourdon, E. Prouzet and V.B. Cajipe. *Journal of Solid State Chem*. **129,** 157-159, 1997

[12] A. A. Grabar, I.V. Kedyk et. al. *Optics Communications* **188**(1-4), 187-194, 2001

[13] ANSI/IEEE, Std 179 – IEEE Standard on Piezoelectricity, p. 242 (IEEE, Inc. 345 East 47th Street, New York, NY 10017, USA, 1987

[14] G. Dittmar and H. Schafer. *Zeitschrift fuer Naturforschung* **29B**(5-6), 312-7, 1974

[15] P. P. Guranich et. al. *Ukr. J. Phys*. Opt. V**2**, №4

[16] M.M. Maior, P.H.M. van Loosdrecht, et. al. *J. Phys.: Condens. Matter,* **5**, 6023, 1993

[17] Yu. Tyagur. *Ferroelectrics*, **345**: 91 – 101, 2006

[18] M.M. Maior, Yu. M. Vysochanskii, I.P. Pritz, et.al. *Inorganic materials*, **27**, 503, 1991

[19] K. Morija, K. Iwauchi et.al. *J. of the Phys. Soc. of Japan*, Vol. **64,** No.5, 1775-1784, 1995

[20] Y. Tyagur, I. Tyagur, A. Kopal, L. Burianova, P. Hana. *Ferroelectrics*, **320**: 35-42, 2005